Delft University of Technology
Master Thesis

Remote sensing data as a soil moisture indicator for grass-covered dikes

Denise Caljouw

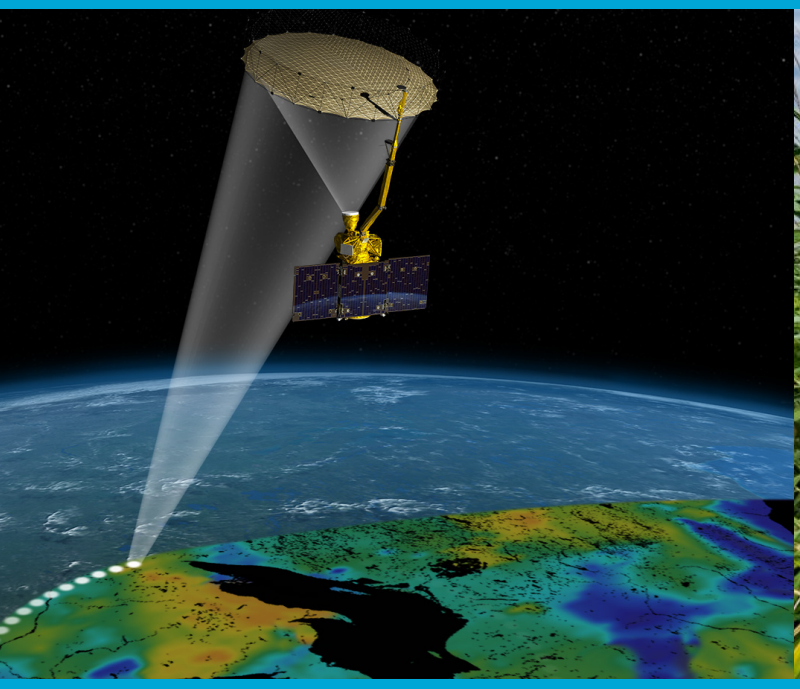

TU Delft Delft University of Technology

HKV LIJN IN WATER

Remote sensing data as a soil moisture indicator for grass-covered dikes

by

D. Caljouw

to obtain the degree of Master of Science

at the Delft University of Technology,

Student number:	4454014	
Thesis committee:	Prof. dr. ir. M. Kok,	TU Delft, chair
	Prof. dr. ir. S.C. Steele-Dunne,	TU Delft
	Dr. S.L.M. Lhermitte,	TU Delft
	Ir. N. van der Vliet,	HKV lijn in water

Abstract

Dikes hold back water and protect the land behind it from flooding. Due to rising sea levels, land subsidence and more extreme weather patterns, the function of dikes become increasingly important. To ensure dike safety, dikes are regularly inspected. With about 22,500 kilometers of dikes in the Netherlands, this is a very slow, costly and time consuming process. Remote sensing could contribute to dike inspections as it can screen large areas in a short time period and more continuously monitor inspection parameters. Several studies have already assessed the use of remote sensing for different inspections parameters such as deformation, grass cover quality and seepage detection. An important parameter that affects dike stability is soil moisture, as effective stress and shear strength are directly related to soil moisture content. Intense periods of drought can lead to low soil moisture values which consequently decreases dike stability. On the other hand, excessive soil moisture can lead to excess pore water pressure and to a decrease in shear strength. Remote sensing would be an ideal way to monitor soil moisture within grass-covered dikes on large scale. In this study, it was assessed if remote sensing data can give a proxy for soil moisture for grass-covered dikes. This was investigated by using open-access optical and SAR remote sensing data, as this would be an ideal data source since it is freely available. Remote sensing data was obtained from satellite missions Landsat 7/8 and Sentinel 1/2. The majority of the research was conducted for two grass-covered regional dikes.

First of all, it was assessed if a lagged relationship could be found between the average soil moisture value of a pixel, extracted from in-situ soil moisture sensors at 20 cm depth, and retrieved vegetation indices (GRR, MSR, NDVI, RVI and NDII) of a pixel. Pearson correlation coefficients were calculated for the harmonized Landsat 7 and 8 data set as the number of data from the single satellite missions was limited. Results show that (1) at location Bermweg a weak correlation was found (R=0.32-0.40) for the MSR, NDVI, RVI and NDII when the optimal lag of around 30 days was applied. A negligible correlation was found for the GRR (R=0.19); (2) at location Geerweg, for one pixel, a negligible (R=0.12-0.16) correlation was found for all vegetation indices, except the NDII, when the optimal lag of 23 days was taken into account. A negative correlation was found for the other pixel. For the NDII a negligible correlation (R=0.13-0.28) was found for the two pixels when the optimal lag of 31 day was applied. The grass-cover at location Bermweg was maintained by grazing whereas at location Geerweg the grass was maintained by both grazing and mowing.

Secondly, it was investigated if a (lagged) relationship could be found between SAR backscatter and in-situ soil moisture measurements at 20 cm depth. An increase in soil moisture results in an increase in backscatter. Since SAR measures only the top few centimeters of the soil, a lag was taken into account. In addition, it is known that there is a lagged correlation between root-zone soil moisture and LAI, which is also sensitive to backscatter (Jamalinia et al., 2019). A Pearson correlation analysis was performed to assess if there was a (lagged) relationship between soil moisture and retrieved backscatter. Only negative and negligible positive correlations were found, showing that SAR backscatter cannot give a proxy for soil moisture, as a positive correlation was expected.

Lastly, a relationship was examined between cumulative precipitation deficit, which can give a proxy for soil moisture, and vegetation indices. The sample size of Landsat 8 and the harmonized Landsat 7 and 8 data set were large enough to demonstrate statistical significance ($N > 31$). Results show that (1) at location Bermweg the optimal correlation was found for both data sets when a cumulative precipitation deficit period of around 15 days was taken into account. The correlation was negligible (R=0.24-0.36) for the harmonized Landsat 7 and 8 data set (statistically significant, with the exception of the NDVI and NDII) and moderate (statistically significant) for Landsat 8 (R=0.38-0.56); (2) at location Geerweg the cumulative period resulting in the optimal correlation was different for each satellite mission. A statistically significant weak correlation (R=0.47-0.57) was found for the harmonized Landsat 7 and 8 data set when a cumulative period of 20 days was taken into account. For Landsat 8 a statistically significant moderate correlation (R=0.49-0.62) was found for a cumulative period of 90 days. The overall pattern of the calculated correlation coefficients, when different cumulative periods were taken into account, vary largely for each satellite mission. All in all, no universal relationship could be found.

The study has shown that vegetation indices and SAR backscatter cannot give an indication of soil moisture

within dikes. No strong relationship was found between soil moisture and vegetation indices which can be assigned to noise introduced by various factors like management practices (i.e. mowing, grazing), other key factors influencing vegetation state (i.e. nutrient availability, radiation), low spatial resolution, and scene-to-scene variability. These factors also influence the vegetation index and overrule the true soil moisture conditions. Moreover, the results show that cloud contamination hinders the use of optical remote sensing data for dike inspections as satellite imagery might not be available for extended periods of time, disabling to gain insight into the dynamics of vegetation indices over time. The insensitivity of SAR backscatter to soil moisture can be assigned to the fact that several parameters (i.e. surface roughness, vegetation, dike slope) can affect backscatter as much, or more than, soil moisture. Furthermore, the backscatter signal was extracted from a relatively small area and thus contains a large amount of noise. This also explains why backscatter was unable to give an indirect proxy of soil moisture by estimating the LAI.

Acknowledgements

With the finalizing of this thesis my master Civil Engineering, Water management at the TU Delft comes to an end. I look back at my study time at the TU Delft as a great time.

First of all, I would like to express big appreciation to Nils van der Vliet, for his good supervision, guidance and encouragement. Every week we had a meeting to discuss the process of my thesis where you always helped me when I lost track. Thanks for always making the meetings easygoing by having a healthy laugh. Furthermore, I would like to show my gratitude to Matthijs Kok, my committee chair, for always being available for meetings and giving me guidance throughout the thesis. Stef Lhermitte and Susan Steele-Dunne, thank you for giving me your specialist view on my project.

Secondly, I would like to thank Bart Strijker for providing me with the soil moisture data. You were always open to discussing my findings during meetings which really helped me along the way. I would also like to thank Joost Stenfert for his enthusiasm and good ideas which helped me shape my research. Thanks to the other colleagues at HKV, where I had great support for writing my thesis. You were always available for discussion on my topics and helping me out.

Finally, there were a lot of people who supported me throughout my thesis. First of all, my family. Thank you for supporting me throughout and giving me feedback on my thesis. Also, I would like to thank my roommates for all the laughs, support and being such good listeners. Lastly, I would like to thank Robert for his great advice, feedback and for helping out where needed.

Rotterdam, November 2021
D. Caljouw

Acronyms

BOA Bottom Of Atmosphere

GEE Google Earth Engine

GRR Green Red Ratio

KNMI Koninklijk Nederlands Meteorologisch Instituut

L7 Landsat 7

L8 Landsat 8

LAI Leaf Area Index

MSR Modified Simple Ratio

NDII Normalised Difference Infrared Index

NDVI Normalized Difference Vegetation Index

NIR Near Infrared

RADAR Range Detection and Ranging

RVI Ratio vegetation index

SAR Synthetic Aperture Radar

SRF Spectral Response function

SWIR Short Wave Infrared

S1 Sentinel-1

S2 Sentinel-2

TOA Top Of Atmosphere

VI Vegetation Index

Contents

1

Introduction

Dikes, also called levees, embankments, or dams, are man-made structures that play a major role in flood protection. The primary function of a dike is to hold back water and protect the land behind it from flooding (Reijers et al., 2014). Dikes are becoming increasingly important, as sea levels keep rising, land subsides and extreme weather patterns increase due to climate change. With hundreds of millions of people around the world living in low elevation coastal zone (i.e. areas less than 10 meters above sea level), dikes are crucial barriers (Neumann et al., 2015).

In the Netherlands, dikes are visually monitored by inspectors who have a crucial role in finding (potential) weaknesses in the dike. With 60% of the Netherlands below sea level, these inspections are of great importance (Jonkman et al., 2008). Visual inspections are a slow, costly and time-consuming process, with about 22,500 kilometers of dikes in the Netherlands (Jorissen et al., 2016). During an inspection, inspectors look at different quality indicators which could indicate a change or loss of the dike structure. There are dozens of parameters that have to be inspected, such as quality of grass-covers, deformations, and saturation (Bakkenist, 2012). The frequency of inspection differs per parameter and also depends on factors such as the type of flood defence (primary or regional) and the probability of flooding (Bakkenist et al., 2012).

Soil moisture is one of the most important factors affecting dike stability. Especially in peat dikes, where effective stress and shear strength are directly related to water content, deformations are largely controlled by soil moisture (Hack et al., 2008). Intense periods of drought can lead to low soil moisture, which can lead to reduced shear strength which consequently decreases the stability of dikes (Jamalinia et al., 2020). Desiccation of dike soils can eventually lead to horizontal displacements. This happened in 2003 in Wilnis, the Netherlands, when a period of drought led to a dike breach. Over 2,000 people had to be evacuated, 600 houses were flooded and the actual damage totaled about 10 million euros. On the other hand, excessive soil moisture may soften soils, weaken shear strength, and also decreases dike stability.

Over the last decade, several studies have assessed the use of remote sensing for different dike inspection parameters. Remote sensing could facilitate dike inspections by monitoring large areas of dike in a short time. LiDAR and synthetic aperture radar (SAR) have been investigated for deformation detection (Bishop et al., 2003) (Haarbrink and Shutko, 2006) (Moser and Zomer, 2006) (Closson et al., 2003). Satellite multispectral imagery and polarimetric SAR have shown potential for slide detection, and hyperspectral imagery was used to develop a slide prediction model (Azad Hossain and Easson, 2012) (Aanstoos et al., 2012) (Sehat et al., 2014). Passive microwave radiometry (PMR) and (polarimetric) SAR have been shown to be sensitive to soil moisture, and also to seepage detection (Haarbrink and Shutko, 2006) (Aanstoos et al., 2011). Various studies have also tested thermal remote sensing for seepage detection but show mixed findings (Givehchi et al., 2003) (Moser and Zomer, 2006) (Swart, 2007). Cundill (2016) demonstrated that multispectral broadband sensors with a relatively lower spatial resolution (i.e. 5 meters) performed well when trying to find a correlation between soil moisture and vegetation indices. This study has illustrated the ability of vegetation indices to give an indication of soil moisture. No research has been conducted yet that investigates the use of open data satellite missions. Open data satellite missions would be an ideal data source since it is freely available. As the spatial resolution of satellite data is restricted, it should be seen as an addition to visual inspections, but should not be perceived as a

replacement.

Vegetation is highly responsive to changes in soil moisture. Therefore, monitoring vegetation conditions by using optical remote sensing could be used as an indicator for subsurface conditions (Hopkins, 2009). It has been widely demonstrated in literature that many vegetation indices are more or less related to root-zone soil moisture and that there is always a time lag in which vegetation responds to soil moisture (Wang et al. (2007), Musyimi (2011), Zhang et al. (2018), Zhang et al. (2011), Buitink et al. (2020)). As root-zone soil moisture is a key factor in vegetation health, vegetation indices could give an indication of soil moisture within a dike. Hasan et al. (2013) concluded that grass growing over areas with cracks and fractures was stressed or dying due to lack of moisture, while it grew green in adjacent areas. Jamalinia et al. (2019) has demonstrated that there is a strong, lagged correlation between the leaf area index (LAI) and the water root-zone content. Furthermore, a strong correlation was found between root-zone water content and the factor of safety of a dike. As the amount of vegetation strongly affects the water flux into the dike and consequently impacts the factor of safety of a dike, vegetation could be used as an indicator to detect vulnerable areas of dike in an early stage. Several studies have also shown the potential of active microwave radar to map changes of surface soil moisture content (Srivastava et al. (2006), Balenzano et al. (2010), Hasan et al. (2013)). SAR is well-known for it's potential of retrieving soil moisture content of the top few centimeters, and several studies have successfully demonstrated the use of SAR to detect soil moisture content changes (Srivastava et al. (2006) Balenzano et al. (2010) Hasan et al. (2013) (Dabrowska-Zielinska et al., 2018)). A major advantage of SAR over optical satellite imagery is that it can penetrate clouds and imagery can be obtained in all weather conditions.

There is a clear need to continuously monitor soil moisture values within dikes, not only in time but also spatially, to make local inspections more effective and increase dike safety. Vegetation indices and SAR backscatter obtained from remote sensing data could potentially be used to give a proxy for soil moisture. The objective of this thesis is to assess if vegetation indices and SAR backscatter obtained from remote sensing satellites can be used as a soil moisture indicator for grass-covered dikes, with the aim of identifying vulnerable areas of interest for further investigation.

1.1. Problem statement

Dikes are built to prevent flood events along coasts, rivers, and artificial waterways. As a significant part of the Netherlands is below sea level, it is very important to monitor dike stability. One of the main factors affecting dike stability is soil moisture, as effective stress and shear strength are directly related to water content, and deformations are largely controlled by soil moisture (Hack et al., 2008). Monitoring soil moisture is therefore crucial and will have even greater importance in the future as dry periods are expected to occur more frequently due to climate change (Philip et al., 2020). Strijker (2021) has demonstrated that the drying out of dikes is a very dynamic and complex process and shows that the cumulative precipitation deficit from April 1st onwards, which is currently used as a drought indicator for dikes in the Netherlands, cannot always give a good indication of soil moisture within dikes. The study highlights the need for other soil moisture indicators. Ground-based methods are measurements at point scale, which means they cannot provide spatially distributed information. Furthermore, it is costly to install sensors. Remote sensing would therefore be an ideal way to monitor soil moisture in grass-covered dikes on large scale. In literature, several studies can be found which show the potential of using remote sensing to give a proxy for soil moisture. SAR data has the potential to give a proxy for surface soil moisture of the dike, and vegetation indices can give an indication of soil moisture in the subsurface as it responds to water content variations in the root-zone. Remote sensing could contribute to more continuously monitoring soil moisture values within grass-covered dikes on large scale to identify vulnerable areas and make local inspections more effective. This would result in better management practices and make inspection planning of dikes more effective.

1.2. Scope

To limit the scope of the study, this research will focus on the potential of optical remote sensing imagery and SAR remote sensing imagery to give an indication of soil moisture in grass-covered dikes. The focus will be on open-access satellite missions, as this would be an ideal data source as the data is freely available. The research is conducted for grass-covered dikes. Since open data satellite data does not have a very high spatial resolution, only broad (> 40 meters) dikes were chosen as study sites to avoid contamination of pixels from other surfaces. The majority of the research is conducted for two grass-covered regional dikes. The geographical scope is set in the Netherlands.

The type of data used in this thesis is satellite imagery, in-situ soil moisture measurements, and precipitation deficit data. Satellite imagery is acquired from open data satellite missions Sentinel-1/2 and Landsat 7/8, based on their high revisit time and relatively high spatial resolution. The part of the research using in-situ soil moisture measurements as ground truth data is limited to the study period of April 2020 up until September 2021. The study period of the remaining part of the research is restricted to the dates from which the satellite imagery is available on the Google Earth Engine platform.

1.3. Objective and research questions

The objective of this study is to assess the relationship between optical and SAR remote sensing data, obtained from satellite imagery, and soil moisture indicators for grass-covered dikes, with the aim of identifying vulnerable areas for further investigation.

This research aims to give an answer to the main research question:

"How can remote sensing data give insight into soil moisture and contribute to dike inspections on grass-covered dikes?"

To answer the main research question, the following sub-research questions will be investigated to simplify the process of answering.

1. How strong is the lagged relationship between vegetation indices obtained from optical remote sensing and soil moisture?
2. How strong is the relationship between backscatter obtained from SAR remote sensing and soil moisture?
3. How strong is the relationship between vegetation indices obtained from optical remote sensing and precipitation deficit?
4. Can spatial-temporal variations of soil moisture be distinguished by vegetation indices and SAR backscatter obtained from remote sensing data?
5. How can remote sensing data contribute to dike inspections on grass-covered dikes?

1.4. Report outline

The outline of the report is as follows. After this introduction, Chapter 2 provides background information that is relevant to follow the research purpose and methodology. Afterwards, Chapter 3 consists of two parts: first of all, an introduction of the study locations, followed by a description of the data used in this research. Chapter 4 contains a description of the research methodology. Following this, results are presented in Chapter 5. Subsequently, the main topics of discussion and implications on the results are discussed in Chapter 6. Lastly, overall conclusions and recommendations are presented in Chapters 7 and 8 respectively.

2

Background information

2.1. Basics of remote sensing

Remote sensing is the acquiring of information about an object or area from a distance by measuring the reflected or emitted electromagnetic radiation (De Jong et al., 2004). Electromagnetic energy is produced by the vibration of charged particles and travels in the form of waves through the atmosphere and the vacuum of space. All materials on earth with a temperature above 0 Kelvin are able to radiate electromagnetic waves of all various wavelengths. The most well-known natural source of electromagnetic radiation is the sun. Artificial radiation occurs when a remote sensing instrument, such as a laser, sends its own energy pulse towards the earth. Remote sensing sensors can measure the electromagnetic radiation emitted by objects at the earth's surface. Sensors that use natural radiation from the sun are called passive sensors and those that provide their own source of radiation are called active sensors.

The total range of wavelengths is referred to as the electromagnetic spectrum (see figure 2.1). The amount of energy reflected from a surface at a specific wavelength is referred to as spectral reflectance. For different objects, a reflectance curve can be established which shows the percentage of reflectance for each wavelength. Objects or surface features can be detected and discriminated because they reflect and absorb different amounts of energy in different bands of the electromagnetic spectrum (Sivakumar et al., 2004). Remote sensing can be used for various applications. Such as monitoring deforestation, examining the health of plants and crops and detecting changes in land use and cover.

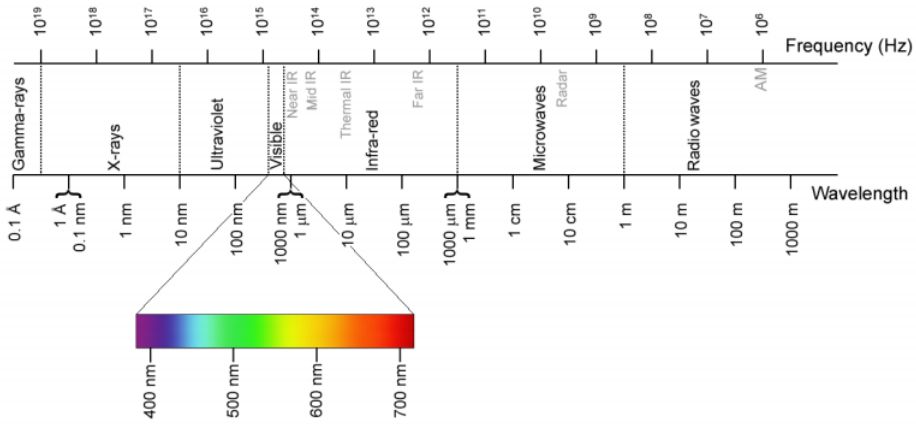

Figure 2.1: The electromagnetic spectrum (Cundill, 2016).

A remotely sensed image is composed of pixels, which all together form an image. Each pixel represents an area on earth and has a certain size, this is referred to as the spectral resolution. The spectral resolution is different for each sensor type. Each pixel is associated with an average reflection value measured in a given wavelength. For each pixel, the measurements are stored as Digital Numbers (DN-values). In optical remote sensing for each

measured wavelength range, a separate data set is stored, which is called a band. Imaging radar acquires an image in which each pixel contains a digital number according to the strength of the backscattered energy that is received from the ground (Bakker et al., 2004).

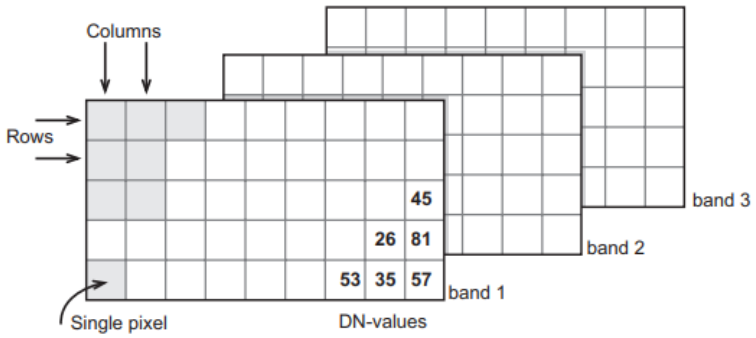

Figure 2.2: An image file comprising of Digital Numbers for each band (Bakker et al., 2004).

The spatial, spectral and temporal resolution of satellites are important factors that determine the type and quality of the information stored within a pixel. The spatial resolution refers to the size of one pixel in the satellite image. This determines the amount of detail that can be seen in a satellite image. The spectral resolution is the ability of a sensor to define finer wavelengths. The finer the spectral resolution, the narrower the wavelength range for a particular band. The temporal resolution specifies the revisiting frequency of a satellite mission over the same area. There is a trade-off between spatial and temporal resolution. The higher the spatial resolution, the lower the temporal resolution and vice versa. When the spatial resolution of a sensor is higher, the field of view is smaller thus more time will be needed to cover the same area.

There are two main types of satellite data used in remote sensing: optical and radar imagery. Optical satellite data is a great way to view the world just as the human eye does. Because optical remote sensing uses the natural energy from the sun as their radiation source, it functions only in the daytime. Radar sensors, on the other hand, can obtain imagery both day and night because it sends out their own pulses. Radar imagery can be obtained in almost all weather conditions and can penetrate through clouds. The difference between optical and radar satellite data lays within the electromagnetic spectrum. Microwave remote sensing (radar) operates in the microwave portion of the electromagnetic spectrum, generally using wavelengths between 1 cm and 1 m. Optical remote sensing measures in the visible and infrared region (400 to 2000 nanometers) (Bakker et al., 2004).

2.1.1. Optical remote sensing

The different bands with their own wavelength and bandwidth can be used to discriminate between different objects or surface features. For example, healthy vegetation is a good absorber of electromagnetic energy in the visible region. Chlorophyll, the pigment in plant leaves, strongly absorbs energy in blue and red wavelengths and reflects more green wavelengths. This is why our eyes perceive healthy vegetation as green. Furthermore, healthy plants have a high reflectance in the near-infrared (NASA, 2021c). The reflectance curve of unhealthy vegetation differs from that of healthy vegetation, making it able to make a distinction between the state of vegetation when using remote sensing sensors. Another way to discriminate different objects is by combining different bands. Combining wavelength bands can provide more information than the bands on their own since all objects have a distinctive reflectance pattern.

For example, the Normalized Difference Vegetation Index (NDVI) is used to give an indication of the vegetation health by the property of chlorophyll. Chlorophyll strongly reflects in the near-infrared and red bands and, therefore, is a good indicator for healthy vegetation.

The NDVI is defined by:

$$NDVI = \frac{\rho_{NIR} - \rho_{RED}}{\rho_{NIR} + \rho_{RED}} \tag{2.1}$$

In the formula, ρ stands for the band corresponding to the specified wavelengths. The NDVI provides a value between +1 and -1, where negative values (-1) of NDVI correspond to water, values close to zero (-0.1 to 0.1)

correspond to barren areas of rock, sand or snow and positive values represent vegetation (NASA, 2021c).

2.1.2. Radar remote sensing

The most common form of imaging active microwave sensors is radar. Active microwaving imaging techniques use wavelengths between 1 cm and 1 m. Within the microwave region, there are several wavelength ranges that are given a code letter. SAR uses the C-band portion of the spectrum, which can penetrate up to 5 cm deep below the soil surface. Images are formed by sending out their own pulses of microwave energy with their transmitter and detecting the backscattered portion of the signal with its receiver. Because they actively send out their own pulses, the signal characteristics (e.g. wavelength, polarization, incidence angle, etc.) are fully controlled and can be adjusted according to the desired application. Also, they can function during the night and therefore acquire data at any time (for Remote Sensing, 2007). Due to its long wavelengths compared to optical remote sensing, radar can penetrate through clouds and can measure in all weather conditions (Bakker et al., 2004). The intensity of the backscattered energy depends on the interaction of the energy with several parameters. These parameters include characteristics of the radar system (wavelength, polarization, viewing geometry, etc.) as well as the characteristics of the surface (landcover type, topography, relief, etc.) (for Remote Sensing, 2007). A lot of studies have used backscatter intensities for identifying crop types and canopy biophysical parameters including Leaf Area Index, biomass and height (Mandal et al., 2020). Volume scattering (the scattering of radar within a medium) depends on the physical properties of the object such as leaf size, density, height, presence of lower vegetation, etc. together with the characteristics of the radar used (Bakker et al., 2004).

Effect of sensor characteristics

Polarization, wavelength (frequency) and incidence angle are the most influential SAR parameters.

Polarization Polarization refers to the orientation of the electric field. Since SAR is an active sensor, it can control the polarization of the emitted signals. SAR is a phase-preserving dual polarization system and can transmit a signal in either horizontal (H) or vertical (V) polarization. It supports operation in single polarization (HH or VV) and dual polarization (HH+HV or VV+VH). Using different polarizations and wavelengths, information can be collected that is useful for specific applications (for Remote Sensing, 2007). Depolarization happens when the outgoing signal has a different polarization than the incoming signal. In SAR the main source of depolarization is volume scattering. A horizontal polarized wave might hit vegetation, bounce back and forth among them, and be backscattered to the satellite in a vertically polarized state. Cross polarization (HV or VH) is therefore very sensitive to vegetation parameters (McNairn and Shang, 2016).

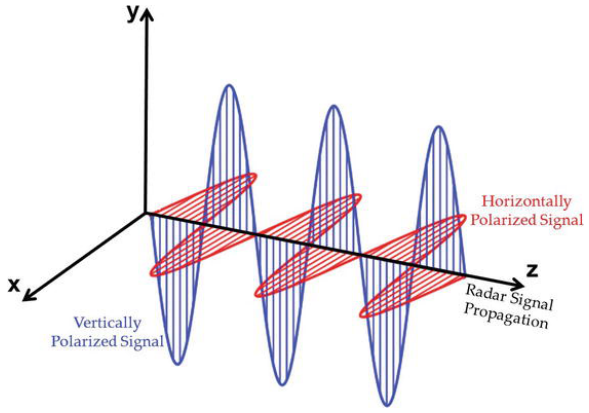

Figure 2.3: Horizontally and vertically polarized radar signal. (Dabboor and Brisco, 2018)

Wavelength Longer wavelengths are able to penetrate further than shorter wavelengths. Therefore, different radar bands can best be used with different types of vegetation. C-bands are most suitable to measure shorter crop canopies and can penetrate up to 5 cm into the ground.

Incidence angle Radar sensors are side-looking instruments. The incidence angle is the angle between the radar sensor and the normal to the ground surface. Figure 2.4 shows the effect of the incidence angle on the backscatter intensity for smooth, moderately rough and rough surfaces. Smooth surfaces act as a mirror when the incidence angle is small. When the angle decreases, the reflected pulses are directed away from the antenna.

However, for rough surfaces, most of the emitted pulses are scattered in a random direction. When the incidence angle is larger than 20°, rough surfaces still produce a lot of random scattering which result in a higher backscatter than for smooth surface at the same incidence angle (Emery and Camps, 2017).

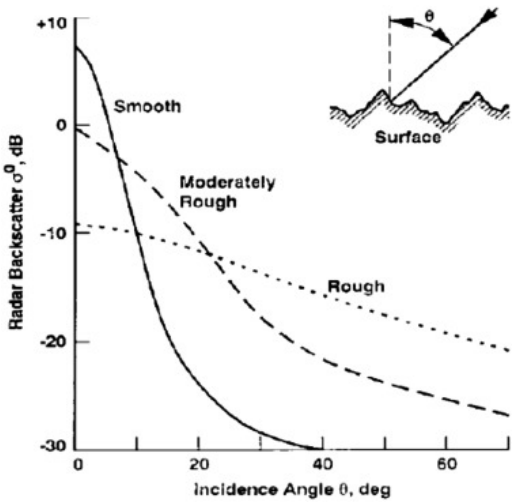

Figure 2.4: The relationship between the incidence angle and the radar backscattered intensity (Emery and Camps, 2017)

2.2. Remote sensing for potential use in dike inspection

Several studies have demonstrated that vegetation indices are more or less related to root-zone soil moisture content and that there is always a time lag in which vegetation responds to soil moisture (Wang et al. (2007), Musyimi (2011), Zhang et al. (2018), Zhang et al. (2011), Buitink et al. (2020)). Zhang et al. (2011) showed that the NDVI showed a significant lag response to soil moisture in grasslands and shrublands and suggests that a lag needs to be taken into account when VIs are used to estimate soil moisture. Research conducted by Wang et al. (2007) demonstrated that the NDVI can give a representation of soil moisture at 10 to 50 centimeters depth for shrub and grass vegetation in semi-arid and humid climate conditions. Sriwongsitanon et al. (2016) has shown that the Normalized Difference Infrared Index (NDII) appears to correlate well with the moisture content in the root-zone of plants and could therefore might be a good proxy for the vegetation quality. A study by Cundill (2016) has assessed if there is a correlation between vegetation indices and soil moisture on a grass-covered peat dike by using high spatial resolution imagery. The study has demonstrated that even when using a relatively lower spatial resolution (i.e. 5 meters), a strong correlation was found between soil moisture and the GRR, MSR and RVI ($R > 0.56$). The relationship between vegetation indices and soil moisture is complicated by many factors such as the time lag in which vegetation responds to soil moisture, seasonality, vegetation types and soil properties (Zhang et al., 2018).

SAR is well-known for its potential for retrieving soil moisture content. Several studies have successfully demonstrated the use of SAR to detect soil moisture content changes (Srivastava et al. (2006) Balenzano et al. (2010) Hasan et al. (2013) (Dabrowska-Zielinska et al., 2018)). Paloscia et al. (2013) tested and validated a soil moisture content (SMC) algorithm for GMES Sentinel-1 characteristics. Overall, most studies show that VV-polarization is less affected by vegetation and should therefore be most sensitive to soil moisture (Bousbih et al. (2017), Benninga et al. (2020)). Liu et al. (2017) assessed the capability of pattern analysis based on the soil moisture retrieval from Sentinel-1. The study confirms that the spatial-temporal pattern of soil moisture can be analysed using Sentinel-1 imagery. However, soil moisture estimation using SAR is very challenging as it is influenced by parameters such as surface roughness and vegetation cover (Romshoo et al., 2002). The magnitude of sensitivity to these parameters depends on surface and vegetation characteristics. As vegetation biomass increases, radar shows higher sensitivity to vegetation parameters compared to surface characteristics. However, the sensitivity to surface soil moisture is higher than to vegetation water content and surface roughness. The study shows that retrieval of volumetric soil moisture is strongest at lower angles of incidence and that under vegetated conditions, surface soil moisture changes can be monitored. However, the sensitivity to these parameters differs largely per area. Surface roughness and vegetation cover could affect backscatter as much, or more than, soil moisture. There is no simple or straightforward method to correct for these parameters (Jackson et al., 1996). Many soil Sentinel-1 soil moisture retrieval products take into account the effect of these different parameters in

order to acquire an accurate estimate of backscatter. Bauer-Marschallinger et al. (2018) developed a soil moisture content product based on a change detection algorithm which assumes constant surface roughness and vegetation conditions. The spatial resolution of these products is relatively low as the data needs to be aggregated to reduce the noise level of backscatter (Esch, 2018).

In literature, numerous studies demonstrate the synergy between optical and SAR radar imagery to retrieve soil moisture content. Liu et al. (2021) combined remote sensing from Sentinel-1 radar and Sentinel-2 optical satellites to quantitively retrieve soil moisture content. Foucras et al. (2020) succeeded in estimating surface soil moisture at a spatial resolution of 500 meters with an algorithm by combining remote sensing data from Sentinel-1 radar, Sentinel-2 optical and MODIS. Studies mentioned above show that SAR and optical data might be a powerful tool to give a proxy for soil moisture in grass-covered dikes.

2.3. Dikes

Dikes are crucial barriers that hold back the water and protect the land behind it from flooding. They are becoming increasingly important as sea level rises and land subsides. A dike breach can result in serious flooding, which can lead to enormous economic damage and a significant loss of lives (Jonkman et al., 2008). In general, four types of dikes can be distinguished: sea dikes, river dikes, dikes around lakes and dikes along canals.

Sea dikes are primary flood defences that have to resist a combination of high water and wave action. The period of high water is relatively short (number of hours) and the water will rise very fast. Sea dikes, therefore, have gentler outer slopes to decrease the wave run-up. The body of the dike is in general composed out of sand because this is the cheapest material. The sand is generally covered with an impermeable clay layer. Clay would be the best material to use for the core of the dike. However, it is too expensive. The subsoil of sea dikes that is available is generally sufficient and can be used (Verhagen, 1998).

River dikes are primary flood defences that are attacked by a relatively slow varying water level and minor wave attack. The period of high water is relatively long (number of days) and the water will rise very slowly. River dikes often have a steeper outer slope and gentler inner slope. Their core generally consists out of sand with a clay layer on top. The subsoil sometimes has to be removed and replaced by sand when it consists of soft peat layers (Verhagen, 1998).

Dikes along canals and inland waterways are regional flood defences. The regional flood defences protect the surrounded area from 'inside water'. This is excess water from the polder pumped onto the storage canals. Water levels inside the storage canals are regulated by human intervention. Water enters the canal through rainfall and inflow from surrounding polders. Water flows out of the canal by drainage to the outside water bodies (rivers or sea) and seepage. Regional flood defences often have steeper slopes than primary flood defences. The core of the dikes often consists of peat and clay layers, because these structures were constructed with locally available materials. Currently, most of the reinforcements of regional flood defences are made with clay (Lendering, 2015). The results of failure are not as catastrophic as the failure of primary flood defences, as the water that may cause inundation is not as large. Therefore, the return period is smaller. However, regional flood defences have become of increasing importance since the growing population have necessitated building in low-level polders (Verhagen, 1998).

The composition of the dike core and base depends on the properties of the different types of soil. Sand is very stable, but also permeable. Peat, on the other hand, is impermeable but can be easily compressed due to its high amount of organic matter. Also, the volumetric weight of peat decreases when it becomes dry affecting the stability. Clay is very impermeable, however easily deforms when it gets wet (Jonkman, 2014).

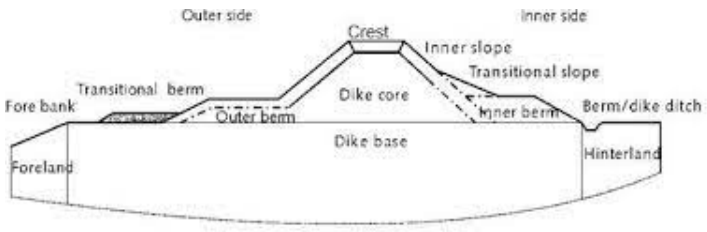

Figure 2.5: General dike profile with the most important elements of a dike (Jonkman, 2014)

2.4. Soil moisture and dike stability

Dike stability is defined by the shear resistance of the soil masses which is the resistance to failure. The stability of a slope depends on the ratio between shear strength and shear stress, which can be expressed in terms of the factor of safety. Stability is strongly influenced by its water content as it changes its weight and strength. Low soil moisture values induced by droughts can lead to reduce shear strength and consequently decrease the stability of dikes (Jamalinia et al., 2020). On the other hand, excessive soil moisture may soften soils, weaken shear strength, and also decreases dike stability.

2.4.1. Drought-sensitive dikes

The core of dikes is usually made of materials that are locally available. Of the 10,000 kilometers of regional dikes in the Netherlands, 3000 km are peat dikes. Dikes are often made out of a mixture of peat and clay. The sensitivity of dikes to drought depends on the amount of organic substances which are present in the clay and peat layers.

During drought, both peat and clay soils suffer from water loss because of the high evapotranspiration (van Haastregt, 2012). Peat consists of a higher amount of organic material than clay, which has a high hydraulic conductivity due to its porous nature. Therefore the weight and volume tend to decrease upon drying (Wong et al., 2008). Therefore, the volumetric weight of peat is much lower than that of other soils and has a higher risk of being pushed aside by water pressure than sand or clay dikes. After periods of dryness, the volumetric weight of peat decreases, affecting the stability and possibly even leading to failure of a dike (Baars, 2004). In August 2003 the peat dike in Wilnis failed after a very dry and warm summer, causing significant damage.

2.4.2. Risks imposed by drought

Drought in dikes can cause failure in several ways. In Wilnis, failure occurred due to the reduction in volumetric weight (Baars, 2004). The specific weight of peat is smaller than the amount of water. Wet peat contains large amounts of water (up to 80% or 90%). When the peat dries out in a dry summer, the specific weight drops significantly, causing the density of peat to be lighter than that of water. This can eventually lead to the peaty soil to float upon the body of water, resulting in the sliding of the soil downwards. This only happens when the body of the dike completely runs out of water and thus there are no cohesive forces between the soil particles and the water inside a dike (Chotkan, 2021).

During intense periods of drought, cracks can be observed in peat and clay dikes. High evapotranspiration and low precipitation rates can cause dry soil with low soil moisture which leads to shrinkage. Shrinkage leads to cracking and reduces shear strength, consequently decreasing the stability of dikes (Jamalinia et al., 2020).

Cracks with an orientation perpendicular to the dike are less dangerous than cracks with a longitudinal orientation (van Haastregt, 2012). Cracks with an orientation perpendicular to the dike may cause contact between the piezometric head on both sides of the dike. This leads to a flow from high to low head. When there are extreme precipitation events, preferential flow can generate friction leading to micro instability of the slope (Nimmo, 2020) (Vorogushyn et al., 2009). Due to the flow of water, pore pressure increases which could lead to the reduction of effective stress as total pressure is the sum of pore pressure and effective stress, which remains constant. Reduction in effective stress leads to a reduction in shear strength (Van Baars and Van Kempen, 2009).

2.5. Soil moisture and vegetation interaction

Water in the unsaturated zone is referred to as soil moisture and forms the link between surface and subsurface processes. The unsaturated zone contains air, water and solids. The volumetric soil moisture content is expressed in volumetric water content (θ) and is the ratio of total water volume and total soil volume.

$$\theta = \frac{Volume of water}{Total soil volume} [m^3 m^{-3}] \tag{2.2}$$

The amount of soil moisture in the unsaturated zone depends on multiple factors. Precipitation, interception, evapotranspiration, soil properties, type of vegetation, etc. are all factors that affect soil moisture. Vegetation meets their water requirement from the water available in the root-zone. However, when the amount of water in the root-zone reaches field capacity, the excess water drains to the lower layers of the ground. Field capacity is the maximum amount of water that can be held in the root-zone. Runoff takes place when excess water can not

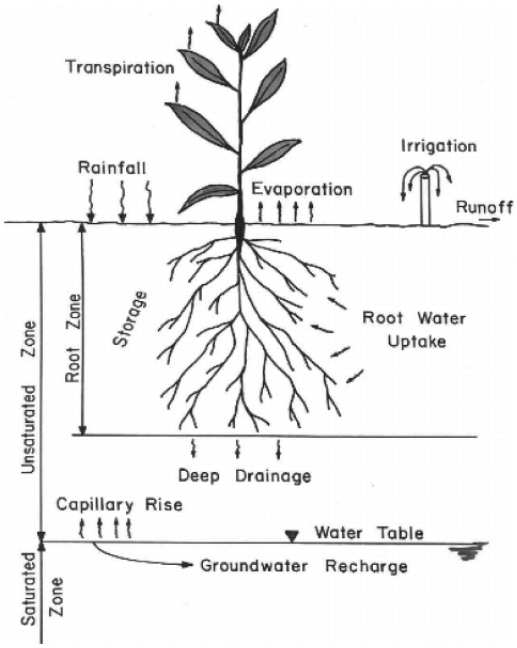

Figure 2.6: A schematic of the root-zone, unsaturated zone and the saturated zone (Šimnek and van Genuchten, 2016)

sufficiently rapidly infiltrate in the soil because the maximum drainage rate is reached (Jamalinia et al., 2019). Surface soil moisture is the water that is in the upper 10 cm of the soil, whereas root-zone soil moisture is the water that is available to plants (USG, 2021).

2.5.1. Droughts

Agricultural drought, defined based on soil moisture availability in the root-zone, strongly affects vegetation health as soil moisture deficits lead to drought stress on plants. Precipitation is the main source of soil moisture and therefore agricultural drought is driven by meteorological drought, which is defined as a shortage of precipitation over a region for a particular duration (Mishra and Singh, 2010). Drought stress on plants occurs when the available soil moisture is lowered to a point such that plants cannot absorb water rapidly enough to replace that lost to the air by transpiration. When soil is very dry, moisture moves very slow which means that water would be lost at the surface by evaporation.

Soil moisture is a good proxy for drought as it reflects recent precipitation and antecedent conditions and can therefore give an indication of agricultural potential and available water storage. The amount of water in the top layers of the soil is correlated with short-term precipitation and can therefore give an indication of meteorological drought. The soil moisture in the root-zone is a key factor of vegetation productivity through the availability of water for transpiration and a direct proxy for agricultural drought. The deeper soil layers are impacted by long-term or hydrological drought as it takes time before any impact in components of the hydrological system (groundwater, streams etc.) are noticed (Sheffield et al., 2004). Hydrological droughts are therefore out of phase with meteorological and agricultural droughts (Wilhite, 2000).

Water repellency can have a large effect in relatively dry soils as infiltration rates of water repellent soils are considerably lower than those in wettable soils. Repellency of soil is strongly related to the amount of organic matter. A high amount of hydrophobic organic compounds in combination with a low soil moisture content leads to a high water repellency (Mao et al., 2019). Regional grass-covered dikes with a core of clay and peat are sensitive to drought and are difficult to wet after a prolonged dry period. The soil is water repellent when it is dry and a major proportion of the water from precipitation may flow rapidly through cracks towards the subsoil, bypassing the layer of peat. This can lead to irregular wetting partners with high variability in topsoil moisture content throughout a layer. As precipitation increases and the soil becomes wetter, infiltration proceeds eventually breaking through the water repellent layer (Dekker and Ritsema, 2000). Droughts can interrupt water infiltration and may therefore decline vegetation growth.

3

Study sites and data description

In the previous chapter background information was provided on remote sensing, the effect of soil moisture on dike stability, and the interaction between soil moisture and vegetation. In this chapter, the study area is introduced. The main part of the research was conducted for two study sites are two grass-covered regional dikes and one grass-covered sea dike in the Netherlands. Furthermore, descriptions of the different remote sensing satellites and ground truth data used in this research are provided.

3.1. Study sites

3.1.1. Grass-covered regional dikes

As mentioned earlier in this thesis, the research is focused on investigating if remote sensing data can be used as a soil moisture indicator of grass-covered dikes. Two grass-covered regional dikes were chosen as study sites, which are both located in the Netherlands. Both dikes are selected because it is reported by the local authorities to be drought sensitive. The core of both dikes consists of a mixture of peat and clay.

The first study site is located in the Geer- en Blankaardpolder (referred to as Geerweg) near Zoeterwoude in the Netherlands and is managed by the Waterboard Rijnland. The dike section is about 55 meters wide with a gentle slope of 1:18. The soil is predominately clay and peat and is covered with grass. The second study site is located at the Bermweg near Rotterdam in the Netherlands and is managed by the Waterboard Schieland en Krimpenwaard. The dike section is about 40 meters wide and has a slope of 1:16. Also, the core of this dike is predominantly clay and peat with a layer of grass on top. Both dikes have ditches on the sides. Figure 3.1 shows a cross-section of the dike at both locations. In-situ soil moisture sensors are located at these study sites and measurements are available since April 2020.

Both dikes are predominantly covered by grass vegetation. Figure 3.2 shows pictures of the two regional grass-covered dikes. The grass-cover at location Bermweg is solely maintained by grazing horses and is not mown. At location Geerweg the grass-covered is maintained by both grazing cattle and mowing. At both locations, a wild life camera is installed which makes photos three times a day. At location Bermweg photos are available since April 2020 and at location Geerweg since May 2021. Photos at location Geerweg show that the grass was mown during June 7th and July 16th 2021.

3.1.2. Grass-covered river dike

The grass-covered river dike which is chosen as a study site is located near Wijk bij Duurstede, the Netherlands. This river dike is a barrier used to regulate or hold back water from the Amsterdam-Rhine canal. No in-situ soil moisture measurements are available for this study site. However, there is an area on the inner slope of the dike which experienced wetting from 2017 up until July 2020 (A. Lievens, personal communication, 14th of April, 2021). Especially during high water periods, one would stand in ankle-deep water. The wet area was caused by a clogged drainage system. A drainage system was installed to discharge water in a controlled manner through the levee to overcome potential seepage problems and promote dike stability. However, due to clogging of the drainage system, problems did occur. In 2020 a reinforcement has taken place and new drainage pipes were installed. The core of the dike consists of different materials such as clay, sand, and peat but is predominantly

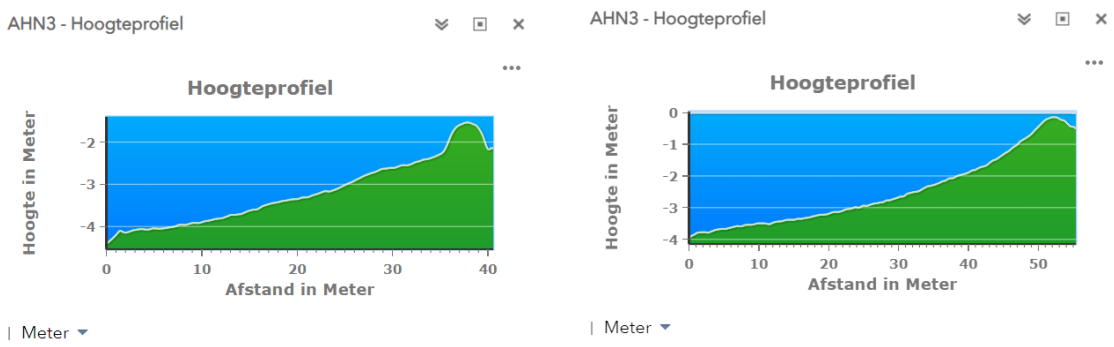

Figure 3.1: Cross-section of the grass-covered regional dike at location Bermweg (left) and location Geerweg (right).

Figure 3.2: Picture of the in-situ soil moisture sensors at a) location Geerweg and b) location Bermweg.

clay (information retrieved from DINOloket). The dike of the base is sand. The dike is managed by Rijkswaterstaat and is about 60 meters wide with a road on a part of the dike which starts at 50 meters (see figure 3.3). Compared to the regional dikes, the slope of this dike is much steeper. The dike has a 1:3 inner slope and a 1:3.5 outer slope.

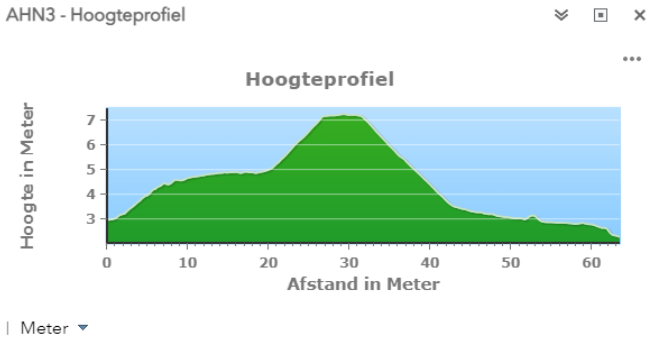

Figure 3.3: Cross-section of the grass-covered river dike at the Amsterdam-Rhine canal.

Figure 3.4 gives an overview of the geographical locations of the study sites.

3.2. Data

The data used in this study include (1) in-situ soil moisture measurements, (2) precipitation deficit data, (3) optical remote sensing data and (4) SAR remote sensing data.

3.2.1. In-situ soil moisture measurements

To investigate if vegetation indices and SAR backscatter obtained from remote sensing data can be used as a proxy for soil moisture in dikes, ground truth data is needed. On the grass-covered regional dikes, in-situ soil moisture measurements are compiled since the beginning of April 2020. On each study site Teros 12 sensors

Figure 3.4: Geographical locations of the study sites.

were placed over the cross-sections of the dike which among other things measures the soil moisture content. Figure 3.5 gives an overview of the two regional grass-covered dikes and the locations of the soil moisture sensors. The Teros 12 sensors use an electromagnetic field to measure the dielectric permittivity of the soil, an electrical property that is highly dependent on the soil moisture content. At location Bermweg there are five soil moisture sensors and at location Geer- en Blankaardpolder four. At location Geerweg no soil moisture measurements are available at the toe of the dike. Depending on the location, sensors provide volumetric soil moisture measurements (m^3/m^3) over depths of 20, 50, 75 and 120 centimeter. Measurements are collected every hour. The locations of the sensors are shown in figure 3.6. The sensors are located relatively close to each other. Only the soil moisture measurements data at a depth 20 cm are used in this research as it is assumed that the majority of the root system is in the top layer of 0-40 cm below the soil surface (Jamalinia et al., 2019). The soil properties of the locations where the different sensors are situated can be found in Appendix A.

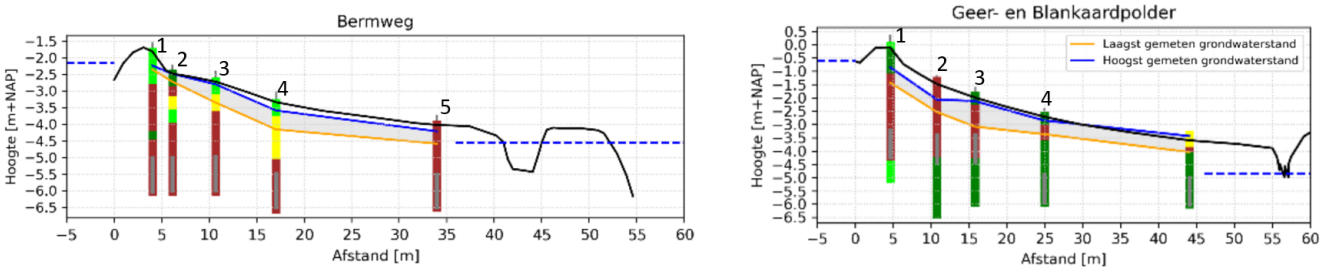

Figure 3.5: Locations of soil moisture sensors at location Bermweg and Geerweg (retrieved from (Strijker, 2021)).

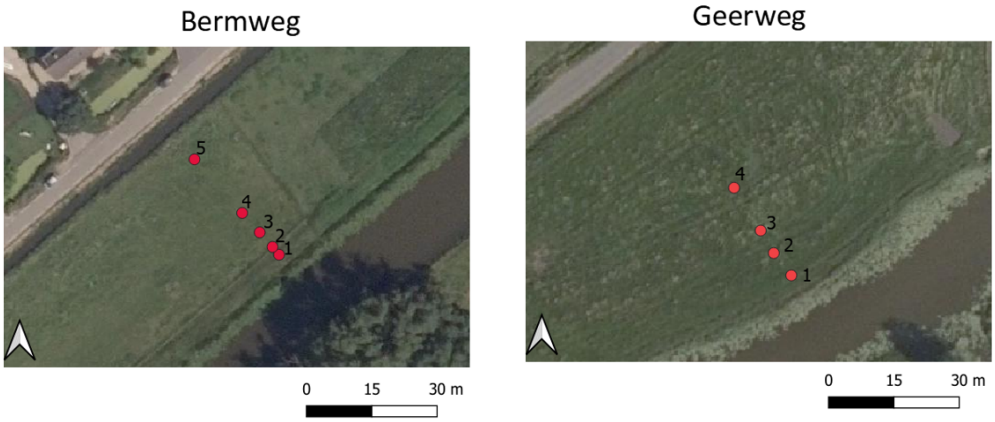

Figure 3.6: Overview of locations of the in-situ soil moisture sensors at location Bermweg and Geerweg.

Figure 3.7 illustrates the soil moisture time series at both study locations at 20 and 50 cm depth. The summer of

2020 is in the top 10 driest years ever recorded in the Netherlands when a maximum precipitation deficit of 253 mm was reached. Precipitation deficits in the Netherlands even exceeded those of 2018 throughout the early summer season (Peters et al., 2020). The effect can be clearly seen in the soil moisture time series of 20 cm depth at both locations. The soil moisture retrieved from sensor 5 at location Bermweg is close to the toe of the dike, where a ditch is located. The groundwater table is relatively high throughout the year due to the geometry of the dike. The soil moisture values are constant throughout the year, which shows that the sensor mainly measures in the saturated zone. Sensors 1 to 4 show a variation in soil moisture at 20 cm depth. At location Bermweg, the soil moisture pattern is quite similar for all sensors. The sensors respond similarly as the soil moisture content is mainly influenced by precipitation and evapotranspiration. At deeper layers, soil moisture changes more slowly. At location Bermweg measurements from a depth of 50 cm show little fluctuations, with the exception of location 1 where short peaks due to rainfall can be seen. The more constant soil moisture trend is because the measurements at 50 cm depth are located closer to the saturated zone. Due to the geometry of the dike, sensor 1 is located furthest away from the groundwater table. Therefore the effect of precipitation can be clearly seen for sensor 1 at 50 cm depth. The top layer responds more quickly to precipitation and droughts than deeper layers. Therefore, the drought in 2020 cannot be observed by the sensors at 50 cm depth, where the soil moisture measurements remain relatively stable. It is interesting to see that soil moisture values measured at 20 cm depth are sometimes higher than at 50 cm depth (i.e. location 3). This could be because the subsoil and porosity is different at 20 and 50 cm depth (Strijker, 2021).

It is interesting to see that at location Geerweg, soil moisture retrieved from sensors 1-4 at 20 cm depth shows a different behaviour during the dry period in 2020. The soil moisture pattern of sensors 3 and 4 is significantly different from sensors 1 and 2. The sensors at locations 3 and 4 do not respond to the rainfall after the dry period in July 2020. This could be due to the difference in subsoil (see Appendix A). When a certain soil moisture threshold is reached in November 2020, sensors 3 and 4 suddenly do respond to precipitation. The difference in behaviour clearly shows that soil moisture content can vary locally. As the subsoil is sensitive to drought and is difficult to wet after a prolonged dry period, preferential flow paths can occur during dry periods which could explain the behavioural difference.

Overall, at 20 cm depth, soil moisture is much more dynamic as it is mainly influenced by precipitation and evapotranspiration whereas, at deeper layers, soil moisture changes more slowly. Graph 3.8 shows the effect of precipitation on the soil moisture time series at 20 cm depth.

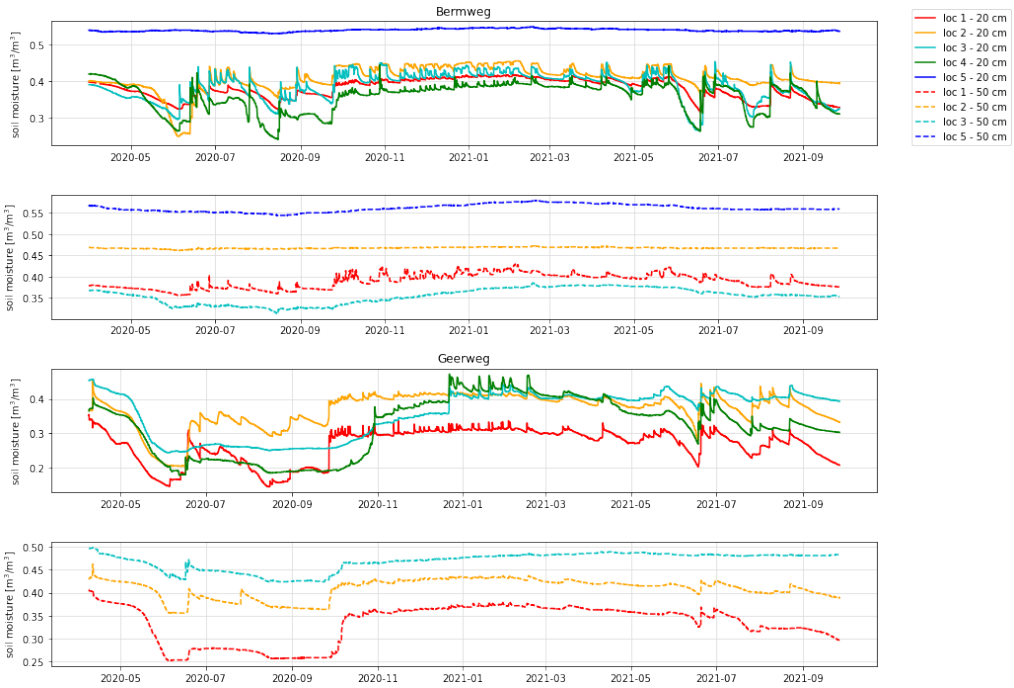

Figure 3.7: Time series of soil moisture for sensors at 20 cm and 50 cm depth at location Bermweg and Geerweg from April 2020 up until September 2021.

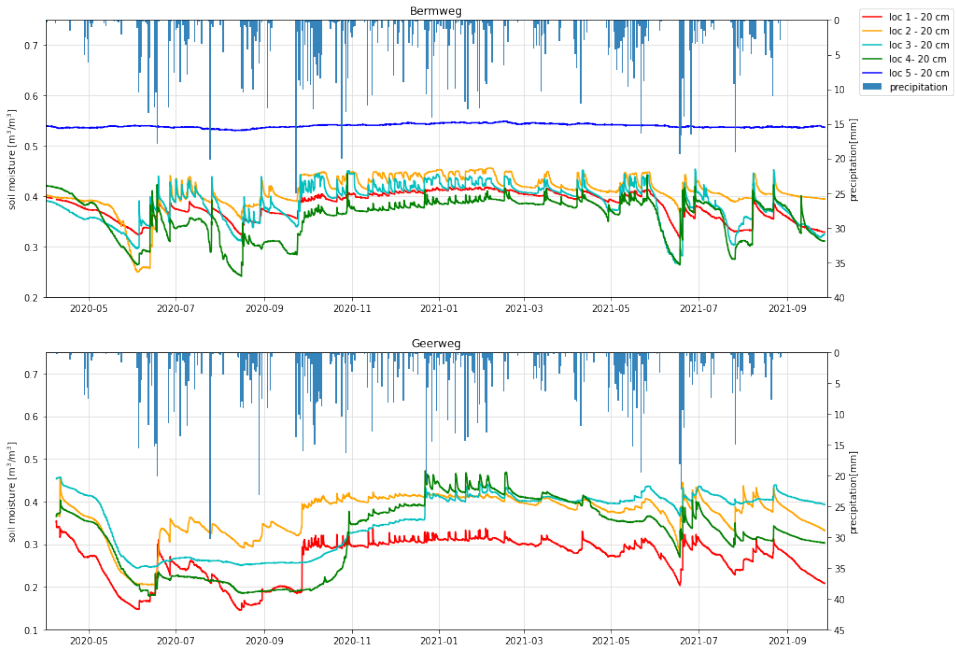

Figure 3.8: Time series of soil moisture at 20 cm depth and cumulative daily precipitation at location Bermweg and Geerweg between April 2020 and July 2021.

3.2.2. Precipitation deficit

Precipitation deficit is defined as the difference between precipitation and evapotranspiration and can give a proxy for soil moisture as a decrease of soil moisture content occurs when the outflux of water is bigger than the influx. To analyze if there is a relationship between precipitation deficit and vegetation indices obtained from optical remote sensing imagery, precipitation deficit data needs to be obtained. In order to calculate the precipitation deficit, precipitation and evapotranspiration data are needed.

Meteobase is a third party that distributes free precipitation and evapotranspiration raster data over the Netherlands. The raster data contains grid cells of 1 km^2 where each pixel is associated with a specific geographical location. The data is retrieved using satellite data after which the KNMI stations are used to calibrate the data (Versteeg et al., 2013). The data is delivered as ASCII files. Figure 3.9 displays a plotted ASCII file. The precipitation time series contains hourly values whereas the evaporation data set contains daily values. The precipitation deficit time series can be obtained by subtracting the daily evapotranspiration values from the daily precipitation values.

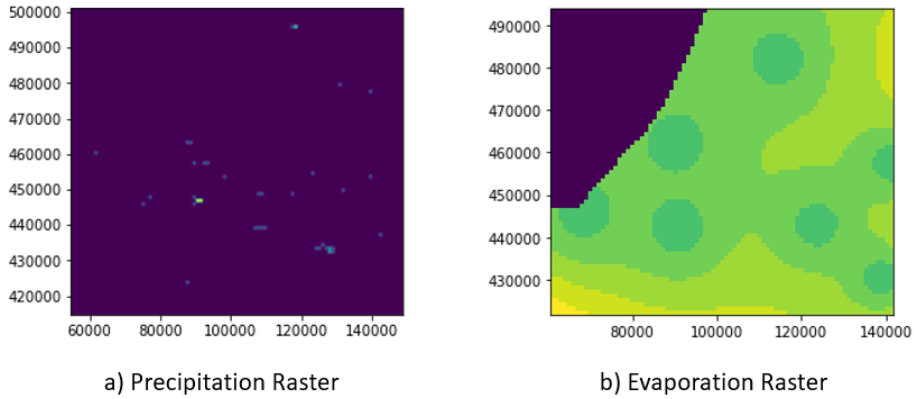

Figure 3.9: Plot of a raster file retrieved from Meteobase. The x and y axis shows the x and y coordinates. Both rasters display January 1st, 2020. No color bar is given, however, values are in millimeters.

3.2.3. Optical remote sensing data

Optical satellite imagery is obtained from satellite missions Sentinel-2, Landsat 7 and Landsat 8. For optical satellite imagery, Bottom of the Atmosphere (BOA) data, also called surface reflectance, will be used. Top of the Atmosphere (TOA) reflectance values represent the "raw" reflectance of the earth as measured from space whereas Bottom of the Atmosphere (BOA) represents the actual reflectance of the areas on the surface of the earth. The BOA values are calculated by eliminating the effect of the atmosphere on the reflectance values. Atmospheric correction is an important step as variations can be introduced due to atmospheric effects, absorption and scattering. The visible and near infrared region of the electromagnetic spectrum are largely affected by atmospheric variations (Bannari et al., 1995).

Sentinel-2

The Sentinel-2 mission consists of two identical satellites. The twin satellites fly in the same orbit but are phased at 180 degrees, allowing a high revisit time of five days. The satellites have a Multispectral Instrument (MSI), a passive sensor, which is based on the push-broom concept. A push-broom sensor works by collecting rows of image data across the entire image swath at once. The MSI samples thirteen spectral bands spanning from the visible (VSI) and the near infra-red to the short wave infra-red (ESA, 2021b). Four bands have a spatial resolution of 10-meter, six bands a 20-meter resolution and three a 60-meter resolution. Table 3.1 gives an overview of the different spectral bands and the spatial resolution for the two satellites Sentinel-2A and Sentinel-2B (ESA, 2021e).

Sentinel-2 MSI		
Band	**Spatial resolution (m)**	**Spectral range (μm)**
1 - Aerosols	60	0.433 - 0.453
2 - Blue	10	0.458 - 0.523
3 - Green	10	0.543 - 0.578
4 - Red	10	0.650 - 0.680
5 - Red Edge 1	20	0.698 - 0.713
6 - Red Edge 2	20	0.733 - 0.748
7 - Red Edge 3	20	0.773 0.793
8 - Near Infrared (NIR)	10	0.785 - 0.900
8a - Near Infrred narrow (NIRn)	10	0.855 - 0.875
9 - Water vapor	60	0.935 - 0.955
10 - Short Wavelengh Infrared - Cirrus	60	1.360 - 1.390
11 - Short Wavelength Infrared (SWIR1)	20	1.565 - 1.655
12 - Short Wavelength Infrared (SWIR2)	20	2.100 - 2.280

Table 3.1: Sentinel-2 MSI spatial and spectral band resolutions (ESA, 2021b).

From the Sentinel-2 mission level 2A data will be downloaded. The level 2A data is pre-processed by performing two tasks. First of all, scene classification provides a pixel classification map and eventually atmospheric correction transforms top-of-atmosphere reflectance into bottom-of-atmosphere reflectance (ESA, 2021a). The images contain 13 spectral bands in the visible, near infrared and short-wave infrared, several L2-specific bands and 3 QA bands, of which one is a bitmask band with cloud information. The resolution of the visible bands and near infrared band is 30 meters. The cloud mask band has a resolution of 60 meters.

Landsat 7/8

The Landsat 7 mission carries the Enhanced Thermatic Mapper (ETM+) passive sensor and orbits the earth with a sixteen day repeat cycle. The ETM+ sensor is based on the whisk-broom concept. The detector sweeps back and forth as they collect data across the image swath. The ETM+ samples eight multispectral bands in the visible to near infra-red, short-wave infrared and long wave infra-red. Landsat 7 has eight spectral bands of which six bands have a spatial resolution of 30-meter, one panchromatic band at 15-meter resolution, and one thermal band at 60-meter resolution. In May 2003 the ETM+ instrument of Landsat 7 failed which leads to a scan line in the satellite imagery.

The Landsat 8 satellite carries two passive sensors: the Operational Land Imagery (OLI) and the Thermal Infrared

Sensor (TIRS). Like Landsat 7, the sensors are based on the whisk-broom concept and covers the entire earth in sixteen days. The OLI collects eight bands within the visible, near infrared and short wave infrared spectral which have a spatial resolution of 30-meter. It measures one panchromatic band, which is at 15-meter resolution. The TIRS samples two additional thermal infrared bands at 30-meter resolution (NASA, 2021a). The spectral and spatial details of Landsat 7 and 8 can be found in table 3.2 and 3.3.

Landsat 7 ETM+		
Band	**Spatial resolution (m)**	**Spectral range (μm)**
1 - Blue	30	0.450 - 0.515
2 - Green	30	0.525 - 0.605
3 - Red	30	0.630 - 0.690
4 - Near Infared (NIR)	30	0.775 - 0.900
5 - Short Wavelength Infrared (SWIR)	30	1.550 - 1.750
6 - Thermal infrared	60	10.40 - 12.50
7 - Short Wavelength Infrared (SWIR)	30	2.090 - 2.350
8 - Panchromatic	15	0.520 - 0.900

Table 3.2: Landsat 7 ETM+ spatial and spectral band resolutions (NASA, 2021b).

Landsat 8 OLI + TIRS		
Band	**Spatial resolution (m)**	**Spectral range (μm)**
1 - Coastal Aerosols	30	0.433 - 0.453
2 - Blue	30	0.450 - 0.515
3 - Green	30	0.525 - 0.600
4 - Red	30	0.630 - 0.680
5 - Near Infrared (NIR)	30	0.845 - 0. 885
6 - Short Wavelength Infrared (SWIR)	30	1.560 - 1.660
7 - Short Wavelength Infrared (SWIR)	30	2.100 - 2.300
8 - Panchromatic	15	0.500 - 0.680
9 - Cirrus	30	1.360 - 1.390
10 - Thermal Infrared	100	10.30 - 11.30
11 - Thermal Infrared	100	11.50 - 12.50

Table 3.3: Landsat 8 OLI and TIRS spatial and spectral band resolutions (NASA, 2021b).

USGS Landsat 7 and 8 Surface Reflectance Tier 1 data sets will be acquired, which is the atmospherically corrected surface reflectance from the Landsat 7 and 8 sensors. The Tier 1 collection meets the geometric and radiometric quality requirements and Tier 2 does not meet these requirements (Engine, 2007). These data have been atmospherically corrected and contain a quality assessment (QA) band which represents a bit-packed combination of surface, atmospheric and sensor conditions.

3.2.4. SAR remote sensing data

To obtain SAR backscatter information, SAR satellite imagery is obtained from the Sentinel-1 satellite mission.

Sentinel-1

The Sentinel-1 mission consists of two single C-band (5.404 GHz) polar-orbiting satellites (Sentinel-1A and Sentinel-B) which share the same orbital plane. They were launched in 2014 and 2015, respectively, and both carry a Synthetic-aperture radar (SAR) instrument which is an active sensor. SAR can obtain imagery during day and night and has the capability to penetrate through cloud cover and most weather conditions. The radar can operate in four modes: Stripmap (SM), Interferometric Wide swath (IW), Wave (WV) and Extra-Wide swath (EW). The spatial resolution depends on the mode: 5-by-5 meters for SM mode, 5-by-20 meters for IW and WV, and 25-by-100 meter for EW mode. The revisit time of Sentinel-1 depends on the latitude and therefore varies globally. The revisit time over the Netherlands is one to two days and the default acquisition mode over land in Europe is the IW mode that provides dual polarization (VV + VH) data (Torres et al., 2012). Dual polarization

means that it receives pulses in both a horizontal and vertical orientation. As a result, the returning frequencies provide measurements of the horizontal and vertical dimensions of targets, supplying better estimates of the size, shape, and variety of targets. Table 3.4 presents a description of the Interferometic Wide swath (IW) mode.

Sentinel-1 - Interferometic Wide swath (IW) mode	
Characteristic	**Value**
Swath width	250 km
Spatial resolution	5 m x 20 m
Incidence angle range	29.1 - 46.0
sub-swaths	3
Azimuth steering angle	+- 0.6
polarization options	Dual HH+HV, VV+VH Single HH, VV
Maximum Nosie Equivalent Sigma Zero (NESZ)	-22 dB

Table 3.4: Characteristics of Interferometric Wide swath mode (ESA, 2021d).

The Sentinel-1 product which is provided by Google Earth Engine is the Sentinel-1 SAR Ground Rage Detected (GRD) image collection. This is already pre-processed with the Sentinel-1 Toolbox using the following steps: thermal noise removal, radiometric calibration and terrain correction and has a spatial resolution of 10x10 meters. A SAR signal contains amplitude and phase information. The GRD image collection only contains amplitude information, which is the strength of the radar signal. The revisit time of the study sites is 2-4 days.

4

Methodology

In the previous chapter, the study areas were introduced and a description was given of the data used in this research. This chapter describes the methods used in this research to answer the research question: “How can remote sensing data give insight into soil moisture and contribute to dike inspections on grass-covered dikes?".

4.1. General approach

Figure 4.1 gives an overview of the methodology of this thesis. This research follows a step-by-step approach that starts with the preparation of the remote sensing data, which includes downloading and pre-processing. Then, vegetation indices were computed for the optical imagery and SAR features were extracted for the SAR imagery. After that, it was investigated if there is a relationship between the retrieved parameters and in-situ soil moisture measurements. Furthermore, it was analyzed if there is a relationship between precipitation deficit and vegetation indices, assuming precipitation deficit can give a proxy for soil moisture. Finally, it was explored if temporal-spatial variations in soil moisture can be detected by SAR backscatter and vegetation indices. The results will give insight if data retrieved from satellites can give a proxy for soil moisture and thus contribute to dike inspections.

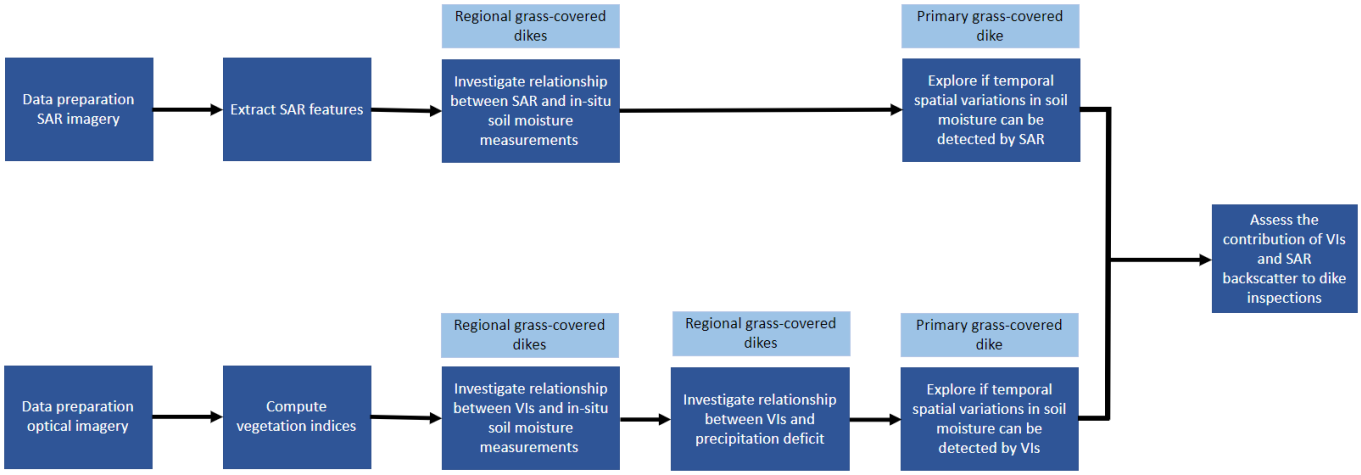

Figure 4.1: Schematic overview of the methodology of this research.

4.2. Remote sensing as a proxy for soil moisture

Figure 4.2 gives a schematic overview of the methodology of this thesis. The goal is to investigate if remote sensing data can give a proxy for soil moisture in grass-covered dikes. This is investigated using two types of

remotely sensed data: optical data and SAR data. Furthermore, two different data sources are used which can give an indication of soil moisture within a dike. First of all, soil moisture measurements are retrieved from in-situ soil moisture sensors on two regional grass-covered dikes. Secondly, precipitation deficit, defined as the difference between precipitation and evapotranspiration, is taken into account as it can give a proxy for soil moisture.

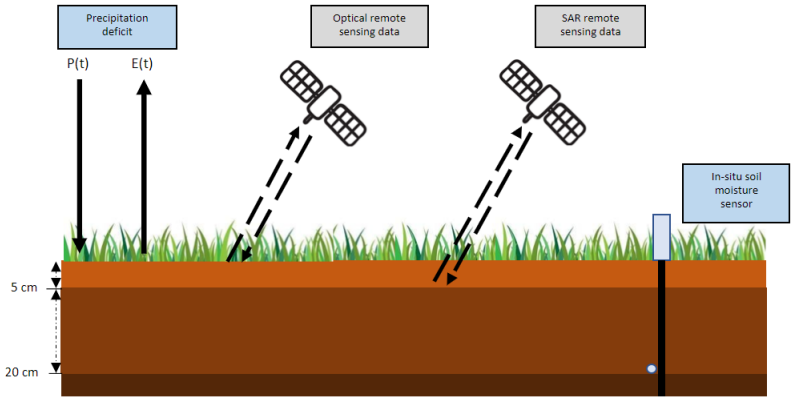

Figure 4.2: Schematic overview of the methodology of this thesis.

4.2.1. Optical remote sensing imagery

It has been widely demonstrated in literature that vegetation indices are more or less related to root-zone soil moisture and that there is always a time lag in which vegetation responds to soil moisture (Wang et al. (2007), Musyimi (2011), Zhang et al. (2018), Zhang et al. (2011) and Buitink et al. (2020)). As root-zone soil moisture is a key factor in vegetation health, vegetation indices could give an indication of soil moisture within a dike. The study considers perennial ryegrass as its grass cover, which has the majority of its root system in the top layer of 0-40 cm below the soil surface. Most grass-covered regional dikes in the Netherlands are mainly covered by ryegrass, likewise the grass-covered dikes in this research.

Vegetation absorbs radiation in different bands and reflects a different percentage of it back to the sensor. The percentage of reflected radiation in specific bands, such as blue, green, red, near infrared (NIR) and short wave infrared (SWIR) varies with plant health. The photosynthetic process absorbs most of the visible light and reflects much in the NIR region. The SWIR band can be used for soil moisture detection. As vegetation health is influenced by water stress, vegetation indices could give an indication of soil moisture. An example of a spectral reflectance curve that distinguishes healthy and unhealthy vegetation by the difference in reflectance pattern can be seen in figure 4.3.

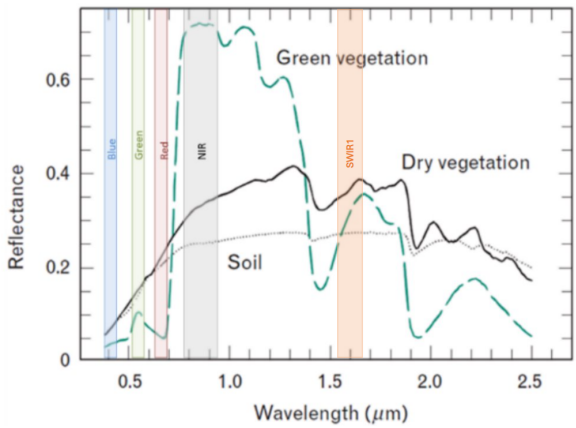

Figure 4.3: Spectral reflectance curve of healthy green vegetation and dry vegetation (retrieved and edited from Didan et al. (2015)). The visible, NIR and SWIR wavelengths are marked.

Vegetation indices were calculated to examine if there was a relationship between soil moisture and vegetation indices obtained from optical remote sensing data. Five different vegetation indices were used: the Green/Red ratio (GRR), Ratio Vegetation Index (RVI), Modified Simple Ratio (MSR), Normalized Difference Vegetation Index (NDVI) and Normalized Normalised Difference Infrared Index (NDII). The first three vegetation indices were selected as they were recommended by Cundill et al. (2014) after testing a large number of indices for the potential use of vegetation indices as a proxy for soil moisture. As the NDVI is the most frequently used spectral vegetation index, this vegetation index was also taken into account. Furthermore, the Normalised Difference Infrared Index (NDII) has been proven to be able to provide a proxy for soil moisture in the root-zone and will therefore also be taken into account (Sriwongsitanon et al., 2015). The vegetation indices which were selected in this study are calculated by the following equations:

$$GRR = \frac{R_{green}}{R_{red}} \tag{4.1}$$

$$RVI = \frac{R_{NIR}}{R_{red}} \tag{4.2}$$

$$MSR = \frac{(\frac{R_{NIR}}{R_{Red}}) - 1}{\sqrt{(\frac{R_{NIR}}{R_{red}})} + 1} \tag{4.3}$$

$$NDVI = \frac{R_{NIR} - R_{red}}{R_{NIR} + R_{red}} \tag{4.4}$$

$$NDII = \frac{R_{SWIR} - R_{NIR}}{R_{SWIR} + R_{NIR}} \tag{4.5}$$

Where R stands for the reflectance value of the specified band. The GRR is used for estimating the greenness of vegetation so it could give an indication of areas affected by long-term shortage of soil moisture (Kanemasu, 1974). Decreasing plant water content results in a greater proportional increase in red reflectance than in green (Carter, 1993). The RVI, MSR and NDVI use the NIR and red band (Jordan (1969), Chen (1996), Carlson and Ripley (1997)). Healthy vegetation strongly reflects NIR and absorbs red light. A higher RVI, therefore, indicates healthier vegetation. The MSR was developed as an improvement over the RVI by combining the simple ratio into the formula. This results in increased sensitivity to vegetation biophysical parameters. The NDVI also uses the NIR and red bands and generates a value between -1 and +1. The NDII can be used to detect plant water stress as solar radiation in the SWIR band is absorbed by liquid water (Hunt Jr and Rock, 1989). Therefore, the reflectance is strongly correlated with root-zone soil moisture. Various studies have demonstrated that there is a strong relationship between vegetation water content and indices based on the NIR and SWIR domain (Datt (1999), Ceccato et al. (2001), Ceccato et al. (2001)). The NDII increases with increasing water content. A combination of SWIR (1645 μm) and NIR is utilized as the NIR is influenced by leaf structure and dry matter, which consequently also influences the SWIR reflectance. Including the NIR can remove this effect (Sriwongsitanon et al., 2015).

4.2.2. SAR remote sensing imagery

The strength of the SAR backscatter signal is directly related to the dielectric constant, which is an important parameter for the study of soil moisture. The dielectric constant of a material is a measure of its electric properties. It consists of two parts (permittivity and conductivity) that are both highly dependent on the moisture content of the material considered. In the microwave region of the electromagnetic spectrum, water has a very high dielectric constant which is at least ten times higher than that for dry soil. A significant change in soil moisture leads to a change in dielectric constant which causes a change in radar backscatter. Therefore, increasing soil moisture results in an increase in backscatter (ESA, 2021c). SAR uses the C-band portion of the spectrum and can therefore penetrate up to 5 cm deep below the soil surface. Furthermore, a study by Jamalinia et al. (2019) investigated how soil-vegetation-atmosphere interaction influences the stability of grass-covered dikes. Results show that there is a lagged correlation between the leaf area index (LAI) and the water root-zone content. As research has shown that there is a strong correlation between backscatter intensity and LAI, SAR backscatter

could give an indirect proxy for soil moisture (Steele-Dunne et al., 2017). The LAI is particularly sensitive to the cross-ratio (VH/VV) (Vreugdenhil et al., 2018).

4.3. Data preparation

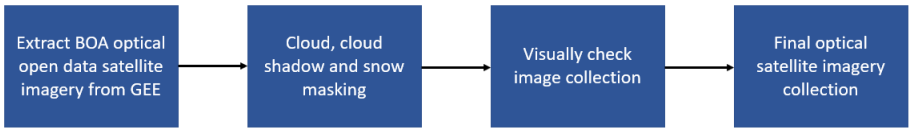

Figure 4.4: Schematic overview of the optical imagery data preparation steps.

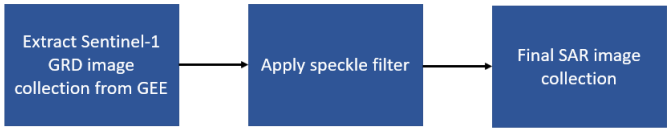

Figure 4.5: Schematic overview of the SAR imagery data preparation steps.

4.3.1. Downloading

To process the satellite imagery retrieved from the different open data satellite missions, a platform is needed to process and analyze this data. Google Earth Engine (GEE) is a cloud computing platform for remote sensing which was extensively used in this research. The main advantage of GEE over other well-known satellite imagery processing programs like QGIS or ArcGIS is that it is cloud-based whereas the other platforms work locally on your computer. This requires high storage space and is also very time-consuming since satellite imagery needs to be downloaded and processed on your computer. GEE, on the other hand, has very powerful servers, making it possible to quickly perform large computations (Amani et al., 2020).

All open-access satellite missions are already on the GEE servers, making them easy and quickly accessible. Satellite imagery from commercial satellite missions which are not available can be uploaded to the servers. Imagery from the different satellite missions used in the research is already available on the GEE servers.

4.3.2. Pre-processing
Optical satellite imagery

Figure 4.4 gives an overview of the pre-processing steps for the optical satellite imagery. Optical satellite sensors cannot penetrate through cloud covers. Cloud contamination is therefore an inevitable problem in optical remote sensing imagery (Li et al., 2020). Hazy clouds and cloud shadows can introduce variations in sensing reflections from the ground and can result in non-representative data. Thick clouds can even block the view completely (Wang et al., 1999). Therefore, the optical imagery which is largely influenced by clouds needs to be filtered out. Furthermore, cloud shadows and snow can result in non-representative reflectance data. To filter out the images influenced by these factors, the acquired data was pre-processed to create a time series of reflectance values from all valid pixels. Pixels influenced by clouds, cloud shadows, and snow were masked out. As it was challenging to filter out all cloud and cloud shadow contaminated imagery, it was important to also visually check the image collection and filter out contaminated images if necessary. Figure 4.6 illustrates the importance of visually checking the image collection after cloud, cloud shadow and snow masking. It shows an example of an image where hazy clouds were not filtered out by the applied masks.

Landsat 7 and 8 The Landsat-7 and Landsat 8 Surface Reflectance Tier 1 data sets were used. Satellite mission Landsat 7 and 8 both contain a quality assessment (QA) band which represents a bit-packed combination of surface, atmospheric and sensor conditions. The L8 QA band contains 16-bit integers which represent certain conditions and is shown in figure 4.7. The double bits (5-6, 7-8, 9-10, 11-12) represent the levels of confidence that a condition exists. Landsat 7 contains such a similar QA band.

There are two bits that represent clouds and cloud shadows, which can be used to filter out images with cloudy conditions, resulting in an image collection with only cloud-free conditions. To filter out the days when snow

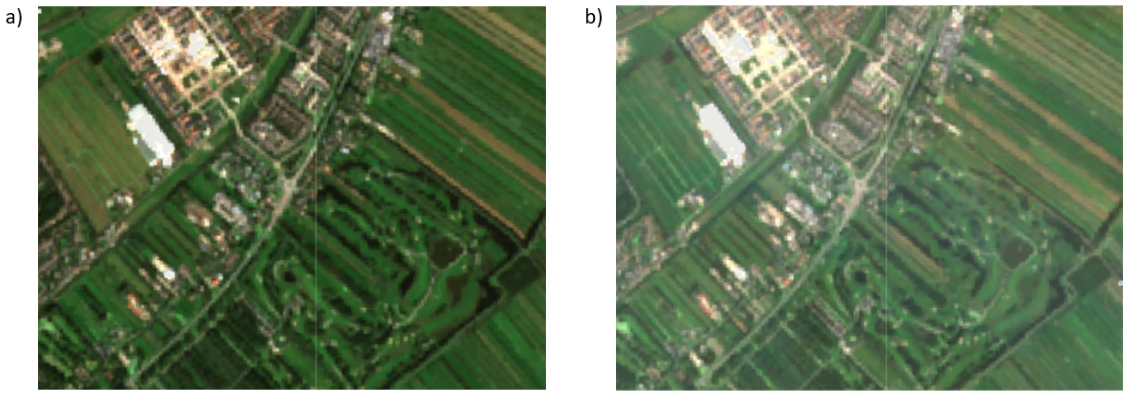

Figure 4.6: The left image a) is retrieved at location Bermweg on September 22nd, 2020 10:40:21 and b) at location Bermweg on the 8th of August 2020 10:56:43 by Sentinel-2. It shows that image b) is contaminated by a very thin cloud.

Landsat 8 OLI, OLI/TIRS Collection 1 QA band bits; Read from RIGHT to LEFT, starting with Bit 0																
Cumulative Sum																
	65553	32767	16383	8191	4095	2047	1023	511	255	127	63	31	15	7	3	1
BIT	15	14	13	12	11	10	9	8	7	6	5	4	3	2	1	0
Description				Cirrus Confidence		Snow/Ice Confidence		Cloud Shadow Confidence		Cloud Confidence		Cloud	Radiometric Saturation		Terrain Occlusion	Designated Fill

Figure 4.7: L8 QA band bits and their explanation (Pareeth et al., 2019).

has fallen, which gives non-representative reflectance data compared to days when there was no snow, the bit representing snow was also used. After applying these bits to filter out these conditions, there were still images containing cloud shadows. Therefore, an extra cloud shadow masking function was applied to the image collection. This function uses the sun elevation and sun azimuth angle to detect cloud shadows. After applying this extra shadow masking function, almost all images containing cloud shadows were masked out.

Sentinel-2

From the Sentinel-2 mission level 2A data was downloaded. Sentinel-2 has a special S2 cloud probability image collection which can be applied to easily identify clouds and shadows. This image collection was used to filter out clouds and their shadows. As this image collection does not filter out images when snow has fallen, a whiteness band was also added. The whiteness band adds up the red, green, and blue band reflectance values. A threshold was chosen for the whiteness band to mask out snow. Not all images contaminated by cloud shadows were filtered out and therefore an extra function was applied which uses the sun azimuth angle to identify cloud shadows.

SAR satellite imagery

Figure 4.5 gives an overview of the pre-processing steps for the SAR satellite imagery. A speckle filtering is an important step in pre-processing SAR images as they are inherently affected by speckle. Speckle is a granular noise, that degrades the quality of the SAR images. This is a result of the interference of waves reflected from many elementary scatters (Filipponi, 2019). Speckle noise affects SAR imagery and results in strong variations in pixels, whereas they have similar backscattering coefficients (Choi and Jeong, 2019). It decreases the radiometric quality of SAR images and makes it difficult to visually interpret the images. Therefore, it is important to use a speckle filter.

Sentinel-1

Imagery from the SAR Ground Rage Detected (GRD) image collection was downloaded. SAR can penetrate

through clouds due to its long wavelengths, enabling it to measure surface reflectance under all weather conditions. The image collection only contains information about the detected amplitude, the strength of the reflected signal. Phase information, which is the fraction of one complete sine wave cycle, was not available. To reduce speckle noise, a speckle filter was applied. The speckle filter used over the SAR imagery is the Refined Lee Filter as it is well-known for its ability to preserve prominent edges, linear features, point target and texture information (Qiu et al., 2004). The Refined Lee Filter uses the K-Nearest Neighbour (KNN) algorithm.

4.4. Vegetation indices as a proxy for soil moisture

An analysis was made to investigate if there is a potential lagged relationship between soil moisture and vegetation indices at two-grass covered regional dikes. A lag was taken into account as it is known that there is always a time lag in which vegetation health responds to soil moisture (Foody, 2003) (Zhang et al., 2011) (Jamalinia et al., 2019) (Buitink et al., 2020). In this research, a relationship was examined for vegetation indices retrieved from three different optical satellite missions: Landsat 7, Landsat 8 and Sentinel-2. In-situ soil moisture values at a depth of 20 cm were used as it was assumed that the majority of the root system is in the top 0-40 cm of the soil surface, and hence soil moisture at 20 cm depth can give a good representation of the soil moisture available to the vegetation. Figure 4.8 gives a schematic overview of the methodology used to examine this relationship. The study period was limited as in-situ soil moisture measurements were only available since April 2020.

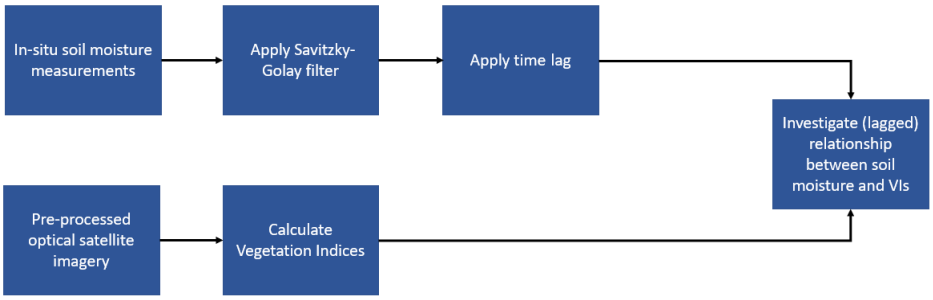

Figure 4.8: Schematic overview of the methodology used to explore the relationship between soil moisture and VIs.

Two main data sets were used: vegetation indices extracted from open data satellite missions and in-situ soil moisture measurements at 20 cm depth. To investigate if there is a potential relationship, the average soil moisture value of a pixel was compared to the vegetation index of a pixel (see figure 4.9). The soil moisture value time series shows some noise and therefore the graphs were smoothed out. The series was filtered with the Savitzky-Golay algorithm (Steinier et al., 1972) which can smooth the data without distorting the signal. The algorithm smooths a signal by fitting a polynomial, in a least squares sense, to a sliding window of data. The parameters to be set by the user are the width of the window and the order of the polynomial to be fitted to the data. A higher peak window size produces a smoother result. A smaller degree of the smoothing polynomial produces a smoother result, however, also increases the filter bias and gives a noisier result. The soil moisture time series is filtered using a moving window of approximately 7 days (167 hours) and a polynomial order of 4.

As the sensors are located close to each other, soil moisture sensors can be located in the same pixel and thus return the same vegetation index value. It was examined for each individual satellite mission and each study location if sensors are located in the same pixel, and if so, the average soil moisture value was taken into account and compared with the retrieved VI from the pixel. As there is a time lag in which vegetation responds to soil moisture, a time lag was taken into account. When for example a 20-day time lag is applied, the vegetation index of the 20th day is compared with the soil moisture from the 1st day.

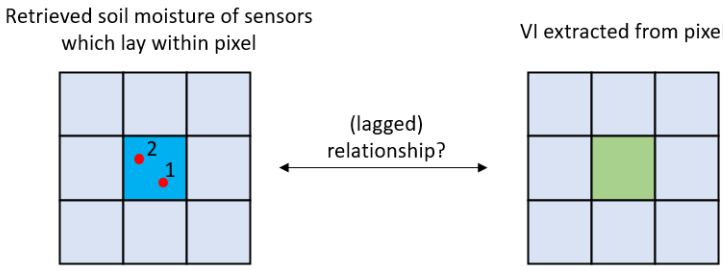

Figure 4.9: Illustration of how a (lagged) relationship is explored between soil moisture and VIs.

As some pixels do not solely cover the dike area but also overlap with the water it will be investigated what the influence is of the presence of both water and vegetation in one pixel. This was done by comparing the spectral response curves of water, vegetation and a pixel containing both vegetation and water. Furthermore, the time series was explored of vegetation indices retrieved from a pixel containing only water of the ditch and a pixel containing only the grass-cover of the dike.

The amount of VI data extracted from a single satellite mission was very limited due to cloud and cloud shadow contamination and the limited study period. Table 4.1 gives an overview of the amount of satellite imagery extracted from the different satellite missions. Merging VIs from different satellite missions is therefore beneficial, as it increases the number of data points. However, VIs obtained from different satellite missions, which have different sensors, are not directly comparable due to differences in sensor characteristics (Steven et al., 2003). The main causes of the differences in reflectance values are variations in spectral response functions (SRF) between sensors (Chander et al., 2012). The SRF describes the relative sensitivity to energy of different wavelengths. Figure 4.11 shows the different spectral response functions from Landsat 7 and Landsat 8.

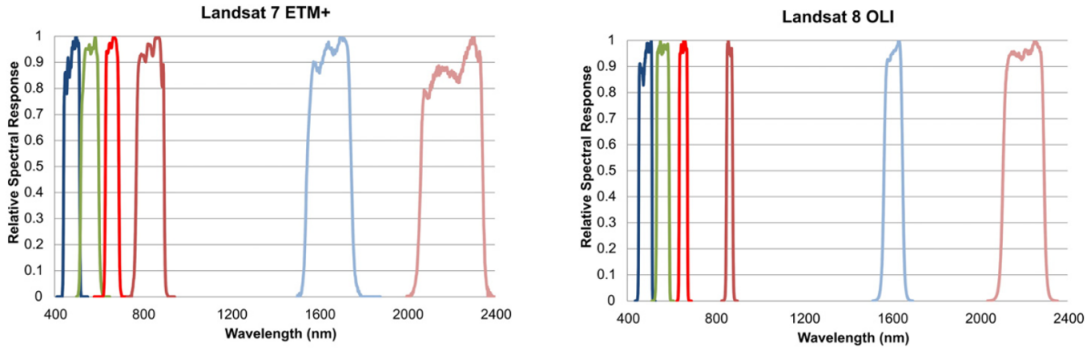

Figure 4.10: Landsat-7 ETM+ and Landsat-8 OLI spectral response functions for the approximately corresponding reflectance bands used in this research (source: Roy et al. (2016)).

In order to merge reflectance values, a translation function needs to be applied in order to convert the reflectance values of one sensor, to equivalent values of another sensor, by adjusting for sensor characteristic differences. Roy et al. (2016) presented a transformation function between the Landsat 7 ETM + and Landsat 8 OLI sensor data. As the orbit and sensing geometries of the Landsat-8 OLI and Landsat-7 ETM + provide swath edge overlapping paths, the pixel locations are the same, enabling to merge the data easily after applying a translation function. The translation functions for the different bands can be found in figure 4.11. The reflectance values from Landsat 8 were translated using the transformation functions from the OLS regression type, and then merged to the reflectance values from Landsat 7.

During the non-growing season, most vegetation is dormant and therefore it was expected that during this period vegetation indices cannot give a proxy for soil moisture, assuming water availability in the root-zone is the main controlling factor for vegetation health (Wang et al., 2007). Hence, vegetation indices are only able to give an indication of soil moisture during the growing season, which is officially from the 1st of April up until the 1st of October (Rivierenland, 2021). The seasonal cycle can significantly influence vegetation indices. Seasonal factors can be seen as expected variations from trends throughout a seasonal period. Vegetation indices were extracted

Location	Satellite mission	Sensors located in pixel	Images
Bermweg	Landsat 7	1, 2, 3, 4, 5	4
	Landsat 8	1, 2, 3, 4, 5	12
	Sentinel-2	1, 2, 3	7
	Sentinel-2	4	7
Geerweg	Landsat 7	1, 2, 3	4
	Landsat 7	4	4
	Landsat 8	1, 2, 3	9
	Landsat 8	4	9
	Sentinel-2	1, 2	7
	Sentinel-2	3	7

Table 4.1: Overview of the imagery used for different optical satellite missions.

	Regression type	Between sensor OLS transformation functions and RMA regression coefficients
Blue λ (~0.48 μm)	RMA	OLI = −0.0095 + 0.9785 ETM
	OLS	OLI = 0.0003 + 0.8474 ETM+
	OLS	ETM+ = 0.0183 + 0.8850 OLI
Green λ (~0.56 μm)	RMA	OLI = −0.0016 + 0.9542 ETM
	OLS	OLI = 0.0088 + 0.8483 ETM+
	OLS	ETM+ = 0.0123 + 0.9317 OLI
Red λ (~0.66 μm)	RMA	OLI = −0.0022 + 0.9825 ETM
	OLS	OLI = 0.0061 + 0.9047 ETM+
	OLS	ETM+ = 0.0123 + 0.9372 OLI
Near infrared λ (~0.85 μm)	RMA	OLI = −0.0021 + 1.0073 ETM
	OLS	OLI = 0.0412 + 0.8462 ETM+
	OLS	ETM+ = 0.0448 + 0.8339 OLI
Shortwave infrared λ (~1.61 μm)	RMA	OLI = −0.0030 + 1.0171 ETM
	OLS	OLI = 0.0254 + 0.8937 ETM+
	OLS	ETM+ = 0.0306 + 0.8639 OLI
Shortwave infrared λ (~2.21 μm)	RMA	OLI = 0.0029 + 0.9949 ETM
	OLS	OLI = 0.0172 + 0.9071 ETM+
	OLS	ETM+ = 0.0116 + 0.9165 OLI

Figure 4.11: Surface reflectance sensor transformation functions (Landsat 7 ETM+ to Landsat 8 OLI and vice versa) (source: Roy et al. (2016)).

for large areas of the dike over several years to investigate to explore during which months of the growing season the seasonal cycle dominates the effect of soil moisture. To get a good overview of the seasonal cycle, a long time series is required. Data from Landsat 7 and 8 is available since 2014, whereas data from Sentinel-2 is only available since 2017. Imagery from Landsat 7 contains a scan line and therefore vegetation indices were retrieved from Landsat 8. Furthermore, in-situ soil moisture patterns were compared to extracted vegetation indices at both study sites to investigate during which months VIs could potentially give an indication of soil moisture. As there is a time lag of vegetation response to soil moisture, a lag was taken into account. The optimal lag of soil moisture on vegetation for grass-covered dikes is unknown, however various studies in literature have demonstrated an optimal lag response time for grassland of 10 to 56 days (Wang et al. (2007), Liu et al. (2011), Zhang et al. (2018)). Therefore, a 30 day lag was chosen. As soil moisture measurements were only available since April 2020, precipitation deficit was used to give an indication of the soil moisture trends in the months prior to April 2020.

Exploratory data analysis

It is recommended to visualize both time series, before complex time series analysis is performed (Shumway et al., 2000). Therefore, retrieved VI values and the (lagged) soil moisture time series were visually analyzed to evaluate if high vegetation index values correspond with high soil moisture values and vice versa. An exploratory data analysis is very important to evaluate the potential relationship and understand the structure of the time series. Furthermore, it can also expose outliers (Chatfield and Xing, 2019). Outliers were further explored by analyzing the satellite imagery and by checking photos taken by the wild life camera, which is installed at both study locations.

Evaluation of the Vegetation Index and soil moisture correlation

As shown in table 4.1 the amount of vegetation index data is restricted as a lot of the satellite imagery is contaminated by clouds or cloud shadows. Since the amount of vegetation index data is limited, a correlation analysis cannot demonstrate statistical significance, as calculating Pearson correlations is only recommended when the sample size is at least 25 (David, 1938). However, they are useful to examine at which time lag a potential correlation can be found between the vegetation indices and soil moisture values. A Pearson correlation analysis will only be performed for the merged Landsat 7 and 8 data set as the sample size was largest and therefore also results in the most reliable outcome. Wang et al. (2007) found an optimal lag response time of 10 days between NDVI and soil moisture for grasslands in a humid region. Liu et al. (2011) demonstrated that there was a 17 to 22 day lagged correlation between soil moisture at 10 cm depth and vegetation indices using the red, green, NIR and SWIR bands for an open grassland in a semiarid region. Zhang et al. (2018) showed that the lag response of NDVI and NDWI (using the NIR and SWIR band) to soil moisture varies among grasslands between 8 and 56 days. The time lag between soil moisture and vegetation indices is dependent on many factors such as vegetation type, soil properties and climate. As these factors were different in these studies, correlation coefficients were computed for a lag up to 40 days. Furthermore, scatter plots were used to visualize a potential relationship between the vegetation indices and the soil moisture measurements at a depth of 20 cm. The optimal lag is defined as the highest correlation coefficient when all the correlation coefficients of all lags are compared.

Pearson correlation coefficients are a measure of the strength of a linear association between two variables and is applicable because a linear relationship exists between surface soil moisture and vegetation indices (Narasimhan et al., 2005). Equation 4.6 shows how the Pearson correlation coefficient is calculated. The x and y represent the individual sample points, in this case the vegetation index values and in-situ soil moisture measurements, whereas n defines the sample size. A Pearson correlation value is returned between - 1 and + 1 which indicates how strongly two variables are linearly related.

$$R = \frac{\sum_{i=1}^{n}(x_i - \bar{x})(y_i - \bar{y})}{\sqrt{\sum_{i=1}^{n}(x_i - \bar{x})^2}\sqrt{\sum_{i=1}^{n}(y_i - \bar{y})^2}} \tag{4.6}$$

4.5. SAR as a proxy for soil moisture

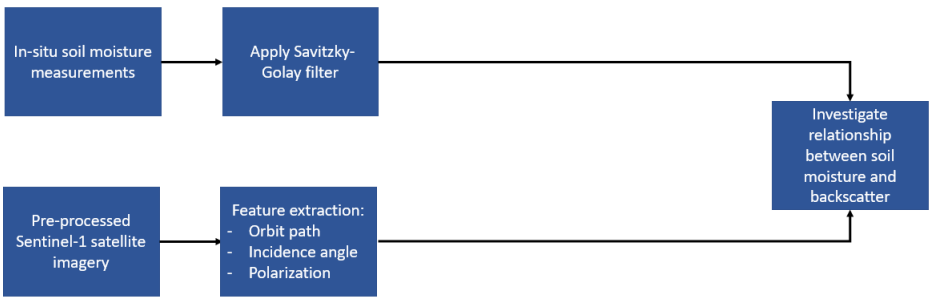

Figure 4.12: Schematic overview of the methodology used to explore the relationship between soil moisture and SAR backscatter.

A significant change in soil moisture leads to an increase in backscatter. It was therefore investigated if there is a relationship between retrieved SAR backscatter and soil moisture measurements at 20 cm depth for the two regional grass-covered dikes.

Sentinel-1 uses the C-band portion of the spectrum, which can penetrate up to 5 cm deep below the soil surface. Hence, the SAR signal only provides information about the soil surface. However, the soil moisture sensors located at the regional dikes only provide measurements at 20 cm depth. A study by Carranza et al. (2018) shows that there is a lagged cross-correlation between soil moisture values at 5 cm (surface) and 40 cm depth (subsurface values) in grass fields. In this study, a 1 to 2 day lead of surface soil moisture is observed. Hence, it was assumed that there is also a lagged relationship between soil moisture at 5 cm and 20 cm. Furthermore, Jamalinia et al. (2020) has demonstrated that there is a lagged correlation between the leaf area index (LAI) and the water root-zone content with an optimal lag at 15 days. Several studies have shown that there is a strong correlation between backscatter intensity and LAI (Steele-Dunne et al., 2017). Therefore, it was explored if backscatter

could be able to give an indication of root-zone soil moisture availability. This was assessed by analyzing if there was a lagged correlation between soil moisture at 20 cm depth and the retrieved backscatter.

All in all, a time lag was taken into account to investigate the relationship between retrieved SAR backscatter and soil moisture at 20 cm depth. Pearson correlations were calculated to measure the strength as a linear relationship exists between surface soil moisture and SAR backscatter (Ulaby et al., 1978) (Zribi et al., 2005) (Moeremans and Dautrebande, 2000). The results from the correlation analysis were analyzed to examine if SAR remote sensing data can be used as a soil moisture indicator. Figure 4.12 gives an overview of the methodology used to explore this relationship.

From the retrieved SAR backscatter, different features were extracted. The incidence angle and direction of the orbit path (i.e. ascending, descending) influences the amount of backscatter retrieved and therefore the images were filtered by orbit mode and their corresponding incidence angles. Increasing incidence angle results in a decreasing penetration depth because the path length through the vegetation is longer with a larger incidence angle (McNairn and Shang, 2016). Images acquired by SAR sensors over the same area but from a different orbit path measure different amounts of backscatter, as orbit paths look at the ground in the opposite direction (see figure 4.13) (Mahdavi et al., 2019). The VV, VH polarization and the cross ratio VH/VV were acquired and filtered by the different incidence angles and orbit directions (table 4.2).

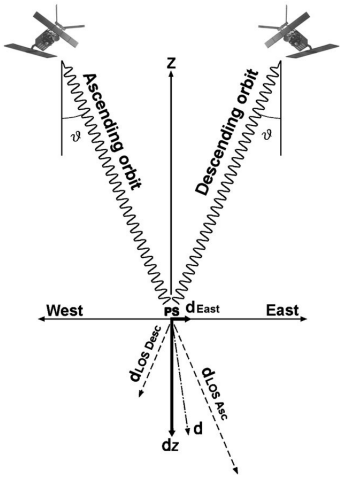

Figure 4.13: Illustration of difference between the ascending and descending orbit path. θ represents the radar look-angle (source: (Vilardo et al., 2009)

Features	**Sentinel-1**
Co-pol intensity	VV
Cross-pol intensity	VH
Intensity ratio cross-co-pol	VH/VV
Orbit	Ascending/Descending
Incidence angle	θ_i

Table 4.2: Overview of the extracted features for Sentinel-1

As SAR backscatter is very noisy, a speckle filter was applied. A speckle filter can suppress noise, however, it cannot remove all noise. To reduce the signal-to-noise ratio, one should retrieve backscatter over an area as large as possible. Averaging out retrieved backscatter can reduce the speckle effect. Therefore, backscatter is retrieved over the area surrounding the soil moisture sensors. To demonstrate that single pixels result in strong variations in backscatter, backscatter retrieved from single pixels (not the average of the whole area) were retrieved and plotted in a graph. The average soil moisture from the sensors was taken into account, assuming that the soil moisture trends are alike over the whole area. A Savitzky-Golay algorithm was applied to smooth out noise from the soil moisture time series. At location Bermweg, soil moisture was averaged for sensors 1-4. Sensor 5 at location Bermweg was excluded, as due to the geometry of the dike and its location close to the toe ditch, the sensor lies in the saturated zone and was therefore only representative for the small are close to the toe. Figure 4.14 gives an illustration of how a relationship is investigated. Only pixels that exclusively cover the dike were

included. Table 4.3 presents an overview of the number of Sentinel-1 imagery that were used for this study. As dikes are sloped, the orbit path (i.e. ascending, descending) can strongly affect the area which is illuminated by the sensor. Therefore, it is analyzed if a particular orbit path illuminates the area of the dike better.

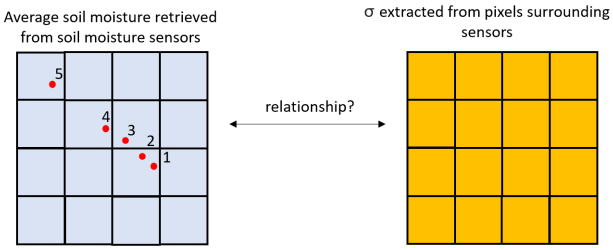

Figure 4.14: Illustration of how a relationship is explored between soil moisture and SAR.

Location	Orbit	Incidence angle	N
Bermweg	Ascending	35	79
		43	77
	Descending	33	75
		42	75
Geerweg	Ascending	33	75
		42	75
	Descending	36	79
		44	77

Table 4.3: Overview of the imagery used from Sentinel-1. N is the amount of satellite imagery extracted for the corresponding orbit and incidence angle during the study period April 2020 - July 2021 (ESA, 2021d).

4.6. Vegetation indices and precipitation deficit

A decrease of soil moisture content occurs when the outflux of water is bigger than the influx. Precipitation deficit, which is defined as the difference between precipitation and evapotranspiration, could therefore give a proxy for soil moisture. Negative values indicate dry conditions and positive values indicate wet conditions (excess precipitation). An analysis was made to investigate the relationship between precipitation deficit and vegetation indices obtained from optical satellite imagery. This study was solely conducted for the regional grass-covered dikes. Equation 4.7 defines the precipitation deficit D(t), where P(t) and E(t) are the precipitation and evapotranspiration.

$$D(t) = P(t) - E(t) \tag{4.7}$$

The effect of precipitation deficit on vegetation health is a slow process of accumulation and is related to both current and earlier precipitation deficit (Wang et al., 2016). A one day precipitation deficit will not lead to significant changes in vegetation health, however, a precipitation deficit over a longer period will. Therefore, it is more convenient to take into account the cumulative conjugates of both variables. This leads to equation 4.8.

$$D_{period} = \int_{t1}^{t2} P(t) - E(t) \tag{4.8}$$

A precipitation deficit of minus 10 mm over a time period means that 10 mm of soil moisture was removed from the soil, which was not replaced by precipitation during this period. The potential evaporation can be estimated using either the Makkink or Penman method (De Bruin and Lablans, 1998). Potential evaporation is the amount of evaporation that would occur if there is no limitation of water. The Makkink formula is as follows:

$$E_{p,MK} = C_{MK} \frac{1}{\lambda} \frac{R_s s}{\gamma} \tag{4.9}$$

The Makkink constant C_{Mk} is equal to 0.65 and R_s is the incoming solar radiation. γ represents the psychrometer constant, λ the latent heat of water evaporation and s defines the slope of the saturated vapour curve. More detail about the exact values and derivation of the Makkink formula can be found in De Bruin and Lablans (1998).

Precipitation and evapotranspiration data for the two study locations can be extracted from two different databases. First of all, there are Koninklijk Nederlands Meteorologisch Instituut (KNMI) weather stations that measure meteorological variables at specific locations. Secondly, Meteobase, a third party, distributes free raster data of precipitation and evapotranspiration in the Netherlands. The raster data are built out of grid cells with a length of 1000 km. This data is retrieved using satellite data, after which the KNMI stations are used to calibrate the data (Versteeg et al., 2013). As the KNMI stations are located far outside the boundaries of the study locations, the Meteobase data will give more accurate values and consequently is a better fit. The precipitation and evapotranspiration data will therefore be extracted from Meteobase.

The precipitation and evapotranspiration data from Meteobase is delivered in ASCII files, which represent raster data. Raster data is gridded data, where each pixel is associated with a specific geographical location. The Meteobase raster data contains grid cells of 1 km^2 and to each pixel, a value is assigned. One raster file represents one time period: daily information for the evapotranspiration and hourly information for the precipitation. Since the data sets have to be in the same time unit in order to calculate the precipitation deficit, the precipitation time series have been re-sampled to daily sums. A precipitation deficit data set was obtained by subtracting daily evaporation values from the daily precipitation values. The cumulative precipitation deficit was calculated by using equation 4.8. The cumulative precipitation deficit was calculated for a certain time period, which is the number of days evaluated prior to the observation date to compute the precipitation deficit. A relationship was explored for time periods of 10 to 90 days. A small period of history will not have an effect on retrieved vegetation indices as only a long period of drought will affect the vegetation state. However, a very large period might introduce noise. Figure 4.15 visualizes how a relationship is investigated between retrieved VIs and cumulative precipitation deficit.

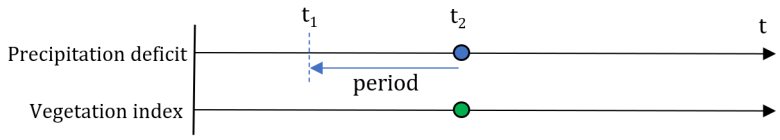

Figure 4.15: Visualization of the methodology used to explore a potential relationship between precipitation deficit and vegetation indices.

Vegetation indices were extracted from satellite missions Landsat 7, Landsat 8 and Sentinel-2. Also, the data from Landsat 7 and 8 was harmonized to increase the vegetation index data set. In section 4.4 it was explained how this data was merged. As the precipitation deficit data was only available for cells with a length of 1000 meters, which is much larger than the area of the dike, average vegetation index values were extracted over a large area of the dike. Only pixels that cover the dike were included. Pixels that also overlap with other land type covers such as water or trees were not taken into consideration as this influences retrieved vegetation indices. As multiple pixels on the dike were taken into account, only satellite imagery in which less than 20% of the region of interest is contaminated by clouds or cloud shadows is included. Table 4.4 shows the number of pixels included to calculate the average vegetation index at each location, and for each satellite mission.

Study location	**Satellite mission**	**N**
Bermweg	Landsat 7	8
	Landat 8	8
	Sentinel-2	107
Geerweg	Landsat 7	8
	Landat 8	8
	Sentinel-2	110

Table 4.4: Table showing the number of pixels (N) included to calculate the average vegetation index at each study location for each satellite mission.

To investigate if there is a relationship between cumulative precipitation deficit and vegetation indices, Pear-

son correlation coefficients were calculated to identify the effect of precipitation deficit on vegetation indices of a grass-covered dike for all different (harmonized) satellite missions. Pearson correlation coefficients were calculated for different time periods: 10 to 90 days. It was analyzed how strong the correlation was for, and if a historical time period could be found for which the correlation is optimal. It was examined if a universal relationship could be found among the results for the different (harmonized) satellite missions. The Pearson correlation equation can be found in equation 4.6. The x and y represent the individual sample points, in this case the precipitation deficit and in-situ soil moisture measurements whereas n defines the sample size. Figure 4.16 illustrates how a relationship between precipitation deficit and vegetation indices was investigated. Table 4.5 gives an overview of the amount of satellite imagery extracted from each satellite mission.

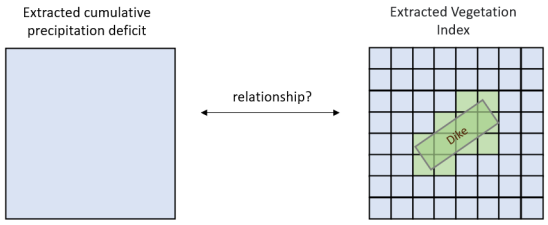

Figure 4.16: Illustration of how a relationship is explored between precipitation deficit and vegetation indices. The cumulative precipitation deficit is calculated using precipitation and evapotranspiration data extracted from a raster file with grid cells of 1 km^2.

Location	Satellite mission	N
Bermweg	Landsat 7	17
	Landsat 8	40
	Sentinel-2	15
Geerweg	Landsat 7	22
	Landsat 8	31
	Sentinel-2	15

Table 4.5: Table showing the amount of imagery (N) used to explore a relationship between cumulative precipitation deficit and vegetation indices for each satellite mission and study location.

4.7. Spatial-temporal analysis

For a river dike section at the Amsterdam-Rhine canal, information was available about specific areas of the dike which experienced wetting at the inner slope of the dike from 2017 up until July 2020 (A. Lievens, personal communication, 14th of April, 2021). At the toe of the dike a drainage system was installed to control seepage. However, clogging of the drainage system led to an increase in phreatic level, which resulted in wetting of the dike at the inner slope. In 2020 the clogging of the drain led to a tremendous increase in pore water pressure, decreasing shear strength and eventually leading to subsidence. In September 2020 actions were taken and a new drainage was installed to prevent seepage problems in the future. The area was very wet and during high water periods, one would even stand ankle-deep in the water (A. Lievens, personal communication, 4th of October, 2021). Figure 4.18 shows the locations which experienced wetting and which did not. It was investigated if a spatial-temporal difference could be observed between the two areas by remote sensing data.

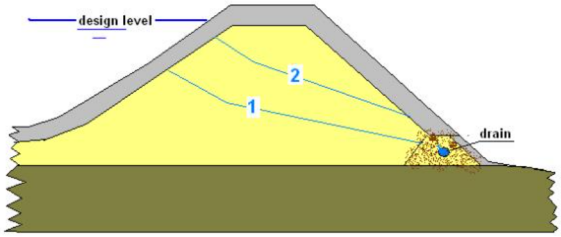

Figure 4.17: Figure illustrating the effect of a drainage system. 1) phreatic level if the drainage is functioning. 2) phreatic level if drainage is malfunctioning (Calle, 2010).

Figure 4.18: River dike section at the Amsterdam-Rhine canal. Between locations 1 and 2 conditions were normal. The area between locations 3 and 4 indicates the area which experienced wetting.

4.7.1. Vegetation indices

It was hypothesized that a difference could be observed between the acquired vegetation indices from the wet area and the non-wet area (referred to as the reference area). It was assumed that overall, vegetation in the wet area had access to larger amounts of water than vegetation in the reference area. Therefore, it is expected that especially during dry periods a difference could be found. A spatial-temporal analysis allows to examine and model the behaviour of different parts of the dike over the years.

Vegetation indices were retrieved from Sentinel-2, Landsat 7 and Landsat 8. Only pixels that cover the wet and reference area (thus not overlap with other elements such as a road, water) were taken into account. Vegetation indices were extracted from all single pixels to investigate if the retrieved VI data was similar for the whole area. To analyze the behaviour of the two areas, the retrieved values over the course of the years were illustrated and interpreted. Mean values of the two different areas were shown with a surrounding polygon representing

plus/minus one standard deviation. The precipitation deficit and daily precipitation rates during these years were displayed to investigate if vegetation index trends can be explained by these meteorological factors. For the precipitation deficit graph, a historical period of 15 days was chosen. A too small period (10 days) of history will not have an effect on retrieved vegetation indices whereas including too much history will result in an excess of data, as periods are included which do not influence the vegetation state. Furthermore, histogram plots that represent the distribution of extracted VIs for each year from the two different areas were shown to demonstrate whether a spatial difference could be observed.

4.7.2. SAR

To investigate if a difference could be found between the behaviour of the allegedly wet area compared to the reference area, SAR backscatter was extracted from pixels in the two different areas. SAR backscatter was averaged out over the whole area to decrease speckle noise. It was hypothesized that since the area is wet, lower backscatter values are retrieved (Liu, 2016). The backscatter of standing water is lower as water is smooth and therefore acts as a mirror. From the retrieved SAR backscatter, a distinction was made between backscatter from the different orbit paths (i.e. ascending, descending) and incidence angles, as this influences the signal. The average backscatter was retrieved for three different polarization channels: VH, VV and cross ratio VH/VV.

It was known that during high water, the wet area was wetter than during low water (A. Lievens, personal communication, 4th of October, 2021). It was therefore investigated if a difference in backscatter retrieval can be observed between the wet and reference area during high water periods and low water periods. Historic water levels were acquired from the Waterinfo website of Rijkswaterstaat from the measuring point at Wijk bij Duurstede, as this can give the best indication of the water levels in the canal near the dike (Rijkswaterstaat, 2021). The three highest and lowest water levels were highlighted in the backscatter plots to examine if a difference can be seen between low and high water periods.

5

Results

This chapter presents the main results related to the research questions. Section 5.1 provides the results of the potential lagged relationship between soil moisture and vegetation indices followed by 5.2, where the relationship between SAR backscatter and in-situ soil moisture measurements was assessed. The results from precipitation deficit as a proxy for soil moisture and its relationship with vegetation indices will be discussed in section 5.3. Lastly, it was assessed if a difference could be found between a wet and non-wet area on a grass-covered river dike by vegetation indices and SAR backscatter. The results from the spatial-temporal analysis are shown in section 5.4.

5.1. Vegetation indices as a proxy for soil moisture

In this section, the results are presented of the analysis if there is a lagged relationship between vegetation indices extracted from optical satellite imagery and in-situ soil moisture measurements at 20 cm depth for two regional grass-covered dikes. This was assessed for five different vegetation indices: the GRR, MSR, NDVI, RVI, and NDII. A lag refers to the time delay that vegetation indices respond to soil moisture.

5.1.1. Study period

It is known that vegetation indices are only able to give an indication of soil moisture during the growing season, which is officially from the 1st of April up until the 1st of October (Rivierenland, 2021). Seasonal factors, which are expected variations from trends throughout a seasonal period, can overrule the response of vegetation to soil moisture. It was investigated if during the whole growing season the main factor for vegetation health is soil moisture or that during some months this effect is overruled by seasonal factors. Vegetation indices were extracted from large areas of the two dikes for several years to get a good overview of the seasonal cycle. Vegetation indices were extracted from Landsat 8 because BOA satellite imagery on Google Earth Engine is available since 2014, whereas data from Sentinel-2 is only available since 2017. As imagery from Landsat 7 contains a scan line error, imagery from Landsat 8 was preferred. The seasonal cycle of the GRR at location Bermweg is shown in figure 5.1. The seasonal cycle of the other vegetation indices and at location Geerweg were similar. The seasonal cycle was clearly visible when the acquired vegetation indices at the study sites were plotted over a longer time period. For the major part, vegetation indices were higher during the growing season than during the non-growing season. Vegetation indices increase at the beginning of the growing season and decrease during the non-growing season.

To examine during which months vegetation indices can give a proxy for soil moisture, vegetation indices were retrieved at location Bermweg and Geerweg and plotted together with the average in-situ soil moisture values at 20 cm depth. Figures 5.2 show the retrieved GRR from Landsat 8 and Sentinel-2 over the dike area at location Bermweg together with the soil moisture time series. A soil moisture lag is applied as there is always a time lag in which vegetation growth responds to soil moisture (Foody (2003), Zhang et al. (2011)). A lag of 30 days was taken into account. As soil moisture values at 20 cm depth were only available since April 2020, the daily precipitation deficit at both locations in the three months prior to April 2020 were investigated to examine if the increase of VIs in April and May can be assigned to the seasonal cycle or that it is due to an increase in soil moisture. The precipitation deficit graphs show that there was an excess of precipitation at both study locations

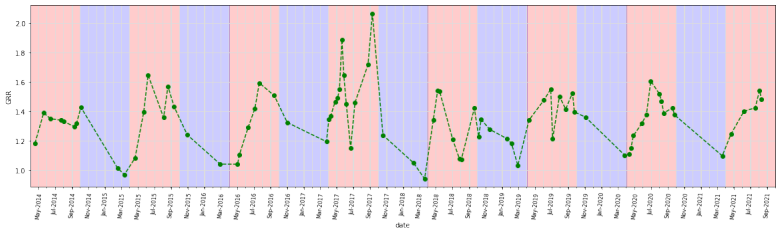

Figure 5.1: Seasonal dynamics of the GRR at location Bermweg. Vegetation indices were extracted from Landsat 8.

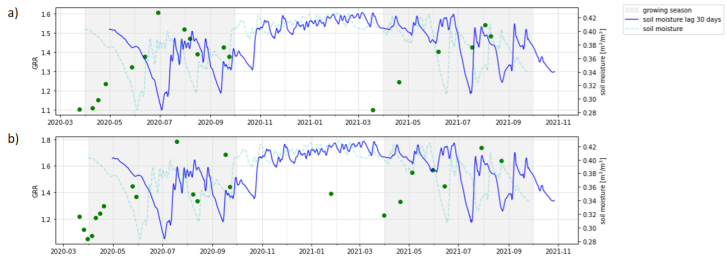

Figure 5.2: Seasonal dynamics of GRR extracted from a) Landsat 8 and b) Sentinel-2 at location Bermweg.

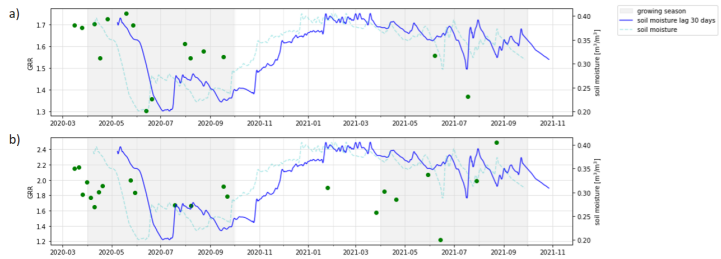

Figure 5.3: Seasonal dynamics of GRR extracted from a) Landsat 8 and b) Sentinel-2 at location Geerweg.

during January to March 2020, and thus soil moisture values are expected to be equal or higher than during April 2020. The trends of the other vegetation indices are similar and can be found in Appendix B. All by all, it can therefore be confirmed that during April and May 2020 and 2021 the increase in VI values is overruled by seasonal factors and soil moisture is not the main controlling factor. Therefore, only vegetation indices acquired during the period June to September were used to examine a potential relationship between vegetation indices and soil moisture.

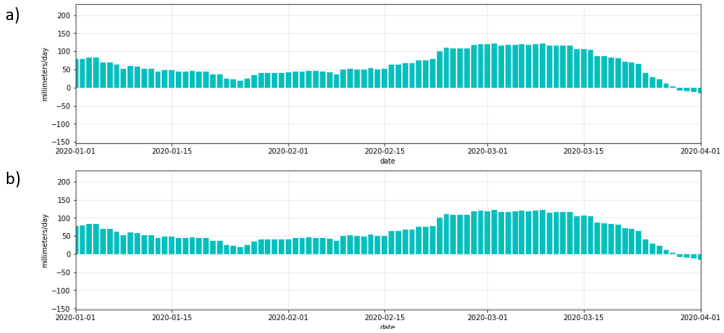

Figure 5.4: Daily precipitation deficit values from January 1st 2020 to April 1st 2021 at a) location Bermweg and b) location Geerweg.

5.1.2. Pixel contamination

As the spatial resolution of Landsat 7 and 8 is only 30 meters, it can occur that different elements are located within the same pixel. At location Geerweg, sensors 1-3 were located in a pixel that partly overlaps with water.

It was therefore explored what the influence is of the spectral reflectance of water on the retrieved vegetation indices. This was examined by exploring the time series of vegetation indices retrieved from a pixel containing only water of the ditch and a pixel containing only the grass-cover of the dike. The values were retrieved from Sentinel-2, as the spatial resolution of Landsat 7 and 8 was too coarse to extract values from pixels containing only water from the toe ditch.

The difference in spectral response between water, vegetation and a mixed pixel are illustrated in figure 5.5. Overall, reflectance values of water are higher in the red, green, blue, NIR and SWIR band. Figure 5.6 gives an overview of the trend of the GRR retrieved from a pixel containing solely water and a pixel containing solely vegetation. The figures of the other vegetation indices can be found in Appendix B. The VIs retrieved from water are not constant throughout the years but fluctuate.

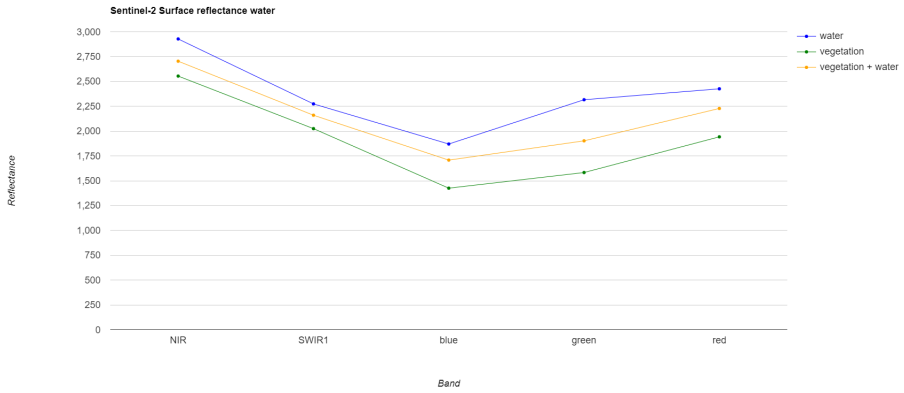

Figure 5.5: Difference between reflectance values of the blue, red, green, NIR and SWIR band for a water and grass pixel at location Geerweg during August 2020. Retrieved from Sentinel-2.

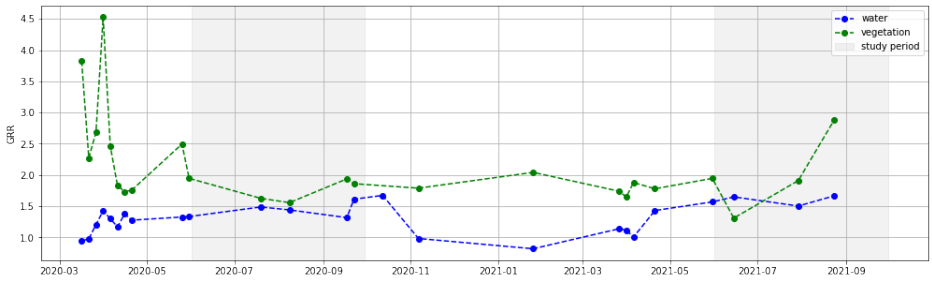

Figure 5.6: Time series of GRR retrieved from water pixel and vegetation pixel acquired from Sentinel-2 at location Geerweg.

5.1.3. Vegetation indices as a proxy for soil moisture

An analysis was made to investigate if there is a potential relationship between vegetation indices extracted from satellite imagery and in-situ soil moisture measurements at 20 cm depth during the period June to September. Since there is a time lag of vegetation response to soil moisture, a lagged relationship was examined to investigate which lag best reflects the vegetation index dependency on soil moisture (Foody, 2003). In-situ soil moisture measurements from different sensors are available from April 2020 up until September 2021 for two study locations: Bermweg and Geerweg. Vegetation indices were extracted from Landsat 7, 8 and Sentinel-2. An analysis of the soil moisture trends can be found in section 3.1. To remove the noise from the soil moisture time series, the series was filtered with a Savitzky-Golay algorithm (see section 4.4 for more information). Figure 5.7 shows an example of how the filtering results in a smoother time series. The soil moisture time series was filtered using a moving window of approximately 7 days (167 hours) and a polynomial order of 4. An example of a filtered soil moisture time series can be found in figure 5.7.

Because multiple images were contaminated with clouds and cloud shadows, VI data during the study period

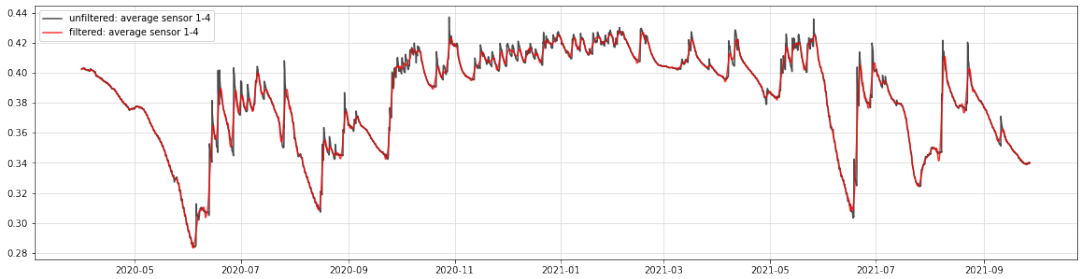

Figure 5.7: Example of filtered soil moisture time series (Average of sensor 1-4 at location Bermweg). The unfiltered profile is illustrated in black and the filtered profile is illustrated in red. Filtering results in a smooth time series.

(June to September) was very limited. The amount of satellite imagery available for the study areas differs for the single satellite missions but lies between four and twelve images. Because the sample size was small, it was necessary to increase the amount of VI data to get a better overview of the trend. One way to enlarge the amount of data is by merging VI extracted from different satellite missions. As discussed in Chapter 4, reflectance values of different satellite missions are not directly comparable due to differences in satellite sensor characteristics (Steven et al., 2003). Therefore, a translation function needs to be applied in order to convert the reflectance values of one satellite to equivalent values of another satellite. Roy et al. (2016) presents a transformation function to harmonize Landsat 7 and 8 data. The data retrieved from Landsat 7 and 8 were merged by applying the transformation function.

In this section the results from the harmonized Landsat 7 and 8 data set are presented. Graphs that demonstrate the relationship between the lagged soil moisture time series and vegetation indices for Sentinel-2 at the two study locations, can be found in Appendix C. No Pearson correlation coefficients were computed for the single missions as the sample size is limited. Pearson correlation coefficients were calculated for the harmonized Landsat 7 and 8 data set as it is useful to examine at which time lag a potential relationship can be found. However, the sample size is small (< 25) and can therefore not demonstrate statistical significance.

Figure 5.8 presents the calculated correlation coefficients between soil moisture and VIs for different time lags at location Bermweg. A positive lag means that soil moisture leads the VI. So a time lag of around 30 days indicates that the VI of the 30th day was compared with the soil moisture from the 1st day. The graph shows that the highest correlation was obtained for all five vegetation indices, utilizing a lag of around 30 days. A weak correlation was found for the MSR, NDVI, RVI, and NDII (R=0.32-0.40) and a negligible correlation with the GRR (R=0.19). The lowest correlation was found for the MSR, NDVI, and RVI when a lag of 0 days was applied and with the GRR and NDII when a lag of 3 days was applied. In both cases correlation coefficients are negative. When the graph was analyzed, an overall increase in correlation coefficients could be observed from a lag of 0 to 30 days. Figure 5.8 shows scatter plots of VIs and soil moisture when a lag of around 30 days was applied at location Bermweg.

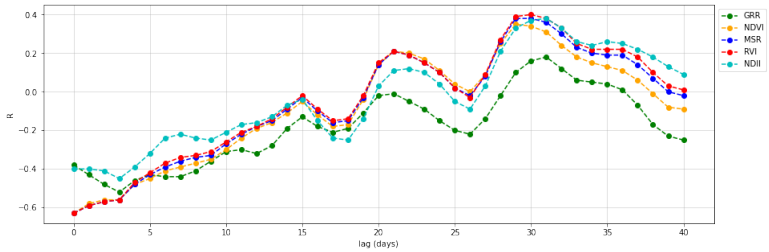

Figure 5.8: Correlation coefficient (R) between vegetation index and soil moisture with time lags up to 40 days for the harmonized Landsat data set at location Bermweg. The lag means that soil moisture leads the vegetation index.

The vegetation indices and soil moisture values were visually analyzed to evaluate if high vegetation index values correspond with high soil moisture values and vice versa. Figure 5.10 illustrates the soil moisture time series with a lag of 30 days and the retrieved VI values. It was expected that vegetation indices decrease when soil moisture decrease, however, this relation cannot always be observed. It was interesting to see that low vegetation index values cannot be detected during the dry period in 2020 by the harmonized Landsat 7 and 8 data

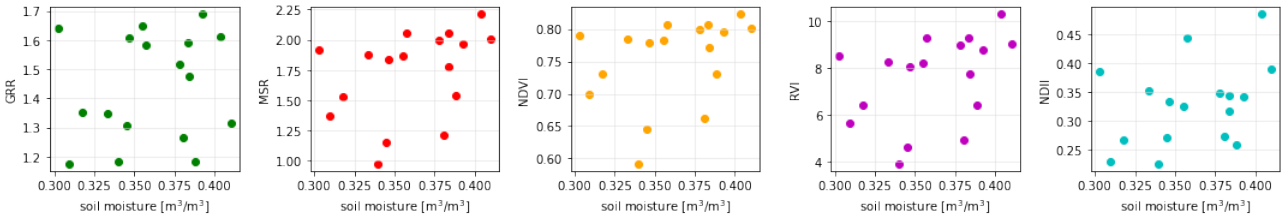

Figure 5.9: Scatter plots of VIs versus soil moisture at a 30 day lag for the harmonized Landsat 7 and 8 data set at location Bermweg.

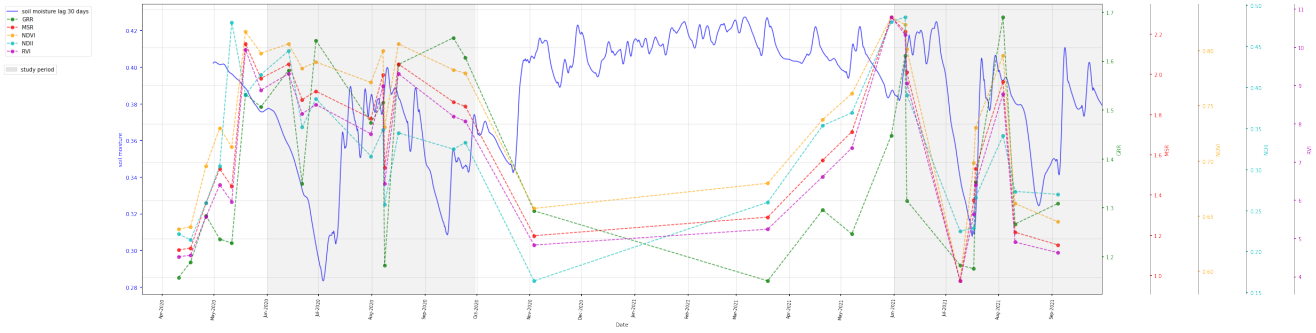

Figure 5.10: Graphs showing the pattern between lagged soil moisture and VIs (extracted from harmonized Landsat 7 and 8 data set) at location Bermweg. Only VIs during June to September were taken into account.

set. Vegetation indices retrieved from the Sentinel-2 satellite mission do indicate low vegetation index values (GRR=1.2, MSR=1.1, NDVI=0.6, RVI=4.3, NDII=0.23) during mid-July 2020. No images were acquired during July 2020 by Landsat 7 and 8 due to cloud or cloud shadow contamination. Furthermore, in June 2020 points could be identified where VIs increase whereas soil moisture values have decreased. Satellite imagery from which these outliers are retrieved were visually checked to investigate if abnormalities could be detected. On the 29th of June, vegetation indices do not decrease, even though soil moisture keeps decreasing. The 29th of June 2020 was a very cloudy day, during which the region of interest was almost the only part of the dike not covered by clouds. Moreover, VI values suddenly decrease from one day to the next on August 7th, 2020. When photos taken with the wildlife camera on these different dates were compared, no large difference could be seen (see figure 5.11). Also, the satellite imagery was not contaminated by clouds or cloud shadows. Additionally, on July 9th and August 10th, 2021 vegetation indices do not correspond to low soil moisture value when a lag of 30 days was applied.

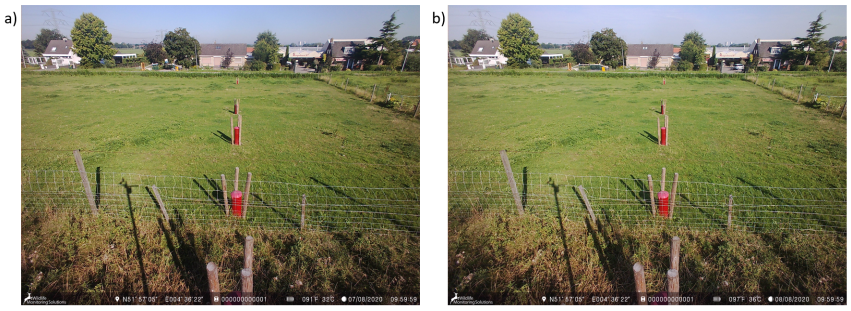

Figure 5.11: Photos giving an overview of location Bermweg during a) August 7th 2020 and b) August 8th 2020.

Interestingly, soil moisture values measured in July 2021 reach values almost as low as in the summer of 2020, which was in the top 10 of driest years ever recorded in the Netherlands. This was unexpected as the local cumulative precipitation deficit at location Bermweg was much higher in 2020 than in 2021 (see figure 5.12) and thus it would be expected that soil moisture values would not reach that low in 2021. The cumulative precipitation deficit, which is a drought indicator used by the KNMI, is the cumulative precipitation deficit from April 1st up until October 1st. Precipitation and evaporation data were extracted from the nearest KNMI weather station, which is Rotterdam. These low soil moisture values in 2021 correspond to low vegetation index values.

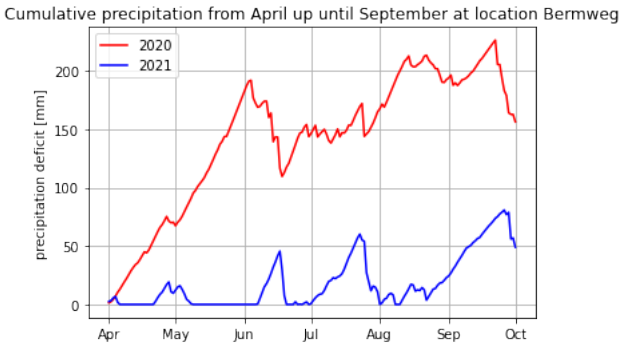

Figure 5.12: Cumulative precipitation deficit from April 1st up until October 1st at location Bermweg in 2020 and 2021.

Furthermore, it was interesting to detect that vegetation indices retrieved from sensor 5 by Sentinel-2 fluctuate throughout the years as much as vegetation indices retrieved from sensors 1-4. Sensor 5 at location Bermweg lies close to the toe ditch. Due to the geometry of the dike, sensor 5 mainly measures in the saturated zone and soil moisture values are almost constant throughout the years. This is contrary to soil moisture values retrieved from sensor 1-4, where values fluctuate and dry periods can be distinguished. Therefore, it was expected that vegetation around sensor 5 has excess to more soil moisture than sensors 1-4. Figure 5.13 shows the difference in retrieved GRR from the different pixels in which the sensors were located. The retrieved vegetation indices of sensor 5 were dynamic throughout the whole year and shows a similar trend to sensors 1-4. Also, extracted vegetation indices retrieved from the pixel where sensor 5 is located were lower throughout the years. It should be noted that it partly overlaps with water and riparian vegetation. The trends of the other vegetation indices can be found in Appendix B and are similar.

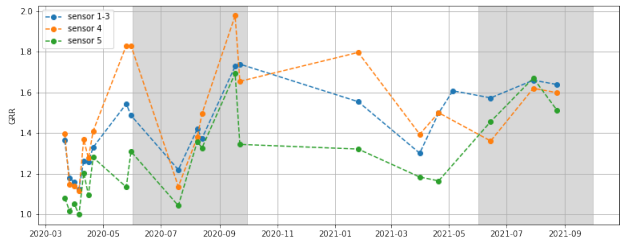

Figure 5.13: Graphs showing the GRR extracted from the different pixels from Sentinel-2 at location Bermweg.

Figure 5.14 presents the correlation coefficient between soil moisture and VIs for different time lags at location Geerweg. Two different graphs are shown as the sensors were located in two different pixels. The graph shows that for sensors 1-3 (left figure), the highest correlation was obtained for the GRR, MSR, NDVI and RVI when a lag of 23 days was applied. However, the calculated correlation coefficient was almost constant from a time lag of 12 to 23 days. The graph shows an increase in correlation from 0 to 12 days, remains stable, and then decreases from 23 days onward. For the NDII the highest correlation was found for a lag of 31 days. All in all, the optimal correlations were negligible (R=0.10-0.28) for all vegetation indices. Negative correlations were found between the GRR, MSR, NDVI, RVI, and soil moisture for the pixels in which sensor 4 was located (right figure). The highest correlation was found for the NDII when a lag of 31 days was taken into account. However, this correlation was negligible (R=0.13). The results clearly show the effect of using single point measurements. At location Geerweg the soil moisture time series of sensors 1 and 2 are very different than those of sensors 3 and 4 during the study period of 2020 (due to local variation). The soil moisture time series of sensors 3 and 4 fluctuate much less than sensors 1 and 2. Therefore, the relation between soil moisture measurements and the retrieved vegetation index was different for the two pixels.

Figures 5.15 and 5.16 illustrate the soil moisture time series with the extracted VIs for sensors 1-3. The optimal lag of 23 days was applied for the GRR, MSR, NDVI and RVI and 31 days for the NDII. The figure shows that during the dry period in July 2020 low vegetation index values can be detected. It was interesting to see that vegetation index values in July 2021 were as low as the dry period of 2020 whereas the decrease in soil moisture in 2021 was not as extreme and long. These extremely low vegetation index values during 2021 can also be detected

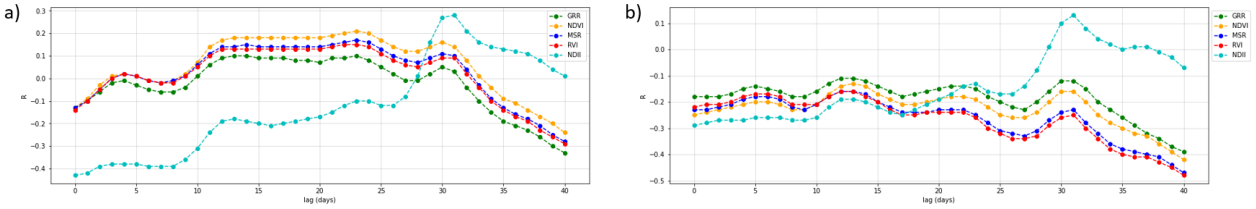

Figure 5.14: Correlation coefficient (R) between vegetation index and soil moisture with time lags up to 40 days for the harmonized Landsat data set at location Geerweg for a) sensors 1-3 and b) sensor 4. The lag means that soil moisture leads the vegetation index.

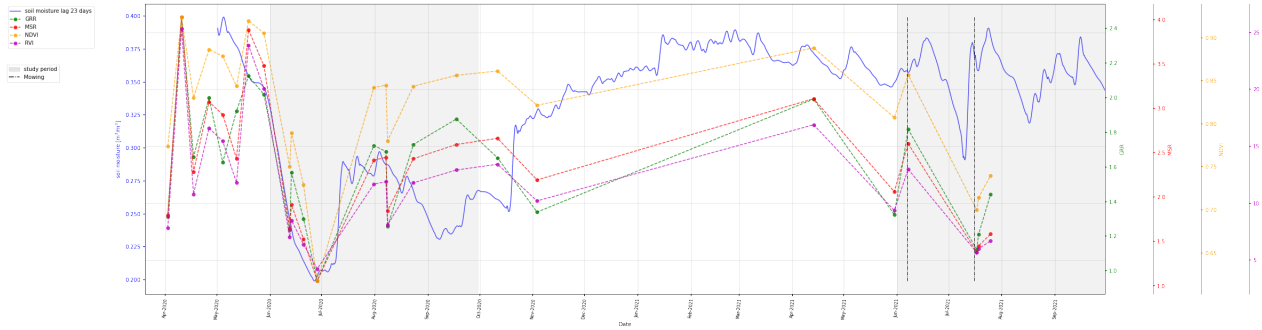

Figure 5.15: Graphs showing the pattern between lagged (23 days) soil moisture and VIs (extracted from harmonized Landsat 7 and 8 data set) at location Geerweg from sensors 1-3. VIs taken into account during June to September contain a vertical dashed line.

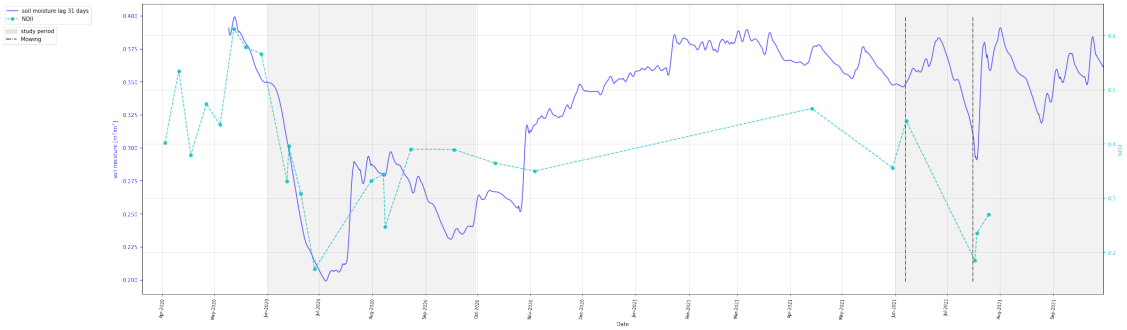

Figure 5.16: Graphs showing the pattern between lagged (31 days) soil moisture and NDII (extracted from harmonized Landsat 7 and 8 data set) at location Geerweg from sensors 1-3. VIs taken into account during June to September contain a vertical dashed line.

by Sentinel-2 during the 14th of June and 29th of July. The grass was mown on June 7th and July 16th, 2021 (indicated by the black dotted line), just before these vegetation indices were retrieved. Mowing can cause a sudden reduction in vegetation index values (Courault et al. (2010), Dusseux et al. (2014)). Figure 5.18 shows the difference in grass-cover before and after mowing. Unfortunately, the camera was only installed in May 2021 and therefore dates of mowing in 2020 were unknown. Furthermore, the sudden decrease in vegetation index from the 7th to the 8th of August 2021 was unexpected. Interestingly, such as sudden decrease can also be observed at location Bermweg during the exact same dates.

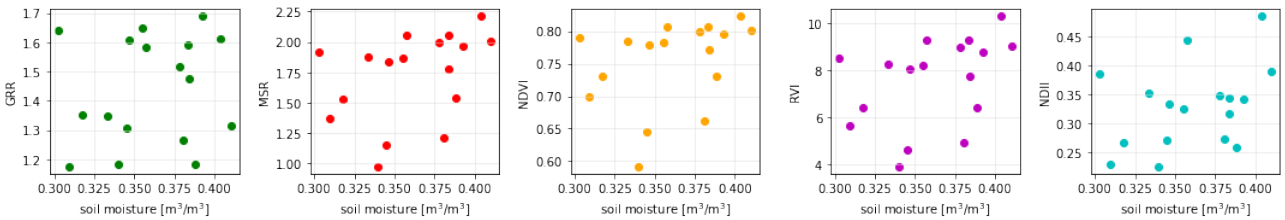

Figure 5.17: Scatter plots of VIs versus soil moisture at a 23 day lag for the GRR, MSR, NDVI, RVI, and a 31 day for the NDII. VIs were retrieved from the harmonized Landsat 7 and 8 data set at location Geerweg.

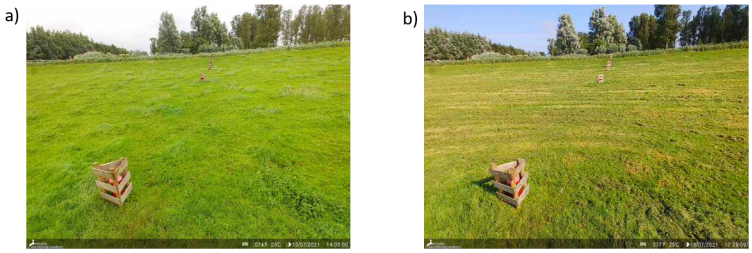

Figure 5.18: Photos giving an overview of location Geerweg (a) before mowing (July 15th, 2020) and (b) after mowing (July 16th, 2021).

5.2. SAR as a proxy for soil moisture

SAR operates at C-band and can therefore penetrate up to 5 cm deep below the soil surface and provide information about the upper part of the soil. Changes in surface soil moisture can be detected by SAR as it leads to a change in dielectric constant which causes a change in radar backscatter. Increasing soil moisture results in an increase in backscatter (ESA, 2021c). As there is a time lag between soil moisture at 5 and 20 cm depth, a time lag needs to be taken into account in the analysis. Furthermore, the study by Jamalinia et al. (2019) demonstrates that there is a lagged correlation between the leaf area index (LAI), which is sensitive to the cross-ratio VH/VV, and the water root-zone content, with an optimal lag at 15 days. To examine if SAR backscatter retrieved from satellite mission Sentinel-1 can give a proxy for soil moisture, a lagged relationship was examined between the in-situ soil moisture measurements at 20 cm depth and the retrieved backscatter at the two regional grass-covered dikes. A distinction was made between the ascending and descending orbit and also their corresponding incidence angle as this influences the signal. Pearson coefficients were calculated to measure the strength of the relationship.

Speckle noise affects SAR imagery and results in strong variations in pixels, whereas they have similar backscattering coefficients (Choi and Jeong, 2019). In order to reduce noise, it is important to retrieve backscatter over a larger area and not only take into account individual pixels. Figure 5.19 shows backscatter retrieved from 30 single pixels of the grass-cover at location Geerweg and shows strong variations for each pixel. To reduce noise, average backscatter was retrieved from several pixels surrounding the soil moisture sensors at both study locations. To further decrease speckle noise a Refined Lee filter was applied. Figure 5.20 shows a comparison of the area around location Bermweg before and after a Refined Lee speckle filter was applied and shows that the filter reduces speckle in the radar imagery.

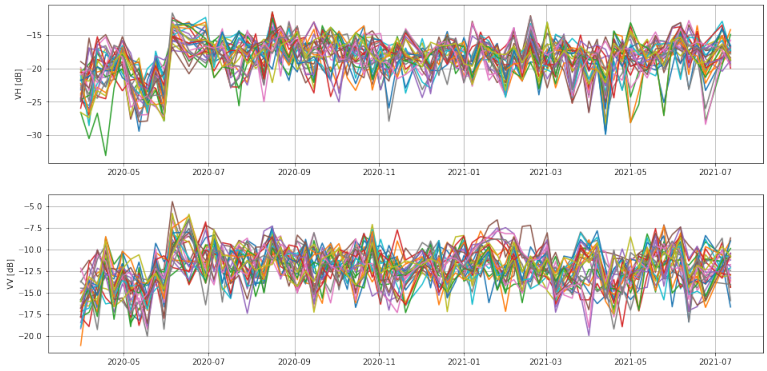

Figure 5.19: Graphs showing retrieved backscatter for polarizations VH and VV of 30 pixels surrounding soil moisture sensors at location Geerweg. Data is retrieved from Sentinel-1 imagery with an ascending orbit and an incidence angle of 33 °.

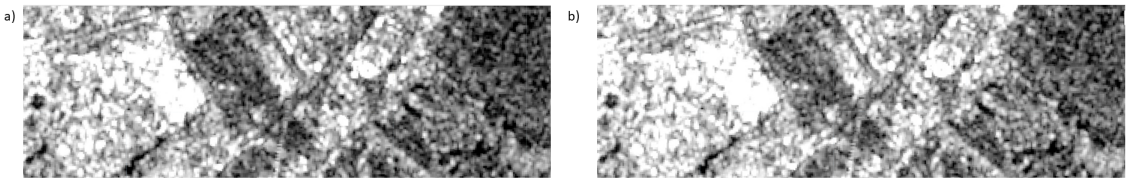

Figure 5.20: Comparison of image with and without Refined Lee speckle filter (S1 Ascending Orbit, image taken on May 2nd 2020). The left image (a) shows the S1 SAR image before speckle filtering was applied. The right image (b) presents the image after which the Refined Lee filter was applied.

As the dike has a slope, the orbit path of the satellite (i.e. ascending or descending) strongly affects the area which is illuminated by the sensor. The slope changes the angle of incidence, which is the angle between the radar sensor and the normal to the ground surface. Figure 5.21 illustrates the effect of a slope. If the area of interest on a dike would be orientated towards the west, the ascending sensor would illuminate this area better than the descending orbit. The slope of the dike could block the view of satellite sensors with a particular orbit path. It was therefore analyzed how the dikes of the study locations are orientated and if a particular orbit path would lead to better results. The region of interest of both dikes is sloped towards the North-West. It was therefore expected that the ascending orbit would better illuminate the region of interest.

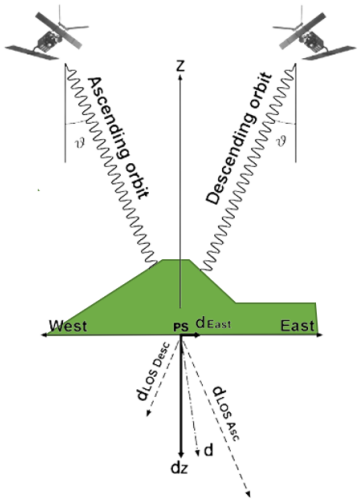

Figure 5.21: Illustration of the effect of the orbit path on the illuminated area. θ represents the radar look-angle. (Retrieved and edited from (Vilardo et al., 2009)).

Figures 5.22 and 5.23 display the retrieved Pearson correlation coefficients (R) between the VH, VV and cross ratio VH/VV when a time lag up to 20 days was taken into account. Only negligible and negative Pearson correlation coefficients were found. Figures 5.24 and 5.25 show the VH, VV and cross ratio VH/VV together with the soil moisture at 20 cm for the ascending orbit at location Bermweg and Geerweg when no lag was taken into account. When visually analyzing the graphs, no obvious relationship can be observed between retrieved backscatter and soil moisture, neither when a lag would be applied. High backscatter values do not correspond to high soil moisture values and vice versa. During the winter, VH and VV backscatter signals fluctuate a lot whereas the soil moisture values stay relatively constant. Furthermore, the overall backscatter retrieved from the VV channel was higher than the backscatter retrieved from the VH channel. The same behaviour can be observed in the graphs obtained from the descending orbits which can be found in Appendix C. The scatter plots between soil moisture and different polarizations are also displayed there, which confirms that the relationship was noisy.

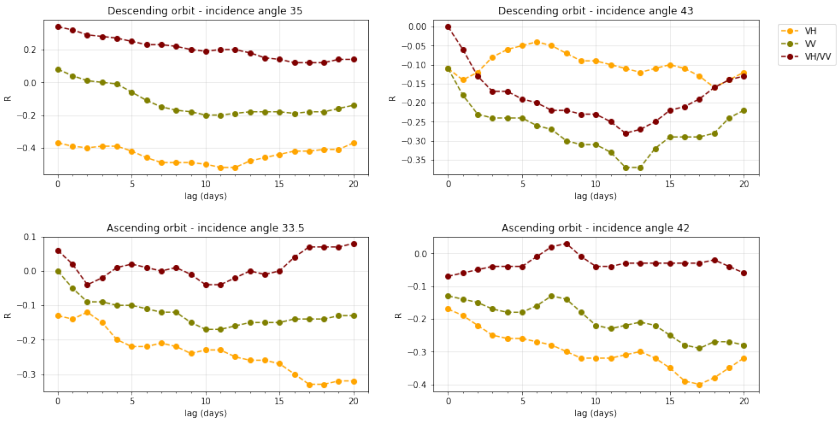

Figure 5.22: Correlation coefficient (R) between backscatter retrieved for polarizations VH, VV, cross ratio VH/VV and soil moisture with time lags up to 20 days at location Bermweg.

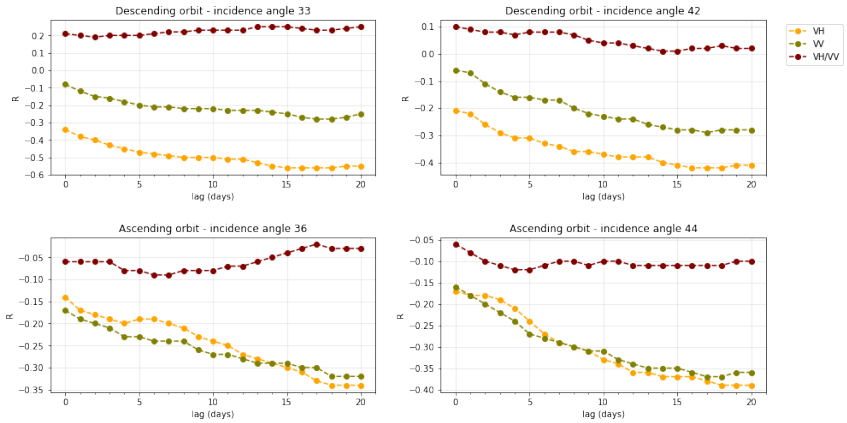

Figure 5.23: Correlation coefficient (R) between backscatter retrieved for polarizations VH, VV, cross ratio VH/VV and soil moisture with time lags up to 20 days at location Geerweg.

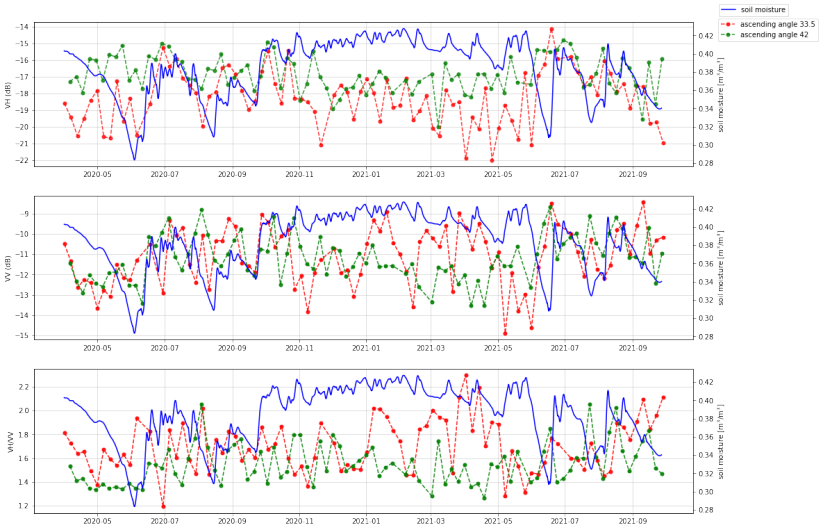

Figure 5.24: Graphs showing retrieved backscatter from satellite imagery with ascending orbit for polarizations VH, VV, cross ratio VH/VV and soil moisture at 20 cm depth at location Bermweg.

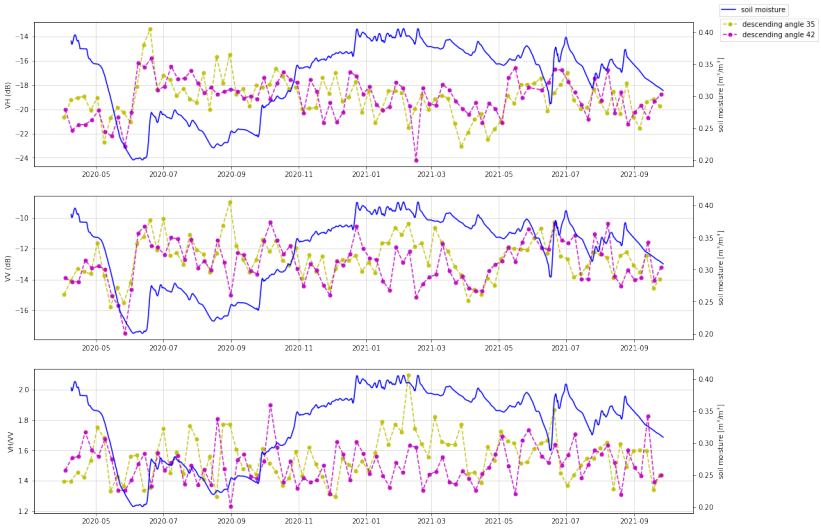

Figure 5.25: Graphs showing retrieved backscatter from satellite imagery with ascending orbit for polarizations VH, VV, cross ratio VH/VV and soil moisture at 20 cm depth at location Geerweg.

5.3. Vegetation indices and precipitation deficit

Precipitation deficit can be used as a proxy for soil moisture since a decrease of soil moisture content occurs when the outflux of water is bigger than the influx. It was assessed if there is a relationship between cumulative precipitation deficit and vegetation indices to explore if vegetation indices could be used to give a proxy for soil moisture within a dike.

Precipitation and evapotranspiration data were extracted from raster data retrieved from Meteobase, which has a cell size of 1 km^2. Data was retrieved from the grid cells where the study sites were located. The time series shown in figure 5.26 shows the precipitation and evapotranspiration for location Bermweg and Geerweg in 2019.

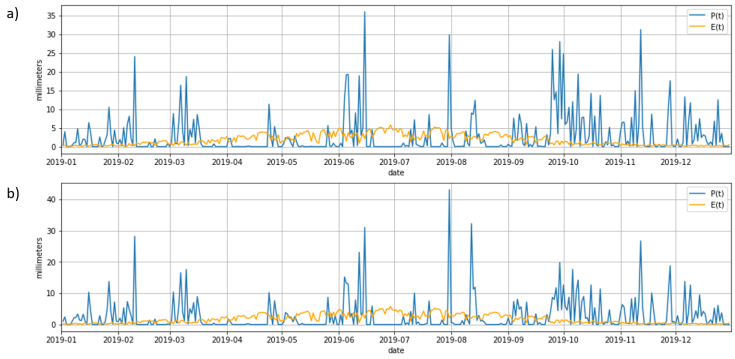

Figure 5.26: Precipitation and evaporation time series for 2019 at a) location Bermweg and b) location Geerweg.

When the precipitation time series is subtracted from the evapotranspiration time series, the precipitation deficit time series is obtained. The cumulative precipitation deficit is defined as the cumulative difference between precipitation and evapotranspiration for a certain time period. This time series can be obtained by using equation 4.7. Figure 5.27 shows the cumulative precipitation time series deficit for a period of 30 days, from 2013 to 2020 at both study locations. Negative values indicate dry conditions and positive values indicate excess precipitation.

Figure 5.27: Cumulative precipitation deficit for a period of 30 days at a) location Bermweg and b) location Geerweg from 2013 up until 2020.

To explore if there is a relationship between precipitation deficit and retrieved vegetation indices, Pearson correlations were calculated for the period June to September. Correlation coefficients were computed between the vegetation indices and the cumulative precipitation deficit for time periods of 10 to 90 days, as a small period of history will not account for enough history and a too large period of history will introduce noise.

The satellite imagery from Landsat 7 and 8 was available since April 2013, whereas the Sentinel-2 data set was available since March 2017. Therefore, the number of samples used to explore a relationship was larger for Landsat 7 and 8 compared to Sentinel-2. The exact number of images used to calculate the Pearson correlation coefficients can be found in section 4.6. Figure 5.28 and 5.29 show the calculated correlation coefficients for the time period 10 to 90 days at location Bermweg and Geerweg respectively for the different satellite missions. Only the graphs for the GRR, MSR and NDII are displayed. The graphs for the other vegetation can be found in

Appendix D. As calculating Pearson correlations is solely recommended when the sample size is at least 25, only the correlations from Landsat 8 and the Harmonized Landsat 7 and 8 data set were tested for their statistical significance and are shown in Appendix D.

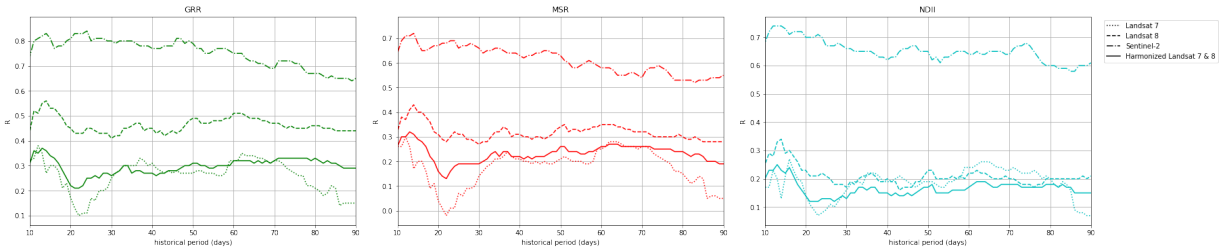

Figure 5.28: Calculated Pearson correlation coefficients (R) between vegetation indices (GRR, MSR, NDII) and cumulative precipitation deficit for different satellite missions at a) location Bermweg and b) location Bermweg during June to September. The historical period refers to the period taken into account when calculating the cumulative precipitation deficit.

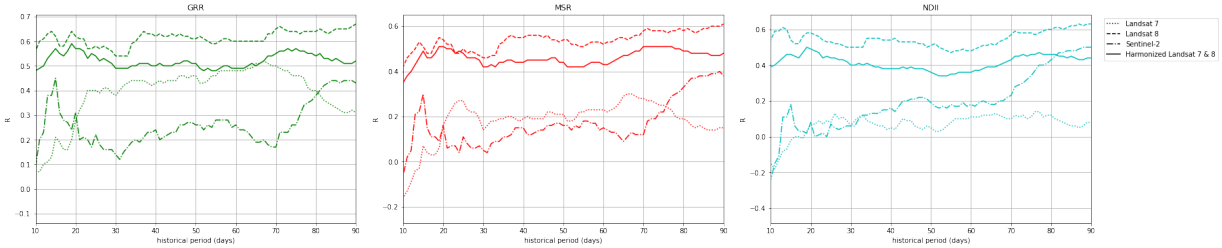

Figure 5.29: Calculated Pearson correlation coefficients (R) between vegetation indices (GRR, MSR, NDII) and cumulative precipitation deficit for different satellite missions at a) location Bermweg and b) location Geerweg during June to September. The historical period refers to the period taken into account when calculating the cumulative precipitation deficit.

The results show that in all graphs, a positive correlation can be found between precipitation deficit and the retrieved vegetation indices. The historical period resulting in the strongest correlation at location Bermweg was found around 15 days for all (harmonized) satellite missions. A strong correlation (R=0.68-0.82) was found for Sentinel-2 and a negligible correlation (R=0.24-0.36) for the harmonized Landsat 7 and 8 data set. The calculated correlation coefficients of the harmonized Landsat 7 and 8 data set were statistically significant ($p < 0.05$) for all vegetation indices except for the NDVI and the NDII. The calculated correlation was weak and statistically significant for Landsat 8 (R=0.38-0.56) and negligible (R=0.12-0.27) for Landsat 7.

At location Geerweg, the historical period leading to the strongest correlation varies largely for each (harmonized) satellite mission. A significant weak correlation was found for the harmonized Landsat 7 and 8 data when a historical period of 20 days was taken into account (R=0.47-0.57). For Sentinel-2, Landsat 7 and Landsat 8 the optimal historical period was around 15, 65, and 90 days respectively. The correlation for Sentinel-2 was weak (R=0.24-0.45), for Landsat 8 moderate statistically significant (R=0.49-0.62), and for Landsat 7 negligible (R=0.06-0.21).

Overall, the GRR has the strongest correlation with precipitation deficit. The GRR uses the red and green bands, whereas the other indices use the red, NIR, and SWIR bands. The GRR is sensitive to changes in green colour. When vegetation experiences water stress, this results in a greater proportional increase in red reflectance than in green (Carter, 1993). The indices using the red and NIR bands (MSR, NDVI, RVI) are more sensitive to chlorophyll variation. Chlorophyll strongly reflects in the near-infrared and red bands, and can therefore give an indication of vegetation health (NASA, 2021c). The NDII uses the NIR and SWIR bands and can be used to detect plant water stress as solar radiation in the SWIR band is absorbed by liquid water.

Many satellite missions show an increase in correlation coefficient as the historical period increases from 10 to approximately 15 days. The trend of the graph for a large historical period differs for each satellite mission and location. Some graphs show a decrease in the correlation coefficient when the historic period becomes very large (over 60 days). In other graphs, however, the correlation coefficient increases or stagnates when a historical period over 60 days was taken into account.

Figure 5.30 illustrates scatter plots between vegetation indices extracted from the harmonized Landsat 7 and 8

data set and precipitation deficit when a historical period of 14 days was taken into account at location Bermweg. The scatter plots show that there is a large amount of noise. Many outliers in the graphs can be assigned to the year 2013. These outliers in the year 2013 could also be found in scatter plots of the NDVI and RVI (see Appendix D). The vegetation index values were relatively low for the corresponding precipitation deficit. When analyzing the precipitation deficit graph of location Bermweg in figure 5.27, the precipitation surplus at the beginning of the year 2013 was lower compared to other years. At location Geerweg, outliers do not specifically correspond to the year 2013 (see figure 5.31).

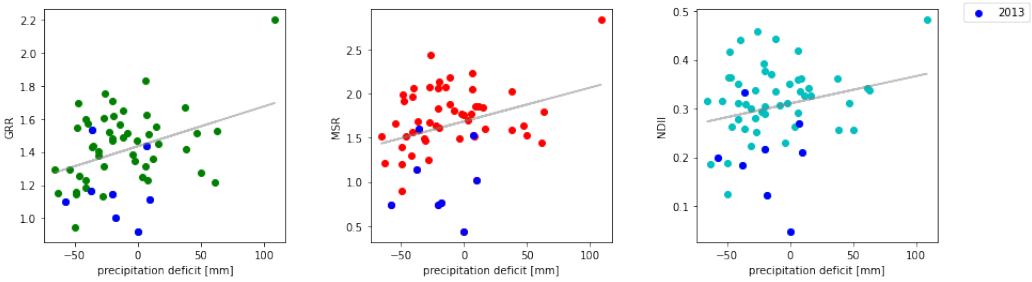

Figure 5.30: Scatter plots between the GRR, MSR, NDII and a cumulative precipitation deficit of 14 days at location Bermweg during June to September. Vegetation indices retrieved during year 2013 are coloured in blue.

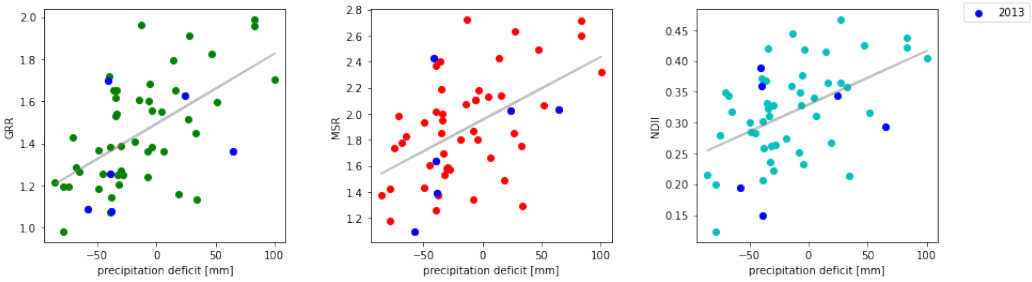

Figure 5.31: Scatter plots between the GRR, MSR, NDII and a cumulative precipitation deficit of 20 days at location Geerweg during June to September. Vegetation indices retrieved during year 2013 are coloured in blue.

5.4. Spatial-temporal analysis

For a river dike section at the Amsterdam-Rhine canal, information is available about a specific area of the dike which experienced wetting at the inner slope of the dike due to a clogged drainage system (A. Lievens, personal communication, 14th of April, 2021). The clogged drainage system led to an increase in pore water pressure, leading to an increase in phreatic level and resulting in a wet area at the inner slope. A spatial-temporal analysis was performed to examine and model the behaviour of the allegedly wet area and the reference area (no wetting), to investigate if a difference could be found by remote sensing data.

5.4.1. Vegetation Indices

Vegetation indices were retrieved from different pixels surrounding the wet and reference area. It was hypothesized that a difference could be observed between the acquired vegetation indices from the non-wet area and the wet area. Especially during dry periods when vegetation in the reference area might experience water stress whereas the wet area does not.

The limitations of spatial resolution of open data satellite missions are clearly highlighted when analyzing this particular problem. As the spatial resolution of Landsat 7 and 8 is quite coarse, 30 meters, these satellite missions were not suitable to extract vegetation indices solely for the inner slope area of the dike, as the area of interest was only 10 meters wide. Results of the Landsat 8 analysis for the two different areas can be found in Appendix D but will not further be discussed.

Figure 5.32 illustrates the mean value of the pixels extracted from Sentinel-2 from the wet and reference area, with a surrounding polygon representing plus/minus one standard deviation. The graph shows that only small differences can be detected between the allegedly wet area and presumed reference area. Vegetation indices retrieved during April 2018 are slightly higher for the wet area, and in 2020 small differences can be detected during April and May. However, from these dates onwards the difference is non-existent. It is known that every year, the first mowing is carried out between the 15th of June and 15th of July, followed by a second mowing in the period ranging from the 15th of August and 22nd of September (K. Speijker, personal communication, September 20 2021). Mowing can cause a sudden reduction in vegetation index values and therefore overrule natural variation of vegetation in response to soil moisture (Courault et al. (2010), Dusseux et al. (2014)). Figure 5.33 shows the distribution of vegetation index values retrieved from the wetted and reference area during the months June to September in 2018, 2019 and 2020. The density curves show no obvious difference between the areas.

The cumulative precipitation deficit for a historical period of 15 days and daily precipitation were also displayed, to analyse if these meteorological indicators could clarify observed vegetation index trends. The effect of precipitation and precipitation deficit on vegetation indices could be seen in the graphs. It was observed that in March 2018, less rain fell compared to March 2019 and 2020. The retrieved vegetation index values were also relatively lower during March 2018. Furthermore, the precipitation deficit in the summer of 2018 was larger when compared to 2019 and 2020. In the vegetation index graphs it can be observed that in the summer of 2018, the retrieved GRR and NDVI are lower than in 2019 and 2020. This distinction cannot be depicted when analyzing the MSR and RVI graphs. Furthermore, it was interesting to see that during dry periods (negative precipitation deficit) more images are retrieved than during wet periods. This effect can be seen during June and July 2018 and during April and May 2020.

5.4.2. SAR

Earlier results (section 5.2) have shown that there was no (lagged) correlation between soil moisture at 20 cm depth and SAR backscatter. This could be due to the fact that the topsoil (~ 5 cm) which is sensed by SAR, is more dynamic than soil moisture at 20 cm depth. At the allegedly wet area, the topsoil was very wet. Therefore it was investigated if a temporal difference could be seen between the wet and reference area by SAR backscatter. A distinction was made between the ascending and descending orbit, and their corresponding incidence angle, as these features influence the signal. To reduce noise, a refined-Lee speckle filter was applied and the average backscatter was retrieved.

Because the wet area was at the inner slope of the dike, which is orientated towards the North-East, it was expected that the descending sensor was able to best illuminate the area of interest. Figures 5.34 and 5.35 illustrate the retrieved backscatter for polarizations VH, VV and cross ratio VH/VV from the descending orbit for the two different areas. Backscatter retrieved from the ascending orbit can be found in Appendix D. Table 5.1 shows

Figure 5.32: Extracted vegetation indices from Sentinel-2 from 2017 up until 2020. The blue line represents the mean values from the pixels within the wetted area and the red line the reference area. The shaded value represents the one standard deviation above or below the mean value. The first chart represents the precipitation deficit when a historical period of 15 days is taken into account. The second chart represents the daily precipitation.

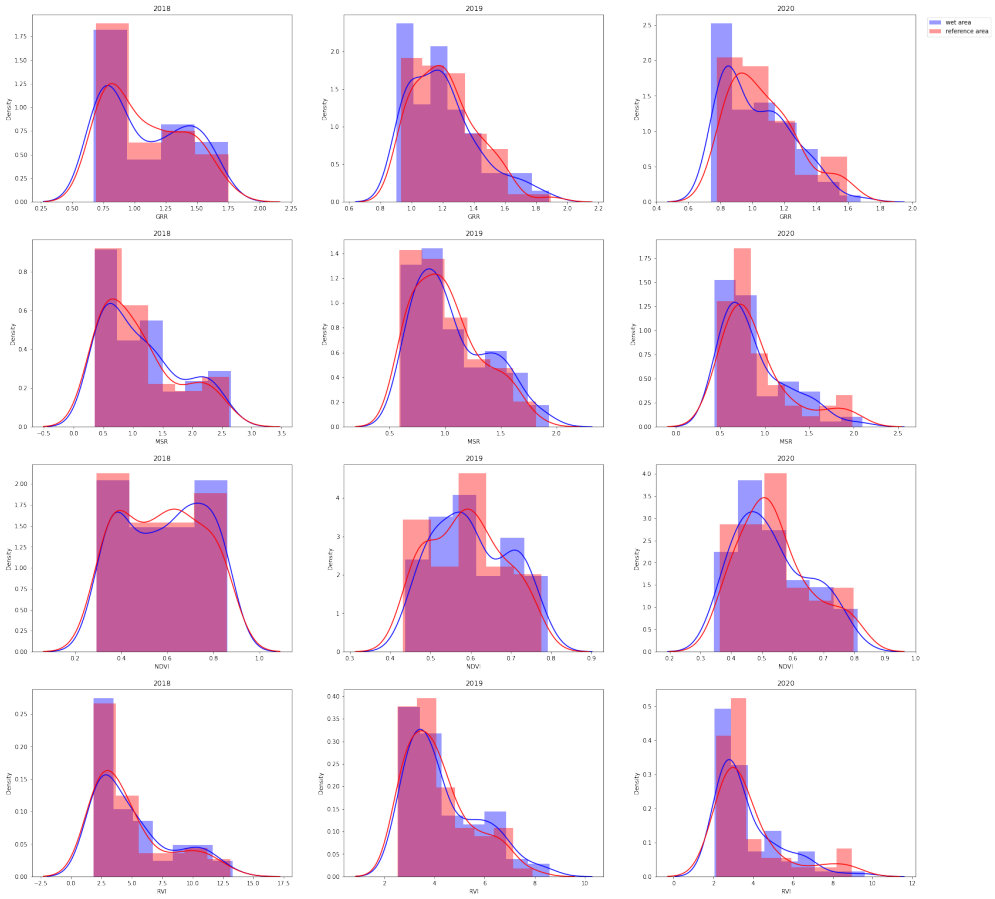

Figure 5.33: Plots representing the distribution of vegetation index values retrieved from the wetted and reference area during June to September.

the mean values of the backscatter retrieved from the wet and reference area. The results show that overall, the backscatter from the wet area is lower throughout the years, for both the ascending and descending orbit. The overall trend of the wet and reference area is very similar. As it was known that the wet area is wetter during high water periods than during low water periods, it was therefore examined if a difference in backscatter can be observed between these two periods. The three highest and lowest water levels were highlighted in the backscatter plots. No larger difference in backscatter could be seen between the two areas during high and low water periods.

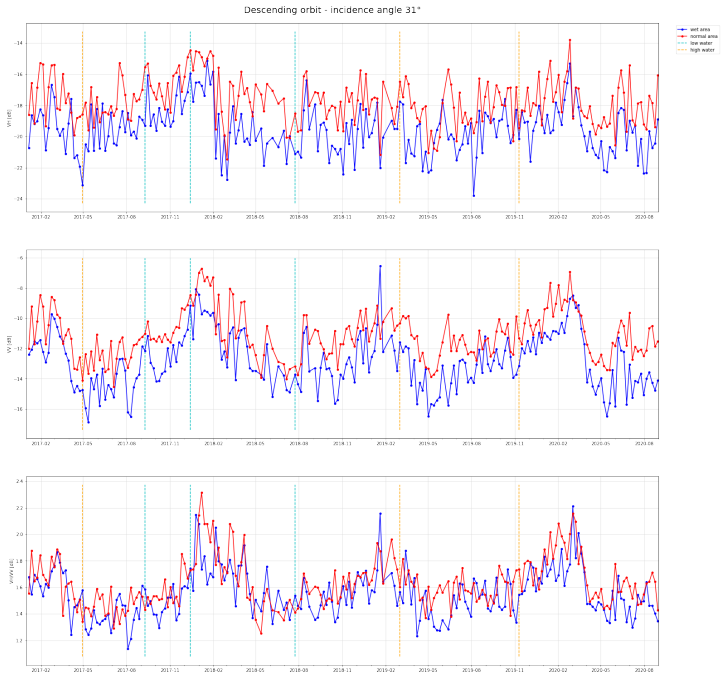

Figure 5.34: Graphs showing the retrieved backscatter for polarizations VH, VV, cross ratio VH/VV at the Amsterdam-Rhine canal. Data is retrieved from satellite imagery with descending orbit and incidence angle 31.

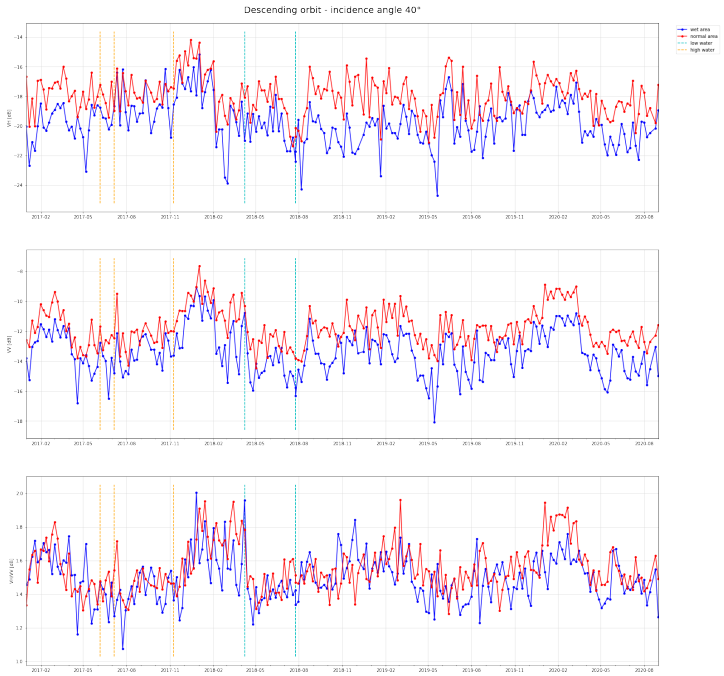

Figure 5.35: Graphs showing the retrieved backscatter for polarizations VH, VV, cross ratio VH/VV at the Amsterdam-Rhine canal. Data is retrieved from satellite imagery with descending orbit and incidence angle 40.

			Mean		
Orbit path	**Incidence angle**	**Area**	**VH**	**VV**	**VH/VV**
Descending	31	Wet	-18.83	-12.13	1.58
		Dry	-17.71	-11.12	1.63
	40	Wet	-19.77	-13.40	1.50
		Dry	-17.98	-11.76	1.55
Ascending	37	Wet	-18.83	-12.12	1.58
		Dry	-16.9	-10.65	1.61
	45	Wet	-19.07	-13.12	1.47
		Dry	-17.36	-11.29	1.56

Table 5.1: Mean values of backscatter retrieved from wet and reference area.

6

Discussion

The results presented in the previous section will be discussed in this chapter. Moreover, the methodological approach conducted to obtain the results will be re-evaluated by taking into account the underlying assumptions and limitations.

6.1. Reflection of results

6.1.1. Vegetation indices as a proxy for soil moisture

It was investigated how strong the lagged relationship is between vegetation indices (GRR, MSR, NDVI, RVI, and NDII) retrieved from optical remote sensing imagery and in-situ soil moisture measurements at 20 cm depth for two regional grass-covered dikes. A lag refers to the time delay that vegetation indices respond to soil moisture.

At location Bermweg the optimal correlation was found when a lag of around 30 days was applied. However, the correlation between the vegetation indices and soil moisture was weak for the MSR, NDVI, RVI, and NDII (R=0.32-0.40) and negligible for the GRR (R=0.19). A general increase in correlation coefficients could be observed when the time lag between soil moisture and vegetation indices increases from 0 to 30 days, after which the correlation decreases again. This demonstrates that there is a time lag of vegetation response to soil moisture. At location Geerweg the optimal correlation (R=0.10-0.21) was found for a time lag of 23 days for all vegetation indices except the NDII for one pixel. For the other pixel, only negative correlations were found. Negative correlations are inconsistent with the expectations that low soil moisture values correspond to low vegetation index values and vice versa. The results for the NDII, which uses the NIR and SWIR bands, gives a different optimal lag. For the two pixels, the optimal correlation (R=0.13-0.28) was found when a 31 day lag was applied. However, this correlation was also negligible. Interestingly, the optimal time lag between soil moisture and the NDII was identical (31 days) at both locations.

The grass-cover at location Bermweg was maintained grazing whereas the grass-cover at location Geerweg was maintained by both grazing and mowing. A negligible correlation could be found at location Geerweg. The results clearly show that mowing overrules the natural variation of vegetation to soil moisture as mowing can lead to a sudden decrease of vegetation indices (Courault et al. (2010), Dusseux et al. (2014)). The effect of grazing was more constant since the grass was maintained by grazing throughout the whole season, which could explain the higher correlation coefficient at location Bermweg. However, also at location Bermweg the correlation is weak. The results should be interpreted with care as statistical significance cannot be demonstrated due to the small sample size.

The results indicate that vegetation indices cannot give an indication of soil moisture dynamics in the root-zone, which demonstrates that many other factors affect the vegetation index. First of all, a direct relationship was assessed between soil moisture at 20 cm depth and vegetation state, whereas vegetation state is not solely dependent on soil moisture but is also affected by other factors such as radiation, temperature, and nutrient availability (Bradley et al., 1998). Secondly, pre-processed imagery was used which is imagery corrected for variations in atmosphere, illumination, and viewing geometry between images, which enables to compare imagery acquired at different epochs (i.e. time of day, season, year). However, it is challenging to convert TOA

reflectance to surface reflectance by performing atmospheric corrections as the impact of aerosols in the visible and NIR spectral range can be difficult to correct because of the complex scattering and absorbing properties of aerosols (Vermote et al., 2016). In August, vegetation values abruptly decrease from one day to another at both study locations. However, when camera photos at location Bermweg are investigated from both days, no large difference can be depicted. This shows that differences might have occurred due to scene-to-scene variability. Furthermore, vegetation indices are not very sensitive to short-term soil moisture variations as vegetation state depends on long-term soil moisture availability (Fensholt and Sandholt, 2003). A short increase or decrease will have minimal to no effect on the vegetation as it takes some time before plants respond to water stress in the root-zone. Also, vegetation can create a small water reserve which helps to sustain during short periods of drought. The analysis also takes into account short-term variations, which influences the calculated correlation coefficients.

The analysis exploring the effect of pixels containing both water and vegetation shows that the retrieved vegetation index values of water fluctuate throughout the years. As the influence of water is not constant, it is necessary to take into consideration that fluctuations in vegetation index values are not only because of changes in vegetation state but could also be because of changes in the spectral reflectance of water. The changes in water reflectance values can be caused by different factors such as algae and soil particles (turbid water). Overall, pixels contaminated with water tend to underestimate retrieved vegetation index values.

Additionally, it was interesting to see that vegetation indices retrieved by Sentinel-2 from the pixel where sensor 5 was located, fluctuate throughout the year as much as vegetation indices retrieved from pixels where sensors 1-4 were located. It was expected that the time series would be less dynamic as the soil moisture time series of sensor 5 at 20 cm depth was constant throughout the year. This is because sensor 5 mainly measures in the saturated zone, due to the geometry of the dike. It is known that when the water table rises close to the surface, the root growth decreases and eventually stops because plants need oxygen for root respiration (Osman, 2018). Therefore, the soil moisture measurements at 20 cm depth might not be representative for water accessible to the root-zone, as the vegetation around sensor 5 responds to soil moisture fluctuations in the topsoil, where soil moisture is not constant and does fluctuate.

Moreover, the results clearly show the limitations of optical remote sensing imagery as due to cloud and cloud shadow contamination, satellite imagery might not be available for extended periods of time. At location Bermweg, the dry period in July 2020 could not be detected by the harmonized Landsat 7 and 8 data set. However, it could be detected by Sentinel-2 imagery. This illustrates that if optical remote sensing data wants to be implemented to contribute to dike inspections, it is important to increase observation frequency to get a complete overview of the data in order to get a better insight into the dynamics of vegetation indices over time. This can be done by merging satellite missions.

In addition to the points mentioned above, it was interesting to see that at location Bermweg, soil moisture values in 2021 reached values as low as in 2020. These low soil moisture values in 2021 were detected by low vegetation index values. However, 2021 was not characterized as a dry year by the Koninklijke Nederlands Meteorologisch Instituut (KNMI) as the local precipitation deficit did not exceed 100 millimeters. The drought indicator used by the KNMI is the cumulative precipitation deficit from April 1st up until October 1st. Only when a precipitation deficit of 150 or 200 millimeters is reached, dike inspections are executed more frequently and measurements are taken (Zoelen (2021), RTL (2013)). The study by Strijker (2021) demonstrates that the drying out of dikes is very dynamic and complex and shows that the cumulative precipitation deficit cannot always give a good indication of soil moisture within dikes. There are a lot of factors such as geometry type, vegetation, and subsoil that affect soil moisture in dikes. It highlights the need of combining various data sources to give a proxy for soil moisture. The results show the potential added value of remote sensing to dike inspections, as (unexpected) low vegetation index values, which go unnoticed by traditional drought indicators such as the cumulative precipitation deficit, could raise red flags. However, low vegetation index values do not always indicate low soil moisture values, especially when grass covers are mown. At location Geerweg, vegetation index values during July 2021 reach values as low as during the dry period in 2020 although soil moisture values during July 2021 are relatively higher. This effect can be attributed to mowing.

Furthermore, the results clearly show the downside of using single point measurements instead of averaging out soil moisture values retrieved from numerous field measurements. At location Geerweg the soil moisture time series of the different sensors were very different during the dry period in 2020, whereas they were located relatively close to each other (within 5 meters). Two of the four sensors did not respond to the rainfall after the dry period in July 2020. This demonstrates that it is difficult to get a representative soil moisture time series if

soil moisture values are based on soil moisture measurements retrieved from a single sensor. The difference in soil moisture time series can be assigned to local variations such as subsoil or preferential flow paths. When the potential relationship between the soil moisture measurements and vegetation indices was assessed, soil moisture values of single sensors were taken into account. However, this might not give an accurate representation of the soil moisture and hence influences the results.

Although no strong relationship was found between soil moisture and vegetation indices in this research, various studies in literature show that there is a correlation between vegetation indices and soil moisture (Wang et al. (2007), Nicholson and Farrar (1994), Musyimi (2011), Zhang et al. (2018)). Cundill (2016) has demonstrated that there is a moderate relationship between vegetation indices obtained from a multispectral camera and soil moisture. The research shows that dike inspectors could potentially use vegetation indices to give an indication of long-term soil moisture. To evaluate if satellite imagery could be used, the index values of different satellite sensors were simulated using sensor specific spectral response functions. Results showed that also remote sensing data from satellites with a relatively low spatial resolution (i.e. 5 meters) performed relatively well in finding a correlation (R>0.550) between vegetation indices acquired from optical remote sensing imagery and soil moisture in grass-covered dikes. However, with the methodology implemented in this study, no strong (lagged) relationship was found between soil moisture and vegetation indices acquired from satellite imagery.

6.1.2. SAR as a proxy for soil moisture

It was investigated how strong the (lagged) relationship is between SAR backscatter amplitude and soil moisture at 20 cm depth at two regional grass-covered dikes. Increasing soil moisture content results in an increase in dielectric constant and should therefore lead to a higher radar backscatter intensity (ESA, 2021c). As SAR measures the top few centimeters of the soil, there is a time lag of 1 to 2 days with the soil moisture in deeper layers (Carranza et al., 2018). Furthermore, it is known that there is a lagged correlation between LAI and the water root-zone content with an optimal lag at 15 days (Jamalinia et al., 2019). Several studies have shown that there is a strong correlation between backscatter intensity and LAI. The LAI is particularly sensitive to the cross-ratio (VH/VV) (Vreugdenhil et al., 2018). Accordingly, it was expected that a lagged relationship could be found between SAR backscatter and soil moisture. Therefore, a time lag was taken into account in the analysis.

Literature shows that VV-polarization is less affected by vegetation and should therefore be most sensitive to soil moisture (Bousbih et al. (2017), Benninga et al. (2020)). However, no (lagged) relationship could be observed between the retrieved backscatter and the soil moisture time series. Negative correlations were calculated for both VH, VV polarized backscatter whereas a positive correlation was expected, as an increase in soil moisture should lead to increasing backscatter values. Overall, the backscatter retrieved from the VH polarization is lower than the backscatter retrieved from the VV polarization. VV signals are related to surface scattering while VH signals are usually more sensitive to volume scattering (i.e. within vegetation). The VH channel measures the part of the waves which are polarized at the surface and returned horizontally to the sensor. This does not happen to a large extent. Furthermore, no lagged correlation could be observed between the cross-ratio VH/VV (most sensitive to LAI) and soil moisture at 20 cm depth. It was assumed that the descending orbit would better illuminate the area of interest at both study locations since the area of interest is sloped towards the North-West. However, backscatter retrieved from the descending orbit did not lead to better results. The backscatter graphs show that during the winter period, the backscatter retrieved from both VH and VV backscatter was very dynamic, whereas soil moisture values were relatively constant. This clearly demonstrates the sensitivity to other factors than soil moisture or LAI.

SAR C-band senses the topsoil, (~ 5 cm) where soil moisture is much more dynamic than soil moisture at 20 cm depth. Moreover, the area over which the backscatter was retrieved was relatively small, leading to relatively high speckle noise. Additionally, the signal interacts with various components of the surface, which can affect backscatter as much, or more than, soil moisture. Topography of the terrain, vegetation density, and surface roughness are all parameters that largely affect backscatter, leading to the insensitivity for soil moisture (Altese et al., 1996). There is no simple or straightforward method to correct for these parameters (Jackson et al., 1996). Grass-covered dikes are covered by relatively dense vegetation which can lead to volume scattering (the scattering of radar within a medium) and introduce another level of complexity. Also, management practices such as mowing or grazing affect the backscatter signal observed by Sentinel-1, as the volume scattering of SAR depends on physical properties of the object such as height (Bakker et al., 2004). Furthermore, the slope affects the retrieved backscatter. When a surface is tilted, without alternating the antenna orientation, the backscatter signal is rotated about the radar line of sight. Also, rainfall and dew affect retrieved backscatter. When data

is acquired shortly after rain or dew, the water present on the vegetation can influence retrieved backscatter. The descending orbit satellite passes over around six o'clock in the morning at both study locations when dew is present on the vegetation. The effect of these parameters should be quantified and removed from the total backscatter to acquire an accurate estimate of the surface soil moisture (Panciera and Monerris, 2013). The use of a soil moisture retrieval algorithm is recommended to take into account these different components. Available Sentinel-1 soil moisture content products like Bauer-Marschallinger et al. (2018) use retrieval methods to estimate soil moisture values, not the directly observed backscatter as the influence of other parameters needs to be estimated as well (ASF, 2021). Spatial resolutions of these products are coarse (1 kilometer) since data needs to be aggregated to lower spatial resolution in order to reduce the noise level of backscatter (Esch, 2018). Furthermore, the sensitivity of backscatter to LAI can only give an indirect proxy of soil moisture, which makes it very complex as there is already a lot of noise present in the backscatter signal.

6.1.3. Vegetation indices and precipitation deficit

It was investigated how strong the relationship is between precipitation deficit and vegetation indices obtained from optical satellite imagery. Precipitation deficit is defined as the difference between precipitation and evapotranspiration. The effect that precipitation deficit has on vegetation health is a slow process of accumulation of precipitation deficit and is related to not only the current but also to the cumulative effect of earlier precipitation deficit (Wang et al., 2016). Therefore, a historical period was taken into account. Correlation coefficients were computed for a historical period of 10 to 90 days. As a larger sample size gives a more reliable result, data from Landsat 7 and 8 was harmonized to increase the number of data points. The sample size of the Landsat 8 data set and the harmonized Landsat 7 and 8 data set was large enough to draw a conclusion about the statistical significance (sample size > 31).

At location Bermweg, the correlation was optimal when a historical period of around 15 days was taken into account for all (harmonized) satellite missions. The optimal correlation for the harmonized Landsat 7 and 8 data set was weak (R=0.24-0.36). The correlations were statistically significant ($p < 0.05$) except for the NDVI and NDII. The calculated correlation coefficients were moderate and statistically significant for Landsat 8 (R=0.38-0.56), negligible for Landsat 7 (R=0.12-0.27) and very strong (R=0.68-0.82) for Sentinel-2. At location Geerweg the optimal correlation coefficient was found for a historical period of around 15, 20, 65 and 90 days for Sentinel-2, the harmonized Landsat 7 and 8 data set, Landsat 7 and Landsat 8 respectively. A statistically significant moderate correlation was found for the harmonized Landsat 7 and 8 data set (R=0.47-0.57). The correlation for Sentinel-2 was weak (R=0.24-0.45), for Landsat 8 moderate statistically significant (R=0.49-0.62) and for Landsat 7 negligible (R=0.06-0.21). Overall, for all satellite missions, the strongest correlation was found for the GRR, which uses the red and green bands.

Although weak to strong correlations were found for the different satellite missions at both locations, the graphs which illustrate the calculated Pearson correlation coefficients for a cumulative period from 10 to 90 days show that the patterns of the graphs from the different satellite missions do not correspond. This is contrary to expectations as an equal pattern was expected as the satellite missions explore the same relationship. However, it should be noted that the different satellite missions extract vegetation indices at different moments in time and therefore use different vegetation index data to calculate the correlation coefficients. Consequently, this influences the results. Furthermore, calculated correlation coefficients do not vary much when the cumulative period taken into account increases from 10 to 90 days. However, it was expected that a short period (< 10 days) of history will not have an effect on retrieved vegetation indices as only a sufficiently long period of precipitation deficit or surplus will affect the vegetation state. When the cumulative period becomes very large (> 60 days) it was expected that correlation coefficients decrease because including too much history will result in an excess of data. This expected pattern cannot be seen in the graphs and show that correlation does not always imply causality.

At location Bermweg many outliers could be detected in the scatter plots showing the relationship between soil moisture and precipitation deficit, of which many correspond to the year 2013. The vegetation index values were relatively low for the corresponding precipitation deficit. Because at the beginning of 2013 the precipitation surplus was very low compared to other years, this could have led to relatively lower soil moisture values at the beginning of the year. This has resulted in lower water availability for the vegetation, restricting vegetation growth and leading to these outliers. Interestingly this consequence cannot be seen at location Geerweg. This clearly shows the dependence on multiple factors which are location-dependent such as subsoil and vegetation.

6.1.4. Spatial-temporal analysis

A spatial-temporal analysis was executed to investigate if a difference could be detected by remote sensing data between the behaviour of an allegedly wet area, due to a clogged drainage, and a non-wet area (reference area). It was hypothesized that a difference could be found between the acquired vegetation indices from the two areas, especially during dry periods, assuming that in the wet area roots had access to more water than in the reference area. Furthermore, it was expected that a difference could be depicted by SAR backscatter, as standing water results in lower backscatter values.

Differences between the two areas found by vegetation indices were negligible, also during dry periods. This could be due to the mowing of the area. The exact dates of mowing are unknown, however, it is known that every year the first mowing is carried out between the 15th of June and the 15th of July and the second time between the 15th of August and 22nd of June (K. Speijker, personal communication, September 20, 2021). This is the period of the year when droughts typically occur. Mowing can result in a sudden reduction in vegetation index values (Courault et al. (2010), Dusseux et al. (2014)). Furthermore, the cut grass is not immediately removed and it can take up to 10 days before this is done (K. Speijker, personal communication, September 20, 2021). Hence, after mowing, the natural variation of vegetation in response to soil moisture is overruled which might explain the fact that no difference could be seen. The effect of precipitation deficit on the overall trend of vegetation indices could be clearly observed. When during March 2018 less rain has fallen compared to 2019 and 2020, this results in lower vegetation indices and show that dry periods (low soil moisture) lead to lower vegetation index values. It was interesting to see that during dry periods, more images were retrieved as there were fewer clouds. This is beneficial for the potential implementation of vegetation indices to monitor dikes during dry periods when monitoring soil moisture is crucial as droughts can lead to a decrease of dike stability.

It was also investigated if a difference could be observed between the two areas by SAR backscatter. The area of interest is sloped towards the North-East and therefore it was expected that the descending orbit can better illuminate the areas of interest. However, results show that backscatter (VH and VV polarization) retrieved from both the ascending and descending orbit demonstrate that the backscatter retrieved from the wet area is lower than the backscatter acquired over the reference area. Wetting can lead to standing water, which leads to lower backscatter values and could explain the lower backscatter signal retrieved from the wet area (Liu, 2016). No larger difference could be observed between the areas during extreme high water periods and extremely low water, although it was known that during high water the allegedly wet area was even wetter. The results should be interpreted with caution, as it could not be validated if after the taken measurements there is no difference anymore in retrieved backscatter signal from the wet and reference area. This is because the backscatter time series available since the installation of the new drainage was too short. In addition, results from section 5.2 showed that the signal interacts with various components on the surface that all largely influence backscatter. Therefore, the observed variation in backscatter signal could be a result of multiple factors of influence and was possibly not significantly affected by the difference in soil moisture.

6.2. Limitations

A major limitation of this research is the lack of cloud-free satellite imagery. Consequently, the part of the research which investigates a lagged relationship between in-situ soil moisture measurement and vegetation indices is based on limited data and cannot demonstrate statistical significance. Furthermore, as the time gap between two satellite images sometimes even exceeds a month, no information is available during this period about the dynamics of the vegetation indices. A more continuous data set is needed to evaluate if the negligible correlation can be assigned to noise introduced by other factors overruling the sensitivity to soil moisture or the lack of data.

In addition, the measured spectral reflectance of optical satellite imagery does not give a direct indication of soil moisture. The amount of soil moisture within the dike is determined by the effect of soil moisture on vegetation health. This is challenging as it takes two steps into one. Soil moisture influences vegetation health and the variation in vegetation health gives a proxy for soil moisture. The same applies to estimating soil moisture values by estimating changes in LAI through backscatter.

Moreover, soil moisture data was retrieved from soil moisture sensors, which are point measurements. The amount of sensors at each study location is very limited. As local conditions influence soil moisture values, a limited amount of sensors makes it difficult to get a representative soil moisture time series for the pixel from which the vegetation indices are retrieved. More field measurements are therefore needed to give an accurate

representation of the average soil moisture within a pixel. Besides, in-situ soil moisture measurements at 20 cm depth were used. However, it is unknown how deep the roots of the vegetation reach at each study location. Root-zone soil moisture is the total water available to vegetation and hence controls surface vegetation health. Furthermore, SAR can only penetrate up to 5 cm deep below the soil surface, whereas soil moisture is much more dynamic than soil moisture at 20 cm depth. In-situ soil moisture measurements retrieved at 20 cm depth do not exactly match the soil moisture measured by SAR, nor when a lag is applied.

Furthermore, raw time series and deseasonalized time series have both been used in literature, and in many cases, both can give good results (Wang et al. (2003), Jackson et al. (2004), Li et al. (2005)). Although, in theory, most time variables contain seasonality which can conceal the underlying correlationship between variables, resulting in over- or underestimates (Kendal and Ord, 1990). As deseasonalizing requires a long term data set, this could not be performed. Therefore this could have led to over- or underestimation of the relationship between vegetation indices and soil moisture.

Another limitation is that open data satellite missions are limited in their spatial resolution. A relatively low spatial resolution influences retrieved values as it increases noise because different elements are located within the same pixel. Some of the retrieved vegetation index data used in this research was extracted from pixels overlapping with water, which consequently affects these measurements.

Additionally, the study period was restricted as data was only available from April 2020 up until September 2021. Therefore, the response of vegetation to soil moisture has not been investigated for the different years and months. However, it is expected that the optimal time lag time could differ from year to year as time lag depends on climatic factors which can change throughout the years (Zhang et al., 2018). Studies from Zhang et al. (2021) and Van Hoek et al. (2016) demonstrated differences in time lag during wet and dry years. Furthermore, it is possible that the time lag differs for each part of the growing season. However, due to the small number of data points, this has not been investigated. Calculating correlations for several years and not distinguishing between different months can underestimate the correlation.

In this study, it a relationship between soil moisture and vegetation indices was assessed. However, other factors also affect vegetation health and hence vegetation indices. The vegetation state is also affected by other climatic conditions such as precipitation, temperature and radiation. Also, nutrient availability and soil texture influence vegetation health (Jamalinia et al., 2019). In addition, the type of vegetation largely influences the response of vegetation to soil moisture as the rooting depth of the vegetation affects the water availability to the plants. This research takes into account soil moisture at 20 cm depth, however, this is not the effective root-zone available water. This could not have been taken into account as neither site-specific soil parameters, vegetation and rooting depth data was available (West et al., 2018). Also, the amount of evapotranspiration depends on the type of plant. The extracted evapotranspiration dataset from Meteobase calculates evapotranspiration based on grass of 12 cm under ideal conditions (no moisture deficiency) (Wolters et al., 2015). As described above, there is a multitude of factors that influence the state of vegetation. Therefore, the relationship between vegetation indices and soil moisture cannot be explained solely by soil moisture.

Moreover, Nicholson and Farrar (1994) demonstrate that there is a precipitation threshold above which NDVI values, and hence other vegetation indices, are less sensitive to precipitation fluctuations. Above this threshold, precipitation is not a limiting factor anymore for vegetation health. When vegetation is saturated, NDVI increases gradually with rainfall, whereas NDVI values rapidly increase with rainfall when vegetation experiences water stress after a dry period. As soil moisture is a function of precipitation and evapotranspiration among other factors such as runoff, infiltration, and percolation, it can be stated that when high soil moisture values are reached, soil saturates, and hence soil moisture is not a limiting factor for vegetation growth. A linear relation was examined and thus this phenomenon has not been taken into account, which might have affected the results.

Precipitation deficit is used in this research as a proxy for soil moisture. Precipitation deficit is a meteorological indicator that only takes precipitation and evapotranspiration into account. However, vegetation health, represented by the calculated vegetation indices, is influenced by various other parameters than just solely precipitation and evapotranspiration. Soil moisture is a function of precipitation among other factors such as runoff, evapotranspiration, infiltration, and percolation. Moreover, the soil type determines how much water is available for the vegetation. A clay dike will dry out to a greater depth than a peat dike. Precipitation deficit is a simplified representation of soil moisture and thus does not give an accurate representation.

Lastly, management practices largely influence vegetation indices. Grass-covered dikes are often mown during

the growing season (April to September) and affects the natural variation of vegetation, as was shown in this study. Also, dikes are sprayed with water during dry periods. No information is available about periods when water spraying has been performed and mowing dates at location Geerweg were only known in 2021 and completely unknown for the river dike at the Amsterdam-Rhine canal. As the dates when management practices were performed were unknown, these moments were not removed from the data set and therefore influence the results. The data used to investigate a lagged relationship between vegetation indices and in-situ soil moisture measurement at location Geerweg was too small to discard the vegetation indices retrieved near the mowing dates. Furthermore, grazing by cattle influences vegetation indices. Both grass-covered regional dikes in this study were grazed.

7

Conclusion

The objective of this study was to assess the relationship between vegetation indices and SAR backscatter obtained from satellite missions and soil moisture on grass-covered dikes. In this section, the key findings obtained from the study are presented.

Main research question: "How can remote sensing data give insight into soil moisture and contribute to dike inspections on grass-covered dikes?"

This study examined the potential of remote sensing data obtained from satellite missions to give a proxy for soil moisture in grass-covered dikes.

It was assessed if the Green Red Ratio (GRR), Modified Simple Ratio (MSR), Normalized Difference Vegetation Index (NDVI), Ratio Vegetation Index (RVI) and Normalised Difference Infrared Index (NDII) obtained from optical satellite imagery could be used as a soil moisture indicator for grass-covered dikes, during the period June to September. In-situ soil moisture measurements at 20 cm depth were available at two study locations for the period of April 2020 to September 2021. A lagged relationship was assessed between the average soil moisture value of a pixel (extracted from soil moisture sensors) and the vegetation index of a pixel. As only a limited amount of satellite imagery was available due to cloud and cloud shadow contamination, vegetation indices retrieved from Landsat 7 and 8 were harmonized to increase the sample size. At location Bermweg, the optimal correlation between vegetation indices and soil moisture was found when a lag of around 30 days was applied. The correlation between the MSR, NDVI, RVI, NDII and soil moisture was weak (R = 0.32-0.40). The correlation with the GRR was negligible (R=0.14). At location Geerweg, the time lag leading to the optimal correlation was different for the NDII compared to the other vegetation indices. The soil moisture sensors were located in two different pixels. For the majority of the vegetation indices, the optimal correlation was found using a lag of 23 days. This correlation was negligible for one pixel (R = 0.12-0.16) and no positive correlation was found for the other pixel. For the NDII an optimal negligible correlation was found for both pixels when a lag of 31 days was applied (R=0.13-0.28). The grass at location Bermweg was maintained by grazing horses whereas the grass at location Geerweg was maintained by both grazing cattle and mowing. Mowing was done twice a year during the growing season. Unlike other studies, which have demonstrated that a correlation could be found between soil moisture and vegetation indices, this research did not potential for vegetation indices to give a proxy for soil moisture on grass-covered dikes (Wang et al. (2007), Nicholson and Farrar (1994), Musyimi (2011), Zhang et al. (2018)). The negligible correlations clearly show that noise was introduced by various factors like management practices (i.e. mowing, grazing), other key factors influencing vegetation state (i.e. nutrient availability, radiation), low spatial resolution, and the presence of scene-to-scene variability within satellite imagery, overruling the effect of soil moisture on vegetation indices. Therefore, vegetation indices could not give a proxy for soil moisture.

No (lagged) relationship could be found between retrieved SAR backscatter and in-situ soil moisture measurements at 20 cm depth. This could be assigned to the fact that the signal was more sensitive to other surface parameters such as surface roughness and vegetation which can affect backscatter as much as, or more than, soil moisture (Altese et al., 1996). Also, the slope of the dike introduces another level of complexity. As discussed, soil moisture data was acquired from 20 cm depth whereas SAR responds to soil moisture only within the first

few centimeters of the soil, where soil moisture is much more dynamic.

Furthermore, in this research, precipitation deficit was used as a soil moisture indicator. The results demonstrate that at location Bermweg, there was a weak to strong correlation (R=0.24-0.82) with the vegetation indices during June to September for the majority of the (harmonized) satellite missions when a cumulative period of 15 days was taken into account. At location Geerweg the cumulative period leading to the optimal correlation differs for each satellite mission and ranges from 15 to 90 days. At both locations, the overall pattern of the correlation coefficients for the different cumulative periods vary largely for each satellite mission. As no universal relationship could be found for the different satellite missions, these results support the previous findings, that vegetation indices cannot give an indication of soil moisture.

All in all, results show that with the method implemented in this research, vegetation indices and SAR backscatter could not give insight into soil moisture. Mapping the relationship between vegetation indices, SAR backscatter and soil moisture is complex because the signal is affected by many factors. If further research proves that remote sensing data can give an indication of soil moisture, remote sensing could facilitate dike inspections by identifying vulnerable dike sections and prioritizing dike inspections during dry periods or deciding if measurements need to be taken during extreme droughts (i.e. water spraying). As the spatial resolution of satellite missions is coarse (meters), small problem areas will not be able to be identified and it can only give a general indication of soil moisture. Moreover, it should be taken into account that the use of optical satellite imagery is limited by cloud contamination. In order for optical satellite imagery to be a valuable screening tool to facilitate dike inspections, it is important to get a good overview of the data. Therefore, imagery acquired from different satellite missions needs to be merged to increase observation frequency.

Research question 1: "How strong is the lagged relationship between vegetation indices obtained from optical remote sensing and soil moisture?"

It was explored how strong the lagged relationship is between vegetation indices (GRR, MSR, NDVI, RVI and NDII) obtained from satellite imagery and in-situ soil moisture measurements at 20 cm depth. A lag was taken into account as there is always a time lag in which vegetation growth responds to soil moisture (Foody, 2003). A potential relationship was investigated during the months June to September as during the non-growing season, most vegetation is dormant and satellite imagery cannot give a proxy for soil moisture (Wang et al., 2007). Vegetation indices retrieved from Landsat 7 and 8 were harmonized to increase the sample size as data was limited. Unfortunately, no statistical significance could be demonstrated due to the small sample size. The optimal time lag was different for each study location. At location Bermweg, the optimal correlation was found when a lag of around 30 days was applied. A weak correlation (R = 0.32-0.39) was found for the MSR, NDVI, RVI and NDII and a negligible correlation (R = 0.14) for the GRR. At location Geerweg, a negligible correlation (R = 0.10-0.21) was found for all vegetation indices, except the NDII, when a 23 day lag was applied. For the other pixel, only negative correlations were found, which is inconsistent with the expectations that high vegetation index values indicate high soil moisture values. For the NDII the highest correlation was found utilising a lag of 31 days, however, this correlation was negligible (R=0.13-0.28). The negligible correlation between vegetation indices and soil moisture at location Geerweg was the result of mowing, which leads to a sudden decrease in vegetation index values (Courault et al. (2010), Dusseux et al. (2014)). Therefore, the natural response of vegetation was overruled and vegetation indices could not give an indication of soil moisture. The weak correlation at location Bermweg shows that vegetation state was not solely influenced by soil moisture. Climatic conditions (i.e. precipitation, temperature, radiation) and soil properties (i.e. nutrient availability) also play a key role in vegetation health (Bradley et al., 1998). Furthermore, the grass-cover at location Bermweg is grazed, which also influences the state of vegetation. In addition, scene-to-scene variability can affect vegetation indices and low spatial resolution can influence retrieved values because pixels do not solely contain vegetation. All in all, the results show that vegetation indices cannot give a reflection of soil moisture dynamics in the root-zone because the presence of noise introduced by various factors overrule the sensitivity of vegetation indices to soil moisture.

Research question 2: "How strong is the relationship between backscatter obtained from SAR remote sensing and soil moisture?"

The relationship between SAR backscatter, retrieved from Sentinel-1, and in-situ soil moisture measurements at 20 cm depth was evaluated. It was hypothesized that SAR could give an indication of soil moisture as an increase in soil moisture content results in an increase in radar backscatter intensity (ESA, 2021c). As soil moisture values were retrieved at 20 cm depth and SAR measures the top few centimeters of the soil, a time lag was taken into account. Furthermore, it is known that there is a lagged correlation between root-zone soil moisture and

LAI (Jamalinia et al., 2019). It was therefore also assessed if the influence of LAI on backscatter could give an indication of soil moisture at 20 cm depth.

A distinction was made between polarization channels (VV, VH and cross-ratio VH/VV), orbit path (i.e. ascending and descending) and incidence angle as this influences the retrieved backscatter. Pearson correlation coefficients were calculated to explore the relationship. The results show that there was no (lagged) relationship between SAR backscatter and soil moisture measurements. For the vast majority of the results negative correlations were found for the VV and VH polarization channels, whereas a positive correlation was expected, as an increase in soil moisture should lead to increasing backscatter values. As discussed, soil moisture measurements of 20 cm depth were taken into account whereas soil moisture in the topsoil is much more dynamic. Furthermore, no lagged correlation was found between soil moisture and the VH/VV ratio, which is most sensitive to the LAI (Vreugdenhil et al., 2018). The results show that SAR backscatter could not give a proxy for soil moisture at 20 cm depth. As discussed, the insensitivity of SAR to soil moisture could be assigned to the interaction with various components such as surface roughness, vegetation and the slope which affects retrieved backscatter. It should be noted that the backscatter signal was extracted from a small area and therefore also a large amount of noise was present in the data. This also explains why the backscatter was unable to give an indirect proxy of soil moisture by estimating the LAI.

Research question 3: "How strong is the relationship between vegetation indices obtained from optical remote sensing and precipitation deficit?"

It was investigated how strong the relationship is between precipitation deficit and vegetation indices. Precipitation deficit, defined as the difference between precipitation and evapotranspiration, could be used as a soil moisture indicator as a decrease of soil moisture content occurs when the outflux of water is bigger than the influx. Cumulative precipitation deficit was taken into account as vegetation health is a slow process of accumulation of precipitation deficit and is related to not only the current precipitation, but also to the cumulative effect of earlier precipitation deficit. It was examined how strong the relationship was between vegetation indices and cumulative precipitation deficit by calculating Pearson correlation coefficients. Correlation coefficients were computed for a cumulative period of 10 to 90 days.

Overall, a weak to strong (R=0.20-0.82) correlation was found between precipitation deficit and vegetation indices retrieved from the different satellite missions. The strongest correlation was found for the GRR, which uses the red and green band, whereas other vegetation indices use the red, near-infrared and shortwave infrared bands. The sample size of the harmonized Landsat 7 and 8 data set was the largest and could therefore demonstrate statistical significance. At location Bermweg, the optimal correlation for all (harmonized) satellite missions was found when a cumulative period of around 15 days was taken into account. A negligible correlation (R=0.24-0.36) was found between precipitation deficit and vegetation indices retrieved from the harmonized Landsat 7 and 8 data set. Correlations were statistically significant except for the NDVI and NDII. At location Geerweg, an optimal moderate correlation (R=0.47-0.57) was found for a cumulative period of around 20 days for the harmonized Landsat 7 and 8 data set. The correlation was statistically significant. The optimal cumulative period for the other satellite missions varied between 15 and 90 days.

The overall pattern of the correlation coefficients for the different cumulative periods varied largely for each satellite mission, calling into question the reliability of the results. In addition, the calculated correlation coefficients do not vary much when the cumulative period taken into account increases from 10 to 90 days, which seems unlikely. All in all, no universal relationship could be found and it can therefore be concluded that vegetation indices cannot give a reflection of precipitation deficit and hence soil moisture. As discussed, it should be noted that precipitation deficit is a simplified representation of soil moisture, as soil moisture is influenced by other factors such as runoff, infiltration and percolation.

Research question 4: "Can spatial-temporal variations of soil moisture be distinguished by vegetation indices and SAR backscatter obtained from remote sensing data?"

A spatial-temporal analysis was executed to investigate if a difference could be detected by remote sensing data between the behaviour of an allegedly wet area and a reference area (no wetting) at the inner slope of a dike. The wet area was the result of a clogged toe drain, which led to an increase in phreatic level.

It was hypothesized that a difference could be found between the vegetation indices retrieved from the wet and reference area, especially during dry periods. This hypothesis was based on the assumption that particularly during dry periods, vegetation located in the wet area had access to water, whereas vegetation in the reference

area experiences water stress. The findings of this report do not support the hypothesis. Only very limited differences could be found during dry periods. The results clearly demonstrate the limitations of using vegetation indices as a soil moisture indicator when grass is intensively managed by practices like mowing during the growing season. As the grass at the study location was mown twice a year during summer, this could overrule the natural variation of vegetation in response to soil moisture during the dry periods. A difference could be found between the wet and normal area by SAR backscatter. The VH and VV polarized backscatter of the wet area was lower than the reference area, which could be the result of the standing water (Liu, 2016). The backscatter of standing water is lower since water is smooth and therefore acts as a mirror. However, as discussed, the observed variation in backscatter signal could be a result of multiple factors of influence, and is possibly not significantly affected by the difference in the wetness of the two areas.

Research question 5: "How can remote sensing data contribute to dike inspections on grass-covered dikes?"

With about 22,500 kilometres of dike in the Netherlands, dike inspections are a slow, costly, and time consuming process (Jorissen et al., 2016). Results show that vegetation indices and SAR backscatter cannot give an indication of soil moisture on grass-covered dikes. However, if further research, implementing another methodology, demonstrates that vegetation indices and SAR can give a proxy for soil moisture, remote sensing data could facilitate visual dike inspections. Remote sensing data could identify the most vulnerable dike sections during dry periods and hence help prioritizing inspections or measures (i.e. water spraying), to avoid excessive drying of the soil during extreme droughts. This could reduce the workload of dike managers. Traditional dike inspections should be continued, as the spatial resolution of satellite imagery is coarse and thus small problem areas will not be able to be identified. However, remote sensing could help as a screening tool and contribute to more continuously monitoring dikes between visual inspections. Optical satellite imagery is limited by cloud and cloud shadow contamination. Therefore, imagery from satellite missions needs to be merged in order to get a good overview of the dynamics of vegetation indices over time. Also, it should be noted that vegetation responds to soil moisture available surrounding its roots. Hence, it depends on the root length of the vegetation to what extend vegetation can give an indication of soil moisture in the subsurface. It should be emphasized that remote sensing information should be used with care, as outliers may be introduced by management practices (i.e. mowing, grazing). Dike management is a crucial limitation on using remote sensing imagery as mowing completely masks the natural variation of vegetation in response to soil moisture, disabling the use of vegetation indices as a proxy for soil moisture. However, remote sensing could still be an interesting tool during extreme events, such as extreme droughts, when little or no mowing is conducted.

Currently, precipitation deficit is a meteorological drought indicator used by the Koninklijk Nederlands Meteorologisch Instituut (KNMI) to give a proxy for drought. The precipitation deficit is defined as the cumulative difference between precipitation and evapotranspiration from April 1st to October 1st. When a certain precipitation deficit is reached, dikes are more intensively inspected. This threshold is determined by the dike manager and lies between 150 or 200 millimeters (Zoelen (2021), RTL (2013)). In 2021 a local precipitation deficit of 75 millimeters was reached at location Bermweg, which does not give an indication to increase inspection frequency. Nonetheless, in 2021, soil moisture values at 20 cm depth reached low soil moisture values, approaching similarly low values as during the drought in 2020. The study by Strijker (2021) confirmed that precipitation deficit cannot always give a good indication of drought within dikes as drying out of dikes is a very dynamic and complex process. This highlights the need of combining various data sources to give a proxy for soil moisture. Remote sensing data would be an ideal source to monitor soil moisture in grass-covered dikes on large scale.

8

Recommendations

In this chapter, recommendations are given based on the discussion chapter, which covers the potential and limitations of remote sensing imagery to give a proxy for soil moisture in grass-covered dikes.

- It is recommended to carry out research that uses ground-based remote sensing data retrieved from a multispectral camera over a long period of time (i.e. whole growing season) in order to exclude noise introduced by atmospheric differences and spatial resolution. Because cloud contamination is of no importance, a more continuous time series is ensured, enabling to gain insight into the dynamics of vegetation indices over time and enabling to demonstrate statistical significance. This investigation can examine if vegetation indices can reflect soil moisture conditions when noise introduced by these factors is eliminated.
- This research clearly shows that vegetation indices are not solely influenced by soil moisture dynamics in the root-zone but also by other factors. It is therefore important to get a better understanding of the relationship between these factors (i.e. nutrient availability, radiation, temperature) and the response of vegetation on grass-covered dikes.
- Mowing significantly affects measurements of the vegetation index, disrupting the relation between vegetation index data and soil moisture. It is therefore recommended to analyse this relation without measurements that are retrieved directly after mowing of the area of observation. This research should be conducted when sufficient data is collected, and dates of mowing are known.
- It would also be interesting to investigate a relationship between vegetation indices and soil moisture during different months of the growing season as studies have shown that the relationship can differ for each month (Rimkus et al., 2017). This can be investigated if there is a sufficient amount of data points for each month.
- Point-measurements do not give an accurate representation of the soil moisture variation within a pixel. It would be beneficial to carry out research using more field measurements in order to get a more accurate representation of the average soil moisture within a pixel.
- The main part of this research is conducted for two grass-covered regional dikes. However, the composition of the dike also determines soil moisture availability to vegetation. Also, the type of vegetation largely influences the response of vegetation to soil moisture (i.e. rooting depth). Further research should therefore take into account other types of dikes and different types of vegetation.
- Cloud and cloud shadow contamination remains an issue for potential implementation of optical remote sensing to facilitate dike inspections as this results in a limited amount of imagery. Hence, if optical remote sensing data wants to be implemented in the future to contribute to dike inspections, it is important to merge imagery from different satellite missions to get more frequent observations and thus a complete overview of the vegetation index dynamics over time. As satellite missions have different sensor characteristics, values should be adjusted and cannot be merged without applying a translation function. Thus,

it is recommended to research how Landsat 7/8 and Sentinel-2 surface reflectance data can be merged. Currently, NASA is conducting research on harmonizing Landsat and Sentinel-2 data.

- If further studies would like to explore the potential of SAR to directly retrieve soil moisture for grass-covered dikes, factors that influence backscatter such as the topography of the terrain, vegetation density, and surface roughness should be taken into account. The effect of these parameters should be quantified and removed to obtain accurate soil moisture results. This can be done using a soil moisture retrieval algorithm that takes into account these different components.

Bibliography

Aanstoos, J. V., Hasan, K., O'Hara, C. G., Dabbiru, L., Mahrooghy, M., Nobrega, R. and Lee, M. A. (2012), Detection of slump slides on earthen levees using polarimetric sar imagery, in '2012 IEEE Applied Imagery Pattern Recognition Workshop (AIPR)', IEEE, pp. 1–7.

Aanstoos, J. V., Hasan, K., O'Hara, C. G., Prasad, S., Dabbiru, L., Mahrooghy, M., Gokaraju, B. and Nobrega, R. (2011), Earthen levee monitoring with synthetic aperture radar, in '2011 IEEE Applied Imagery Pattern Recognition Workshop (AIPR)', IEEE, pp. 1–6.

Altese, E., Bolognani, O., Mancini, M. and Troch, P. A. (1996), 'Retrieving soil moisture over bare soil from ers 1 synthetic aperture radar data: Sensitivity analysis based on a theoretical surface scattering model and field data', Water Resources Research **32**(3), 653–661.

Amani, M., Ghorbanian, A., Ahmadi, S. A., Kakooei, M., Moghimi, A., Mirmazloumi, S. M., Moghaddam, S. H. A., Mahdavi, S., Ghahremanloo, M., Parsian, S. et al. (2020), 'Google earth engine cloud computing platform for remote sensing big data applications: A comprehensive review', IEEE Journal of Selected Topics in Applied Earth Observations and Remote Sensing .

ASF (2021), 'Smap-instrument'.

Azad Hossain, A. and Easson, G. (2012), 'Predicting shallow surficial failures in the mississippi river levee system using airborne hyperspectral imagery', Geomatics, Natural Hazards and Risk **3**(1), 55–78.

Baars, S. (2004), 'Peat dike failure in the netherlands', Official Publication of the European Water Association (EWA) .

Bakkenist, S. (2012), Inspectiewijzers waterkeringen: technische informatie uitvoering inspecties, Technical report, Tech. Report (in Dutch), STOWA, Amersfoort, The Netherlands.

Bakkenist, S., van Dam, O., van der Nat, A., Thijs, F. and de Vries, W. (2012), Bouwstenen professionele inspecties: Handreiking voor het organiseren van inspecties, Technical report, STOWA, Amersfoort, The Netherlands.

Bakker, W. H., Grabmaier, K., Hunmeman, G. a., Van Der Meer, F., Prakash, A., Tempfli, K., Gieske, A., Hecker, C., Janseen, L., Parodi, G. et al. (2004), 'Principles of remote sensing, an introductory textbook', The international institute for geo-informational science and earth observation (ITC), Enschede, the Netherlands .

Balenzano, A., Mattia, F., Satalino, G. and Davidson, M. W. (2010), 'Dense temporal series of c-and l-band sar data for soil moisture retrieval over agricultural crops', IEEE Journal of Selected Topics in Applied Earth Observations and Remote Sensing **4**(2), 439–450.

Bannari, A., Morin, D., Bonn, F. and Huete, A. (1995), 'A review of vegetation indices', Remote Sensing Reviews **13**, 95–120.

Bauer-Marschallinger, B., Freeman, V., Cao, S., Paulik, C., Schaufler, S., Stachl, T., Modanesi, S., Massari, C., Ciabatta, L., Brocca, L. et al. (2018), 'Toward global soil moisture monitoring with sentinel-1: Harnessing assets and overcoming obstacles', IEEE Transactions on Geoscience and Remote Sensing **57**(1), 520–539.

Benninga, H.-J. F., van der Velde, R. and Su, Z. (2020), 'Sentinel-1 soil moisture content and its uncertainty over sparsely vegetated fields', Journal of Hydrology X **9**, 100066.

Bishop, M., Dunbar, J. B. and Peyman-Dove, L. P. (2003), Integration of remote sensing (lidar, electromagnetic conductivity) and geologic data toward the condition assessment of levee systems, in 'Remote Sensing for Environmental Monitoring, GIS Applications, and Geology II', Vol. 4886, International Society for Optics and Photonics, pp. 400–407.

Bousbih, S., Zribi, M., Lili-Chabaane, Z., Baghdadi, N., El Hajj, M., Gao, Q. and Mougenot, B. (2017), 'Potential of sentinel-1 radar data for the assessment of soil and cereal cover parameters', Sensors **17**(11), 2617.

Bradley, L., Kilby, M., Call, R., Kopec, D., Capizzi, J., Langston, D., Claridge, J., Maloy, O., DeGomez, T., Mikel, T. et al. (1998), 'Environmental factors that affect plant growth', Arizona Master Gardener Manual .

Buitink, J., Swank, A. M., van der Ploeg, M., Smith, N. E., Benninga, H.-J. F., van der Bolt, F., Carranza, C. D., Koren, G., van der Velde, R. and Teuling, A. J. (2020), 'Anatomy of the 2018 agricultural drought in the netherlands using in situ soil moisture and satellite vegetation indices', Hydrology and Earth System Sciences **24**(12), 6021–6031.

Calle, E. (2010), 'Schematiseringfactor voor stabiliteitsanalyses (achtergrond en theroei)'.

Carlson, T. N. and Ripley, D. A. (1997), 'On the relation between ndvi, fractional vegetation cover, and leaf area index', Remote sensing of Environment **62**(3), 241–252.

Carranza, C. D., Ploeg, M. J. and Torfs, P. J. (2018), 'Using lagged dependence to identify (de) coupled surface and subsurface soil moisture values', Hydrology and Earth System Sciences **22**(4), 2255–2267.

Carter, G. A. (1993), 'Responses of leaf spectral reflectance to plant stress', American journal of botany **80**(3), 239–243.

Ceccato, P., Flasse, S., Tarantola, S., Jacquemoud, S. and Grégoire, J.-M. (2001), 'Detecting vegetation leaf water content using reflectance in the optical domain', Remote sensing of environment **77**(1), 22–33.

Chander, G., Helder, D. L., Aaron, D., Mishra, N. and Shrestha, A. K. (2012), 'Assessment of spectral, misregistration, and spatial uncertainties inherent in the cross-calibration study', IEEE Transactions on Geoscience and Remote Sensing **51**(3), 1282–1296.

Chatfield, C. and Xing, H. (2019), The analysis of time series: an introduction with R, Chapman and hall/CRC.

Chen, J. M. (1996), 'Evaluation of vegetation indices and a modified simple ratio for boreal applications', Canadian Journal of Remote Sensing **22**(3), 229–242.

Choi, H. and Jeong, J. (2019), 'Speckle noise reduction technique for sar images using statistical characteristics of speckle noise and discrete wavelet transform', Remote Sensing **11**(10), 1184.

Chotkan, S. (2021), 'Predicting drought-induced cracks in dikes with artifical intelligence'.

Closson, D., Karaki, N., Hansen, H., Derauw, D., Barbier, C. and Ozer, A. (2003), 'Space-borne radar interferometric mapping of precursory deformations of a dyke collapse, dead sea area, jordan', International Journal of Remote Sensing **24**(4), 843–849.

Courault, D., Hadria, R., Ruget, F., Olioso, A., Duchemin, B., Hagolle, O. and Dedieu, G. (2010), 'Combined use of formosat-2 images with a crop model for biomass and water monitoring of permanent grassland in mediterranean region', Hydrology and Earth System Sciences **14**(9), 1731–1744.

Cundill, S. (2016), 'Investigation of remote sensing for dike inspection'.

Cundill, S. L., van der Meijde, M. and Hack, H. R. G. (2014), 'Investigation of remote sensing for potential use in dike inspection', IEEE Journal of Selected Topics in Applied Earth Observations and Remote Sensing **7**(2), 733–746.

Dabboor, M. and Brisco, B. (2018), 'Wetland monitoring and mapping using synthetic aperture radar', Wetl. Manag. Assess. Risk Sustain. Solut **1**, 13.

Dabrowska-Zielinska, K., Musial, J., Malinska, A., Budzynska, M., Gurdak, R., Kiryla, W., Bartold, M. and Grzybowski, P. (2018), 'Soil moisture in the biebrza wetlands retrieved from sentinel-1 imagery', Remote Sensing **10**(12), 1979.

Datt, B. (1999), 'Remote sensing of water content in eucalyptus leaves', Australian Journal of botany **47**(6), 909–923.

David, F. N. (1938), Tables of the ordinates and probability integral of the distribution of the correlation coefficient in small samples, Cambridge University Press.

De Bruin, H. and Lablans, W. (1998), 'Reference crop evapotranspiration determined with a modified makkink equation', Hydrological Processes **12**(7), 1053–1062.

De Jong, S. M., Van Der Meer, F. D. and Clevers, J. G. (2004), Basics of remote sensing, in 'Remote sensing image analysis: Including the spatial domain', Springer, pp. 1–15.

Dekker, L. and Ritsema, C. (2000), 'Wetting patterns and moisture variability in water repellent dutch soils', Journal of Hydrology **231**, 148–164.

Didan, K., Munoz, A. B., Solano, R. and Huete, A. (2015), 'Modis vegetation index user's guide (mod13 series)', University of Arizona: Vegetation Index and Phenology Lab .

Dusseux, P., Vertès, F., Corpetti, T., Corgne, S. and Hubert-Moy, L. (2014), 'Agricultural practices in grasslands detected by spatial remote sensing', Environmental monitoring and assessment **186**(12), 8249–8265.

Emery, W. and Camps, A. (2017), Introduction to satellite remote sensing: atmosphere, ocean, land and cryosphere applications, Elsevier.

Engine, G. E. (2007), 'Fundamentals of remote sensing: A canada center for remote sensing remote sensing tutorial'.
URL: https://developers.google.com/earth-engine/guides/landsat

ESA (2021a), 'Level-2'.
URL: https://sentinels.copernicus.eu/web/sentinel/user-guides/sentinel-2-msi/processing-levels/level-2

ESA (2021b), 'Multispectral instrument (msi) overview'.
URL: https://sentinel.esa.int/web/sentinel/technical-guides/sentinel-2-msi/msi-instrument

ESA (2021c), 'Parameters affecting radar backscatter'.
URL: https://earth.esa.int/web/guest/missions/esa-operational-eo-missions/ers/instruments/sar/applications/radar-courses/content-2/-/asset$_publisher/qIBc6NYRXfnG/content/radar-course-2-parameters-affecting-radar-backscatter$

ESA (2021d), 'Sentinel-1 overview'.
URL: https://sentinels.copernicus.eu/web/sentinel/user-guides/sentinel-1-sar/acquisition-modes/interferometric-wide-swath

ESA (2021e), 'Sentinel-2'.
URL: https://sentinel.esa.int/web/sentinel/missions/sentinel-2

Esch, S. (2018), Determination of Soil Moisture and Vegetation Parameters from Spaceborne C-Band SAR on Agricultural Areas, PhD thesis, Universität zu Köln.

Fensholt, R. and Sandholt, I. (2003), 'Derivation of a shortwave infrared water stress index from modis near-and shortwave infrared data in a semiarid environment', Remote Sensing of Environment **87**(1), 111–121.

Filipponi, F. (2019), Sentinel-1 grd preprocessing workflow, in 'Multidisciplinary Digital Publishing Institute Proceedings', Vol. 18, p. 11.

Foody, G. (2003), 'Geographical weighting as a further refinement to regression modelling: An example focused on the ndvi–rainfall relationship', Remote sensing of Environment **88**(3), 283–293.

for Remote Sensing, C. C. (2007), 'Fundamentals of remote sensing: A canada center for remote sensing remote sensing tutorial'.
URL: https://www.nrcan.gc.ca/maps-tools-publications/satellite-imagery-air-photos/tutorial-fundamentals-remote-sensing/9309

Foucras, M., Zribi, M., Albergel, C., Baghdadi, N., Calvet, J.-C. and Pellarin, T. (2020), 'Estimating 500-m resolution soil moisture using sentinel-1 and optical data synergy', Water **12**(3), 866.

Givehchi, M., Vrijling, J., Hartmann, A., Van Gelder, P. and Van Baars, S. (2003), 'Application of remotely sensed data for detection of seepage in dikes', INTERNATIONAL ARCHIVES OF PHOTOGRAMMETRY REMOTE SENSING AND SPATIAL INFORMATION SCIENCES **34**(7/A), 378–382.

Haarbrink, R. and Shutko, A. (2006), New airborne sensor for soil moisture mapping, in 'Proceedings of the Second International Workshop on The Future of Remote Sensing', Citeseer.

Hack, H., van der Meijde, M., van der Schrier, J., Awaju, J., Barritt, S., van'T Hof, J., Maccabiani, J., Maresch, S., Calero, D., Reymer, A. et al. (2008), 'Strength of peat dykes evaluated by remote sensing: Pilot project program flood control 2015, rsdyk2008'.

Hasan, K., Aanstoos, J. V. and Mahrooghy, M. (2013), Stressed vegetation identification by sar time series as an indicator of slope instability in mississippi river levee segments, in '2013 IEEE Applied Imagery Pattern Recognition Workshop (AIPR)', IEEE, pp. 1–4.

Hopkins, W.G., H. N. (2009), Introduction to plant physiology,, New York: Wiley Sons.

Hunt Jr, E. R. and Rock, B. N. (1989), 'Detection of changes in leaf water content using near-and middle-infrared reflectances', Remote sensing of environment **30**(1), 43–54.

Jackson, T. J., Chen, D., Cosh, M., Li, F., Anderson, M., Walthall, C., Doriaswamy, P. and Hunt, E. R. (2004), 'Vegetation water content mapping using landsat data derived normalized difference water index for corn and soybeans', Remote Sensing of Environment **92**(4), 475–482.

Jackson, T. J., Schmugge, J. and Engman, E. (1996), 'Remote sensing applications to hydrology: soil moisture', Hydrological Sciences Journal **41**(4), 517–530.

Jamalinia, E., Vardon, P. J. and Steele-Dunne, S. C. (2019), 'The effect of soil–vegetation–atmosphere interaction on slope stability: a numerical study', Environmental Geotechnics pp. 1–12.

Jamalinia, E., Vardon, P. and Steele-Dunne, S. (2020), 'Use of displacement as a proxy for dike safety', Proceedings of the International Association of Hydrological Sciences **382**, 481–485.

Jonkman, S. (2014), 'An introduction to flood defenses'.

Jonkman, S. N., Kok, M. and Vrijling, J. K. (2008), 'Flood risk assessment in the netherlands: A case study for dike ring south holland', Risk Analysis: An International Journal **28**(5), 1357–1374.

Jordan, C. F. (1969), 'Derivation of leaf-area index from quality of light on the forest floor', Ecology **50**(4), 663–666.

Jorissen, R., Kraaij, E. and Tromp, E. (2016), Dutch flood protection policy and measures based on risk assessment, in 'E3S Web of Conferences', Vol. 7, EDP Sciences, p. 20016.

Kanemasu, E. (1974), 'Seasonal canopy reflectance patterns of wheat, sorghum, and soybean', Remote Sensing of Environment **3**(1), 43–47.

Kendal, M. and Ord, J. (1990), Time series, Charles Griffin.

Lendering, K.T., K. M. J. S. (2015), Flood risk of regional flood defenses, Technical report, Tech. Report (in Dutch), STOWA, Amersfoort, The Netherlands.

Li, H., Robock, A., Liu, S., Mo, X. and Viterbo, P. (2005), 'Evaluation of reanalysis soil moisture simulations using updated chinese soil moisture observations', Journal of Hydrometeorology **6**(2), 180–193.

Li, J., Wu, Z., Hu, Z., Zhang, J., Li, M., Mo, L. and Molinier, M. (2020), 'Thin cloud removal in optical remote sensing images based on generative adversarial networks and physical model of cloud distortion', ISPRS Journal of Photogrammetry and Remote Sensing **166**, 373–389.

Liu, C. (2016), Analysis of sentinel-1 sar data for mapping standing water in the twente region, Master's thesis, University of Twente.

Liu, J., Xu, Y., Li, H. and Guo, J. (2021), 'Soil moisture retrieval in farmland areas with sentinel multi-source data based on regression convolutional neural networks', Sensors **21**(3), 877.

Liu, S., Chadwick, O. A., Roberts, D. A. and Still, C. J. (2011), 'Relationships between gpp, satellite measures of greenness and canopy water content with soil moisture in mediterranean-climate grassland and oak savanna', Applied and Environmental Soil Science **2011**.

Liu, Z., Li, P. and Yang, J. (2017), 'Soil moisture retrieval and spatiotemporal pattern analysis using sentinel-1 data of dahra, senegal', Remote Sensing **9**(11), 1197.

Mahdavi, S., Amani, M. and Maghsoudi, Y. (2019), 'The effects of orbit type on synthetic aperture radar (sar) backscatter', Remote Sensing Letters **10**(2), 120–128.

Mandal, D., Kumar, V., Ratha, D., Dey, S., Bhattacharya, A., Lopez-Sanchez, J. M., McNairn, H. and Rao, Y. S. (2020), 'Dual polarimetric radar vegetation index for crop growth monitoring using sentinel-1 sar data', Remote Sensing of Environment **247**, 111954.

Mao, J., Nierop, K. G., Dekker, S. C., Dekker, L. W. and Chen, B. (2019), 'Understanding the mechanisms of soil water repellency from nanoscale to ecosystem scale: a review', Journal of Soils and Sediments **19**(1), 171–185.

McNairn, H. and Shang, J. (2016), 'A review of multitemporal synthetic aperture radar (sar) for crop monitoring', Multitemporal Remote Sensing pp. 317–340.

Mishra, A. K. and Singh, V. P. (2010), 'A review of drought concepts', Journal of hydrology **391**(1-2), 202–216.

Moeremans, B. and Dautrebande, S. (2000), 'Soil moisture evaluation by means of multi-temporal ers sar pri images and interferometric coherence', Journal of Hydrology **234**(3-4), 162–169.

Moser, G. and Zomer, W. (2006), Inspectie van waterkeringen: een overzicht van meettechnieken, STOWA Amersfoort, the Netherlands.

Musyimi, Z. (2011), Temporal relationships between remotely sensed soil moisture and ndvi over africa: potential for drought early warning, Master's thesis, University of Twente.

Narasimhan, B., Srinivasan, R., Arnold, J. and Di Luzio, M. (2005), 'Estimation of long-term soil moisture using a distributed parameter hydrologic model and verification using remotely sensed data', Transactions of the ASAE **48**(3), 1101–1113.

NASA (2021a), 'Landsat 8 overview'.
URL: https://landsat.gsfc.nasa.gov/landsat-8/landsat-8-overview

NASA (2021b), 'Landsat-8 overview'.
URL: https://landsat.gsfc.nasa.gov/landsat-8/landsat-8-overview

NASA (2021c), 'Normalized difference vegetation index (ndvi)'.
URL: https://earthobservatory.nasa.gov/features/MeasuringVegetation/measuring$_v egetation_2 .php$

Neumann, B., Vafeidis, A. T., Zimmermann, J. and Nicholls, R. J. (2015), 'Future coastal population growth and exposure to sea-level rise and coastal flooding-a global assessment', PloS one **10**(3).

Nicholson, S. and Farrar, T. (1994), 'The influence of soil type on the relationships between ndvi, rainfall, and soil moisture in semiarid botswana. i. ndvi response to rainfall', Remote sensing of environment **50**(2), 107–120.

Nimmo, J. R. (2020), 'The processes of preferential flow in the unsaturated zone', Soil Science Society of America Journal .

Osman, K. T. (2018), Management of soil problems, Springer.

Paloscia, S., Pettinato, S., Santi, E., Notarnicola, C., Pasolli, L. and Reppucci, A. (2013), 'Soil moisture mapping using sentinel-1 images: Algorithm and preliminary validation', Remote Sensing of Environment **134**, 234–248.

Panciera, R. and Monerris, A. (2013), 'Basis of an australian radar soil moisture algorithm theoretical baseline document (atbd)'.

Pareeth, S., Karimi, P., Shafiei, M. and Fraiture, C. (2019), 'Mapping agricultural landuse patterns from time series of landsat 8 using random forest based hierarchial approach', Remote Sensing **11**, 601.

Peters, W., Bastos, A., Ciais, P. and Vermeulen, A. (2020), 'A historical, geographical and ecological perspective on the 2018 european summer drought'.

Philip, S. Y., Kew, S. F., van der Wiel, K., Wanders, N. and van Oldenborgh, G. J. (2020), 'Regional differentiation in climate change induced drought trends in the netherlands', Environmental Research Letters **15**(9), 094081.

Qiu, F., Berglund, J., Jensen, J. R., Thakkar, P. and Ren, D. (2004), 'Speckle noise reduction in sar imagery using a local adaptive median filter', GIScience & Remote Sensing **41**(3), 244–266.

Reijers, V. C., Visser, E. J., Paulissen, M. P. C. P. and de Kroon, H. (2014), De invloed van vegetatie op de erosiebestendigheid van dijken: de start van een monitoringsexperiment naar de effecten van de vegetatiesamenstelling op de erosiebestendigheid van de purmerringdijk, Technical report, Alterra, Wageningen-UR.

Rijkswaterstaat (2021), 'Sentinel-2'.

Rimkus, E., Stonevicius, E., Kilpys, J., Maciulyte, V. and Valiukas, D. (2017), 'Drought identification in the eastern baltic region using ndvi', Earth System Dynamics **8**(3), 627–637.

Rivierenland, W. (2021), 'Maaien'.
URL: https://www.waterschaprivierenland.nl/maaien

Romshoo, S. A., Koike, M., Onaka, S., Oki, T. and Musiake, K. (2002), 'Influence of surface and vegetation characteristics on c-band radar measurements for soil moisture content', Journal of the Indian Society of Remote Sensing **30**(4), 229–244.

Roy, D. P., Kovalskyy, V., Zhang, H., Vermote, E. F., Yan, L., Kumar, S. and Egorov, A. (2016), 'Characterization of landsat-7 to landsat-8 reflective wavelength and normalized difference vegetation index continuity', Remote sensing of Environment **185**, 57–70.

RTL (2013), 'Rijnland gaat kades inspecteren'.
URL: https://www.rtlnieuws.nl/node/2476336

Sehat, S., Vahedifard, F., Aanstoos, J. V., Dabbiru, L. and Hasan, K. (2014), 'Using in situ soil measurements for analysis of a polarimetric sar-based classification of levee slump slides in the lower mississippi river', Engineering geology **181**, 157–168.

Sheffield, J., Goteti, G., Wen, F. and Wood, E. F. (2004), 'A simulated soil moisture based drought analysis for the united states', Journal of Geophysical Research: Atmospheres **109**(D24).

Shumway, R. H., Stoffer, D. S. and Stoffer, D. S. (2000), Time series analysis and its applications, Vol. 3, Springer.

Šimnek, J. and van Genuchten, M. T. (2016), Contaminant transport in the unsaturated zone: Theory and modeling, in 'The handbook of groundwater engineering', CRC Press, pp. 221–254.

Sivakumar, M., Roy, P., Harmsen, K. and Saha, S. (2004), Satellite remote sensing and gis applications in agricultural meteorology, in 'Proceedings of the Training Workshop in Dehradun, India. AGM-8, WMO/TD', Vol. 1182.

Srivastava, H. S., Patel, P. and Navalgund, R. R. (2006), How far sar has fulfilled its expectation for soil moisture retrieval, in 'Microwave Remote Sensing of the Atmosphere and Environment V', Vol. 6410, International Society for Optics and Photonics, p. 641001.

Sriwongsitanon, N., Gao, H., Savenije, H. H., Maekan, E., Saengsawang, S. and Thianpopirug, S. (2016), 'Comparing the normalized difference infrared index (ndii) with root zone storage in a lumped conceptual model', Hydrology and Earth System Sciences **20**(8), 3361–3377.

Sriwongsitanon, N., Gao, H., Savenije, H., Maekan, E., Saengsawang, S. and Thianpopirug, S. (2015), 'The normalized difference infrared index (ndii) as a proxy for root zone moisture storage capacity 2'.

Steele-Dunne, S. C., McNairn, H., Monsivais-Huertero, A., Judge, J., Liu, P.-W. and Papathanassiou, K. (2017), 'Radar remote sensing of agricultural canopies: A review', IEEE Journal of Selected Topics in Applied Earth Observations and Remote Sensing **10**(5), 2249–2273.

Steinier, J., Termonia, Y. and Deltour, J. (1972), 'Smoothing and differentiation of data by simplified least square procedure', Analytical chemistry **44**(11), 1906–1909.

Steven, M. D., Malthus, T. J., Baret, F., Xu, H. and Chopping, M. J. (2003), 'Intercalibration of vegetation indices from different sensor systems', Remote Sensing of Environment **88**(4), 412–422.

Strijker, B. (2021), 'Droogtemonitoring - analyse van de waterhuishouding in boezemkades tijdens perioden van droogte'. unpublished.

Swart, L. T. (2007), Remote sensing voor inspectie van waterkeringen, Swartvast!

Torres, R., Snoeij, P., Geudtner, D., Bibby, D., Davidson, M., Attema, E., Potin, P., Rommen, B., Floury, N., Brown, M. et al. (2012), 'Gmes sentinel-1 mission', Remote Sensing of Environment **120**, 9–24.

Ulaby, F. T., Batlivala, P. P. and Dobson, M. C. (1978), 'Microwave backscatter dependence on surface roughness, soil moisture, and soil texture: Part i-bare soil', IEEE Transactions on Geoscience Electronics **16**(4), 286–295.

USG (2021), 'Soil moisture'.
URL: https://www.drought.gov/topics/soil-moisture

Van Baars, S. and Van Kempen, I. (2009), 'The causes and mechanisms of historical dike failures in the netherlands', E-WAter journal, 2009 .

van Haastregt, B. (2012), Evaluatie droge zomer 2018 waterkeringen, Technical report, STOWA, Amersfoort, The Netherlands.

Van Hoek, M., Jia, L., Zhou, J., Zheng, C. and Menenti, M. (2016), 'Early drought detection by spectral analysis of satellite time series of precipitation and normalized difference vegetation index (ndvi)', Remote Sensing **8**(5), 422.

Verhagen, H. (1998), 'Revetments, sea-dikes and river-levees', IHE lecture note .

Vermote, E., Justice, C., Claverie, M. and Franch, B. (2016), 'Preliminary analysis of the performance of the landsat 8/oli land surface reflectance product', Remote Sensing of Environment **185**, 46–56.

Versteeg, R., Hakvoort, J. H. M., Bosch, S. and Kallen, M.-J. (2013), Meteobase: online archief van neerslag-en verdampingsgegevens voor het waterbeheer, STOWA, Stichting Toegepast Onderzoek Waterbeheer.

Vilardo, G., Ventura, G., Terranova, C., Matano, F. and Nardò, S. (2009), 'Ground deformation due to tectonic, hydrothermal, gravity, hydrogeological, and anthropic processes in the campania region (southern italy) from permanent scatterers synthetic aperture radar interferometry', Remote Sensing of Environment **113**(1), 197–212.

Vorogushyn, S., Merz, B. and Apel, H. (2009), 'Development of dike fragility curves for piping and micro-instability breach mechanisms', Natural Hazards and Earth System Sciences **9**(4), 1383–1401.

Vreugdenhil, M., Wagner, W., Bauer-Marschallinger, B., Pfeil, I., Teubner, I., Rüdiger, C. and Strauss, P. (2018), 'Sensitivity of sentinel-1 backscatter to vegetation dynamics: An austrian case study', Remote Sensing **10**(9), 1396.

Wang, B., Ono, A., Muramatsu, K. and Fujiwara, N. (1999), 'Automated detection and removal of clouds and their shadows from landsat tm images', IEICE Transactions on information and systems **82**(2), 453–460.

Wang, J., Rich, P. M. and Price, K. P. (2003), 'Temporal responses of ndvi to precipitation and temperature in the central great plains, usa', International journal of remote sensing **24**(11), 2345–2364.

Wang, S.-p., Wang, J.-s., Zhang, Q., Li, Y.-p., Wang, Z.-l. and Wang, J. (2016), 'Cumulative effect of precipitation deficit preceding severe droughts in southwestern and southern china', Discrete Dynamics in Nature and Society **2016**.

Wang, X., Xie, H., Guan, H. and Zhou, X. (2007), 'Different responses of modis-derived ndvi to root-zone soil moisture in semi-arid and humid regions', Journal of hydrology **340**(1-2), 12–24.

West, H., Quinn, N., Horswell, M. and White, P. (2018), 'Assessing vegetation response to soil moisture fluctuation under extreme drought using sentinel-2', Water **10**(7), 838.

Wilhite, D. A. (2000), 'Drought as a natural hazard: concepts and definitions'.

Wolters, E., Hakvoort, H., Bosch, S., Versteeg, R., Bakker, M., Heijkers, J., Talsma, M. and Peerdeman, K. (2015), 'Meteobase: online neerslag-en referentiegewasver-dampingsdatabase voor het nederlandse waterbeheer'.

Wong, L., Hashim, R. and Ali, F. (2008), 'Strength and permeability of stabilized peat soil', Journal of Applied Sciences **8**(21), 3986–3990.

Zhang, H., Chang, J., Zhang, L., Wang, Y., Li, Y. and Wang, X. (2018), 'Ndvi dynamic changes and their relationship with meteorological factors and soil moisture', Environmental Earth Sciences **77**. - NDVI increase not significant after precipitation is exceeded.

Zhang, L., Ji, L. and Wylie, B. K. (2011), 'Response of spectral vegetation indices to soil moisture in grasslands and shrublands', International journal of remote sensing **32**(18), 5267–5286.

Zhang, W., Li, Y., Wu, X., Chen, Y., Chen, A., Schwalm, C. R. and Kimball, J. S. (2021), 'Divergent response of vegetation growth to soil water availability in dry and wet periods over central asia', Journal of Geophysical Research: Biogeosciences p. e2020JG005912.

Zoelen, v. B. (2021), 'Waternet begint met officiële dijkinspecties in de regio'.
URL: https://www.parool.nl/nieuws/waternet-begint-met-officiele-dijkinspecties-in-de-regio bb379571/

Zribi, M., Baghdadi, N., Holah, N. and Fafin, O. (2005), 'New methodology for soil surface moisture estimation and its application to envisat-asar multi-incidence data inversion', Remote sensing of environment **96**(3-4), 485–496.

A

Appendix A

A.1. Ground measurements study locations

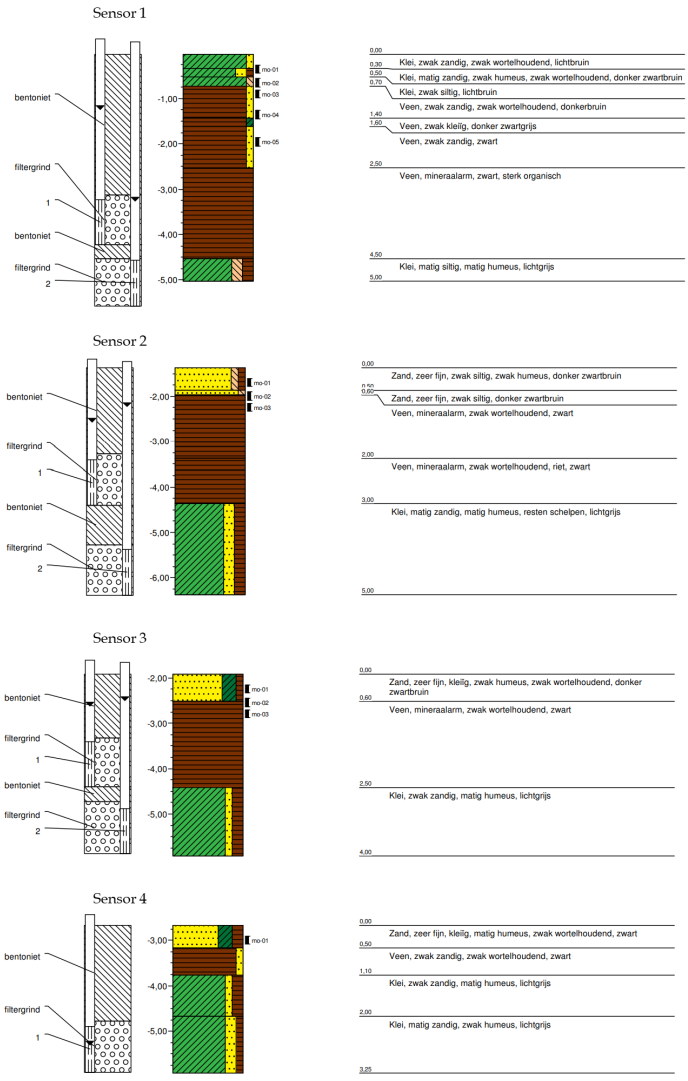

Figure A.1: Illustration of soil properties of the in-situ soil moisture sensors at location Geerweg.

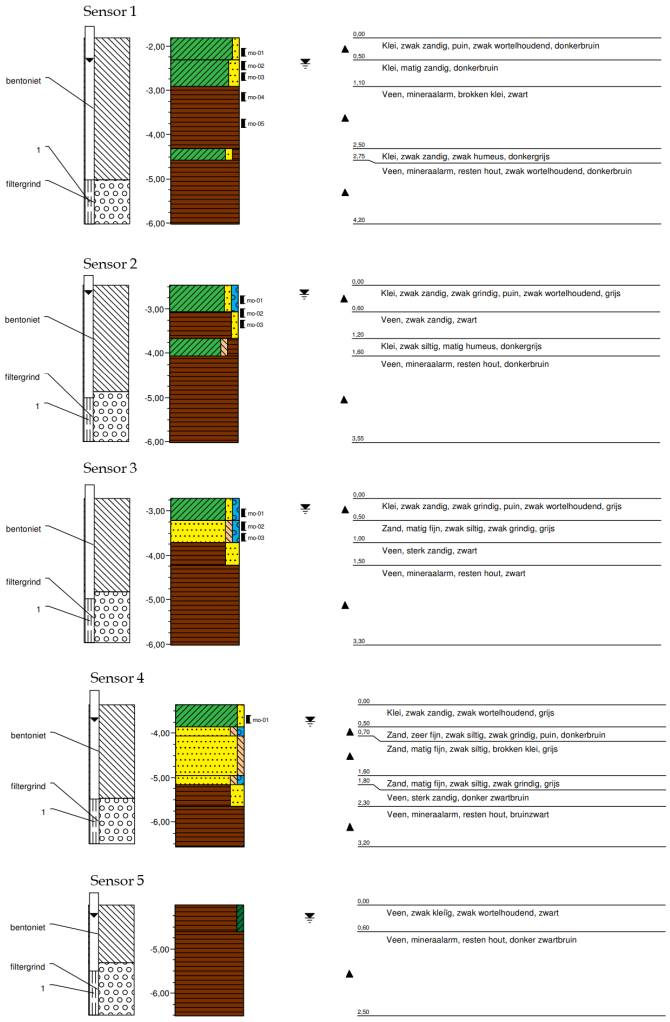

Figure A.2: Illustration of soil properties of the in-situ soil moisture sensors at location Bermweg.

B

Appendix B

B.1. Seasonal dynamics

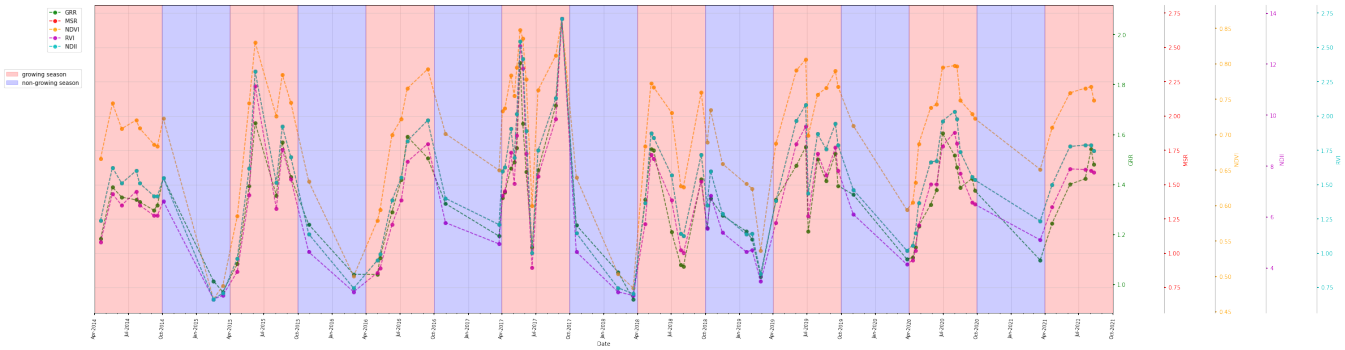

Figure B.1: Seasonal dynamics of GRR, MSR, NDVI, RVI and NDII at location Bermweg. Vegetation indices are extracted from Landsat 8.

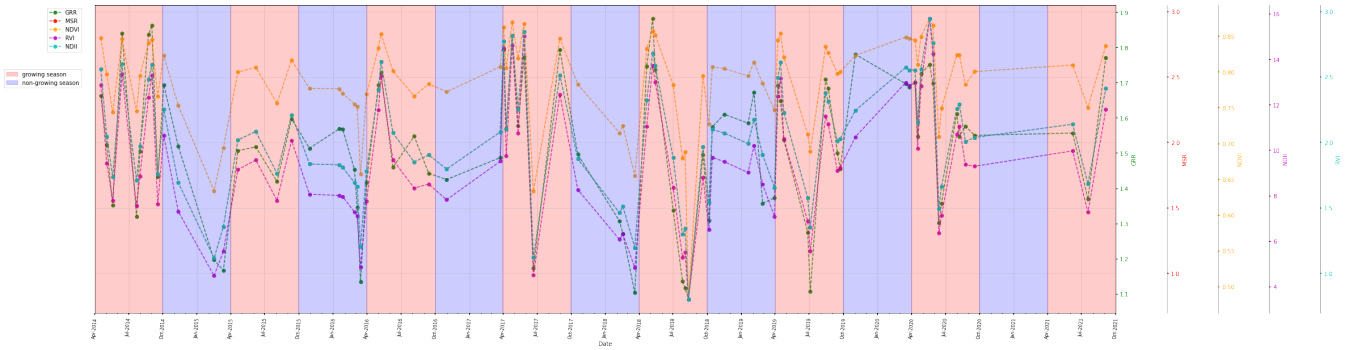

Figure B.2: Seasonal dynamics of GRR, MSR, NDVI, RVI and NDII at location Geerweg. Vegetation indices are extracted from Landsat 8.

B.2. Vegetation indices as a proxy for soil moisture

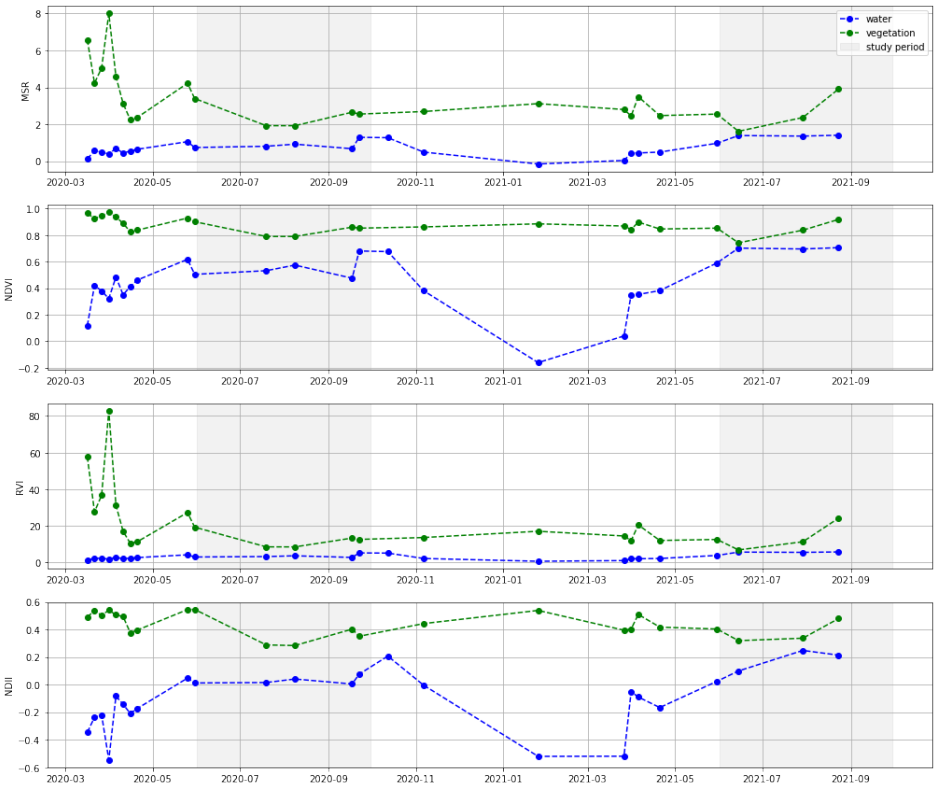

Figure B.3: Time series of MSR, NDVI, RVI and NDII retrieved from water pixel and vegetation pixel acquired from Sentinel-2 at location Geerweg.

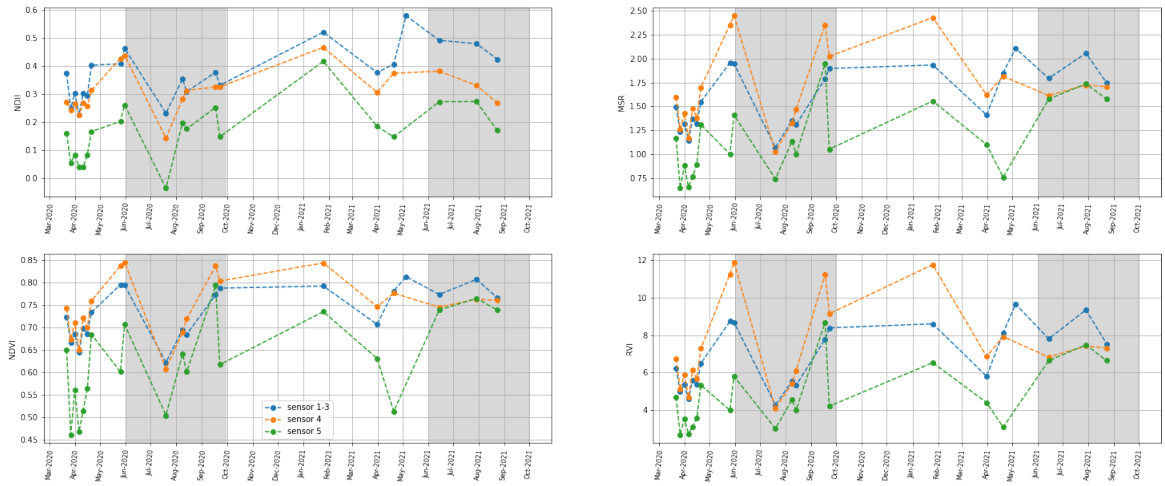

Figure B.4: Graphs showing the GRR extracted from the different pixels from Sentinel-2 at location Bermweg.

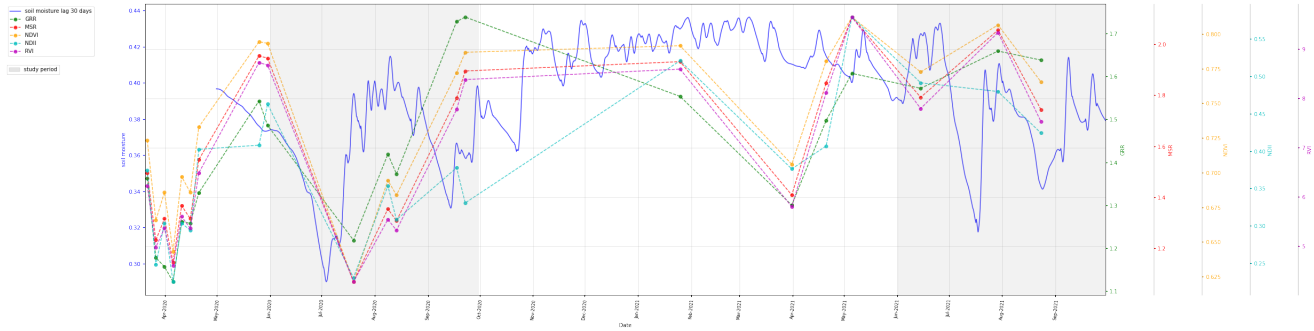

Figure B.5: Graphs showing the pattern between lagged (30 days) soil moisture and VIs (extracted from Sentinel-2) at location Bermweg from sensors 1-3.

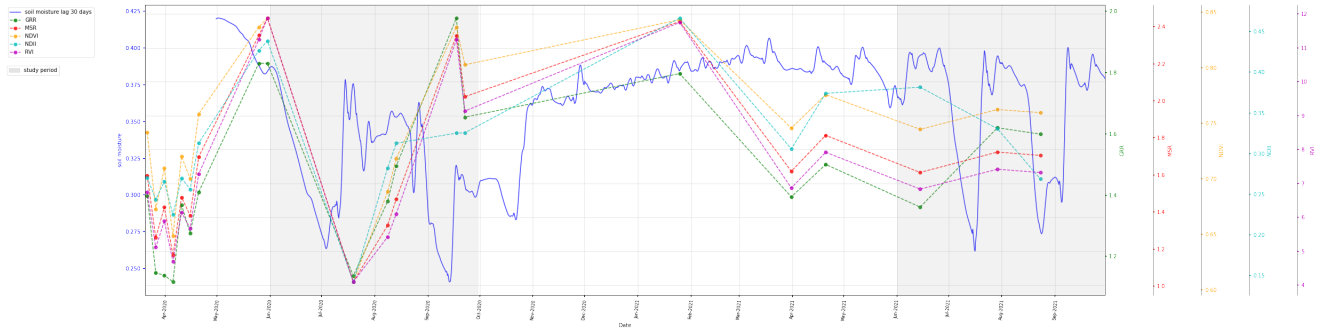

Figure B.6: Graphs showing the pattern between lagged (30 days) soil moisture and VIs (extracted from Sentinel-2) at location Bermweg from sensor 4.

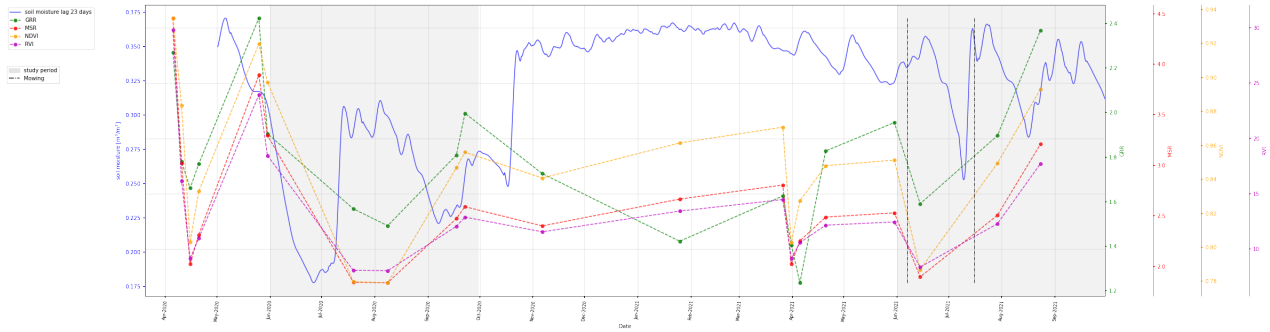

Figure B.7: Graphs showing the pattern between lagged (23 days) soil moisture and VIs (extracted from Sentinel-2 data set) at location Geerweg from sensors 1-2.

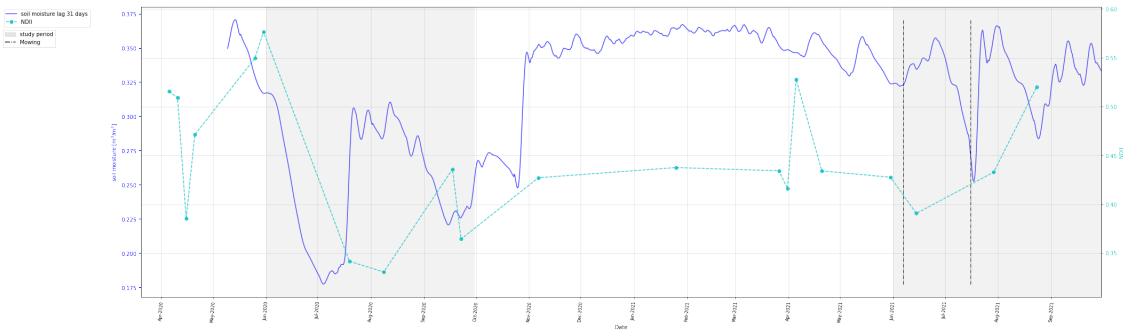

Figure B.8: Graphs showing the pattern between lagged (31 days) soil moisture and NDII (extracted from Sentinel-2 data set) at location Geerweg from sensors 1-2.

	Bermweg					**Geerweg (sensors 1-3)**					**Geerweg (sensor 4)**				
	GRR	**MSR**	**NDVI**	**RVI**	**NDII**	**GRR**	**MSR**	**NDVI**	**RVI**	**NDII**	**GRR**	**MSR**	**NDVI**	**RVI**	**NDII**
lag 0	-0.38	-0.63	-0.63	-0.63	-0.4	-0.13	-0.13	-0.13	-0.14	-0.43	-0.18	-0.23	-0.25	-0.22	-0.29
lag 5	-0.43	-0.43	-0.45	-0.42	-0.32	-0.03	0.01	0.01	0.01	-0.38	-0.14	-0.18	-0.2	-0.17	-0.26
lag 10	-0.31	-0.27	-0.3	-0.26	-0.21	0.01	0.06	0.07	0.05	-0.31	-0.16	-0.21	-0.21	-0.21	-0.26
lag 15	-0.13	-0.03	-0.05	-0.02	-0.04	0.09	0.14	0.18	0.13	-0.2	-0.14	-0.2	-0.17	-0.2	-0.22
lag 20	-0.02	0.14	0.14	0.15	0.03	0.07	0.14	0.18	0.13	-0.17	-0.15	-0.23	-0.19	-0.24	-0.19
lag 25	-0.2	0.02	0.04	0.02	-0.05	0.05	0.13	0.17	0.11	-0.12	-0.2	-0.31	-0.25	-0.32	-0.17
lag 30	0.16	0.38	0.34	0.4	0.37	0.05	0.11	0.16	0.09	0.27	-0.12	-0.24	-0.16	-0.26	0.1
lag 35	0.04	0.19	0.13	0.22	0.26	-0.19	-0.13	-0.09	-0.14	0.13	-0.26	-0.38	-0.3	-0.4	0
lag 40	-0.25	-0.02	-0.09	0.01	0.09	-0.33	-0.28	-0.24	-0.29	0.01	-0.39	-0.47	-0.42	-0.48	-0.07

Table B.1: Pearson correlation coefficients between (lagged) soil moisture and VIs for the harmonized Landsat 7 and 8 data set.

C

Appendix C

C.1. SAR as a proxy for soil moisture

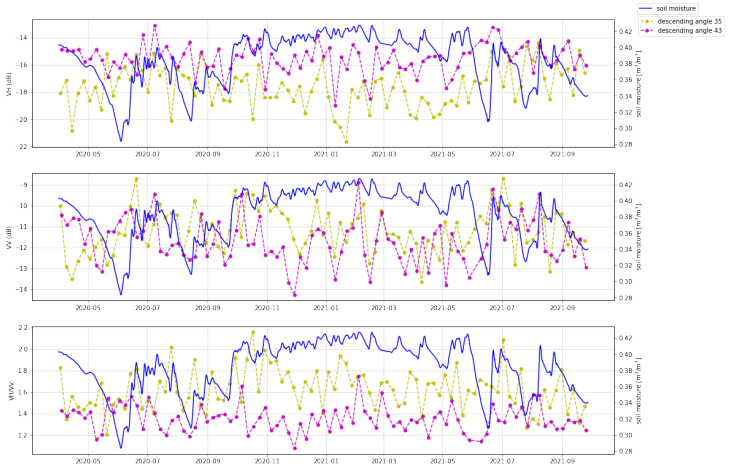

Figure C.1: Graphs showing retrieved backscatter from satellite imagery with descending orbit for polarizations VH, VV, cross-polarization ratio VH/VV and soil moisture at 20 cm depth at location Bermweg.

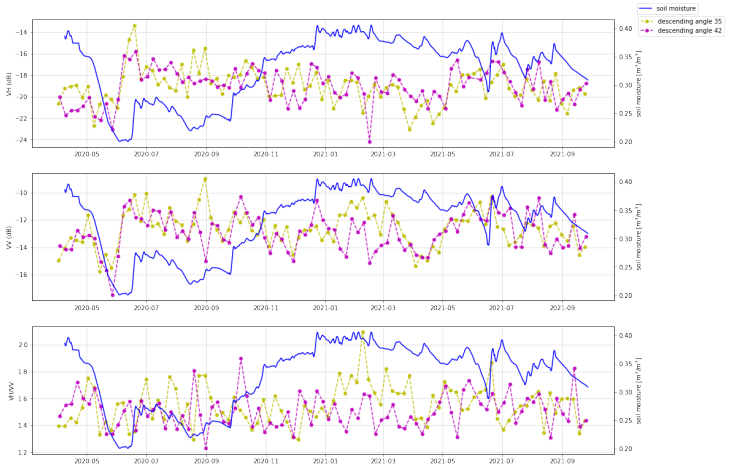

Figure C.2: Graphs showing retrieved backscatter from satellite imagery with ascending orbit for polarizations VH, VV, cross-polarization ratio VH/VV and soil moisture at 20 cm depth at location Geerweg.

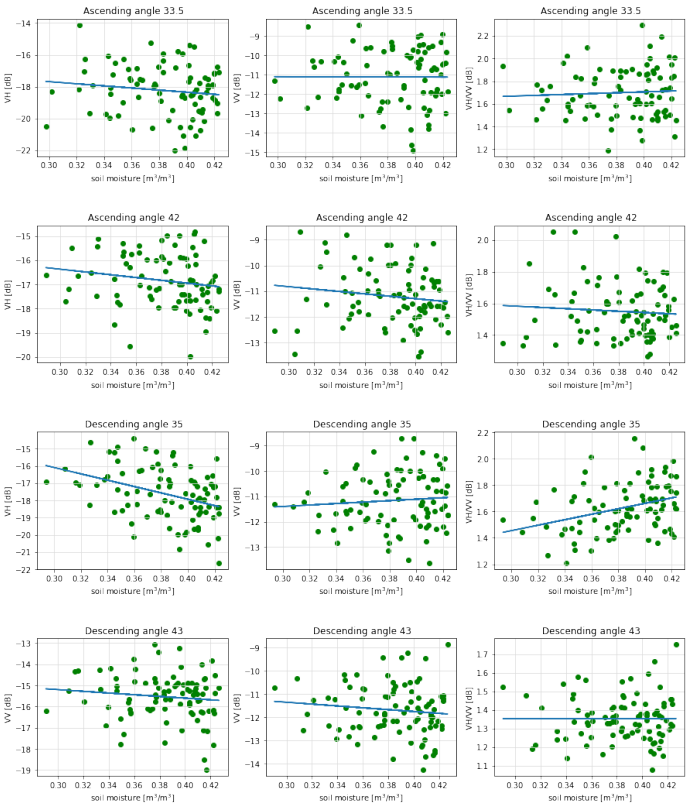

Figure C.3: Scatter plots showing potential relationship between retrieved backscatter and soil moisture at location Bermweg.

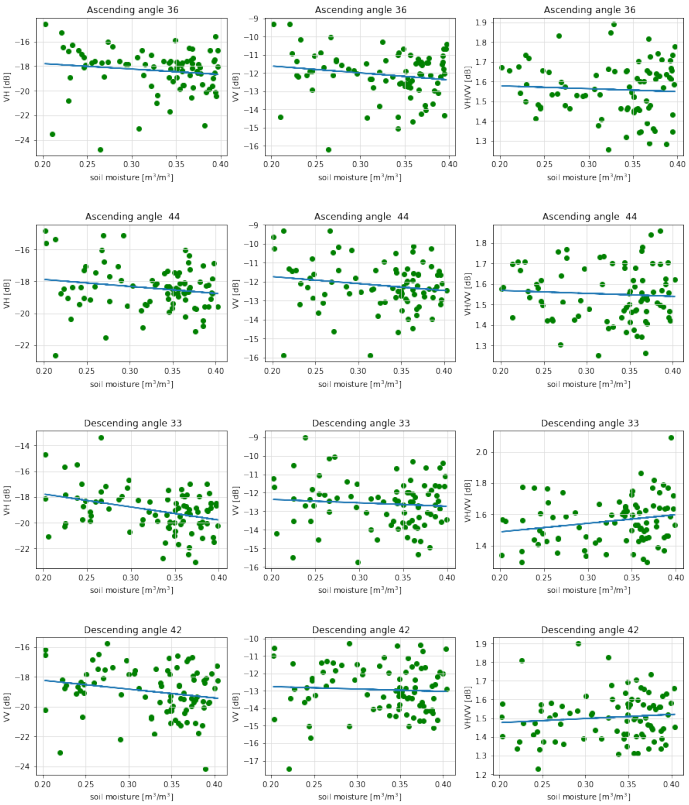

Figure C.4: Scatter plots showing potential relationship between retrieved backscatter and soil moisture at location Geerweg.

D

Appendix D

D.1. Precipitation deficit as a proxy for soil moisture

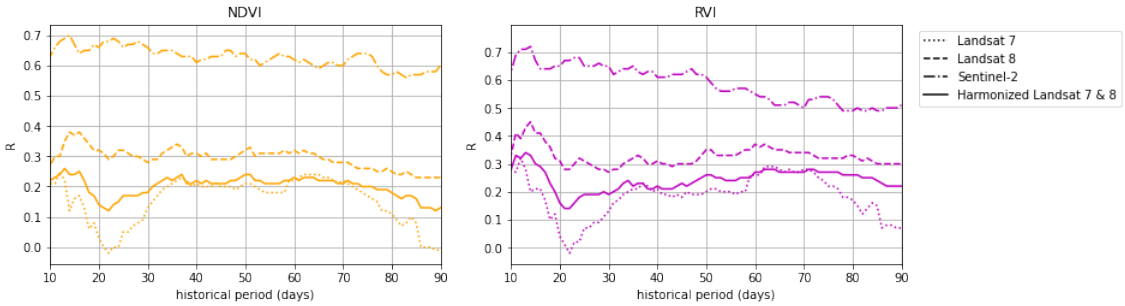

Figure D.1: Calculated Pearson correlation coefficients (R) between vegetation indices (NDVI, RVI) and cumulative precipitation deficit for different satellite missions at a) location Bermweg and b) location Bermweg during June-September. The historical period refers to the period taken into account when calculating the cumulative precipitation deficit.

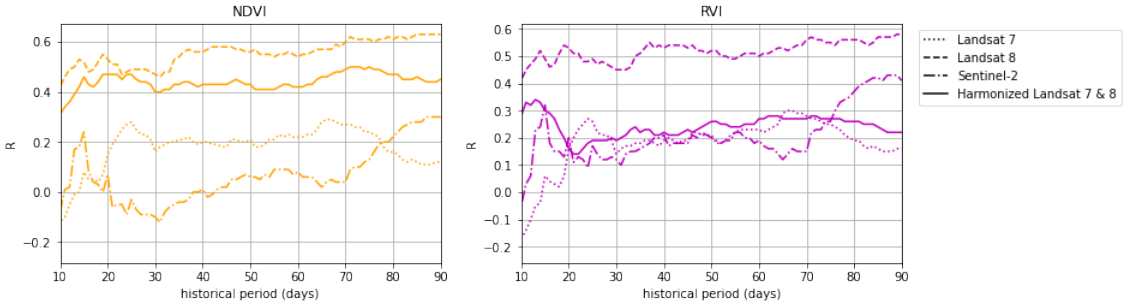

Figure D.2: Calculated Pearson correlation coefficients (R) between vegetation indices (NDVI, RVI) and cumulative precipitation deficit for different satellite missions at a) location Bermweg and b) location Geerweg during June-September. The historical period refers to the period taken into account when calculating the cumulative precipitation deficit.

	Bermweg									
Historical period (days)	**Landsat 8**					**Landsat 7 & 8**				
	GRR	**MSR**	**NDVI**	**RVI**	**NDII**	**GRR**	**MSR**	**NDVI**	**RVI**	**NDII**
10	0.005	0.047	0.091	0.036	0.091	0.020	0.046	0.101	0.053	0.101
15	0.000	0.011	0.019	0.009	0.019	0.010	0.031	0.072	0.023	0.072
20	0.004	0.049	0.045	0.052	0.045	0.100	0.240	0.290	0.226	0.290
25	0.004	0.050	0.045	0.052	0.045	0.062	0.168	0.218	0.155	0.218
30	0.008	0.088	0.082	0.091	0.082	0.052	0.158	0.178	0.155	0.178
35	0.003	0.043	0.040	0.046	0.040	0.044	0.094	0.095	0.101	0.095
40	0.004	0.053	0.054	0.054	0.054	0.042	0.100	0.107	0.103	0.107
45	0.005	0.061	0.071	0.058	0.071	0.032	0.095	0.114	0.092	0.114
50	0.001	0.030	0.041	0.027	0.041	0.018	0.055	0.077	0.050	0.077
55	0.002	0.041	0.054	0.038	0.054	0.028	0.084	0.123	0.076	0.123
60	0.001	0.025	0.044	0.020	0.044	0.017	0.049	0.090	0.041	0.090
65	0.001	0.033	0.061	0.026	0.061	0.019	0.051	0.093	0.042	0.093
70	0.002	0.045	0.084	0.034	0.084	0.017	0.055	0.112	0.041	0.112
75	0.003	0.056	0.107	0.041	0.107	0.012	0.056	0.130	0.039	0.130
80	0.003	0.056	0.113	0.040	0.113	0.013	0.071	0.175	0.047	0.175
85	0.004	0.078	0.148	0.057	0.148	0.018	0.100	0.231	0.069	0.231
90	0.005	0.081	0.149	0.061	0.149	0.028	0.150	0.348	0.101	0.348

Table D.1: Two-tailed p-values between cumulative precipitation deficit and retrieved vegetation indices at location Bermweg. The historical period is the amount of days evaluated prior to the VI observation date to compute the precipitation deficit.

	Geerweg									
Historical period (days)	**Landsat 8**					**Landsat 7 & 8**				
	GRR	**MSR**	**NDVI**	**RVI**	**NDII**	**GRR**	**MSR**	**NDVI**	**RVI**	**NDII**
10	0.001	0.020	0.020	0.023	0.020	0.000	0.009	0.022	0.008	0.022
15	0.000	0.003	0.002	0.005	0.002	0.000	0.000	0.001	0.000	0.001
20	0.000	0.002	0.002	0.002	0.002	0.000	0.000	0.000	0.000	0.000
25	0.001	0.005	0.005	0.005	0.005	0.000	0.000	0.000	0.000	0.000
30	0.002	0.008	0.008	0.010	0.008	0.000	0.002	0.003	0.002	0.003
35	0.000	0.002	0.002	0.003	0.002	0.000	0.001	0.001	0.001	0.001
40	0.000	0.001	0.001	0.002	0.001	0.000	0.001	0.001	0.001	0.001
45	0.000	0.001	0.001	0.002	0.001	0.000	0.001	0.001	0.001	0.001
50	0.000	0.002	0.001	0.003	0.001	0.000	0.001	0.001	0.001	0.001
55	0.000	0.003	0.002	0.006	0.002	0.000	0.002	0.002	0.002	0.002
60	0.000	0.003	0.002	0.004	0.002	0.000	0.001	0.002	0.002	0.002
65	0.000	0.001	0.001	0.002	0.001	0.000	0.000	0.001	0.001	0.001
70	0.000	0.001	0.000	0.001	0.000	0.000	0.000	0.000	0.000	0.000
75	0.000	0.001	0.000	0.001	0.000	0.000	0.000	0.000	0.000	0.000
80	0.000	0.001	0.000	0.001	0.000	0.000	0.000	0.000	0.000	0.000
85	0.000	0.000	0.000	0.001	0.000	0.000	0.001	0.001	0.000	0.001
90	0.000	0.000	0.000	0.001	0.000	0.000	0.001	0.001	0.000	0.001

Table D.2: Two-tailed p-values between cumulative precipitation deficit and retrieved vegetation indices at location Geerweg. The historical period is the amount of days evaluated prior to the VI observation date to compute the precipitation deficit.

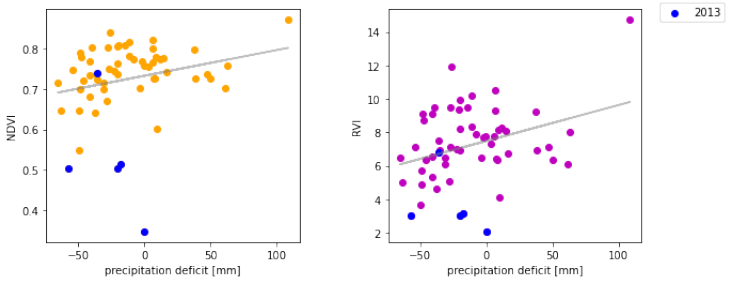

Figure D.3: Scatter plots between the NDVI, RVI and a cumulative precipitation deficit of 14 days at location Bermweg during June to September. Outliers from the year 2013 are coloured in blue.

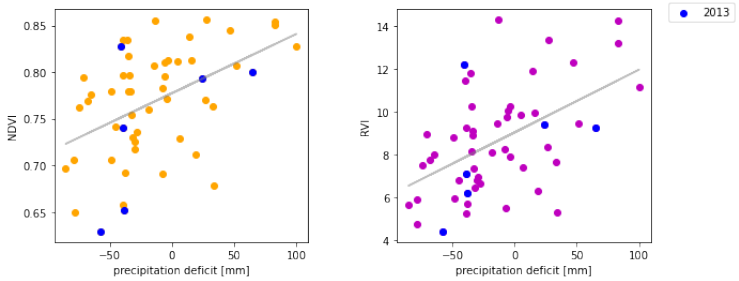

Figure D.4: Scatter plots between the NDVI, RVI and a cumulative precipitation deficit of 20 days at location Geerweg during June to September. Outliers from the year 2013 are coloured in blue.

E

Appendix E

E.1. Spatial-temporal analysis

Figure E.1 displays the extracted vegetation indices from Landsat 8 at the Amsterdam-Rhine canal. Differences can be found, however as it covers not only the region of interest these results are not further interpreted.

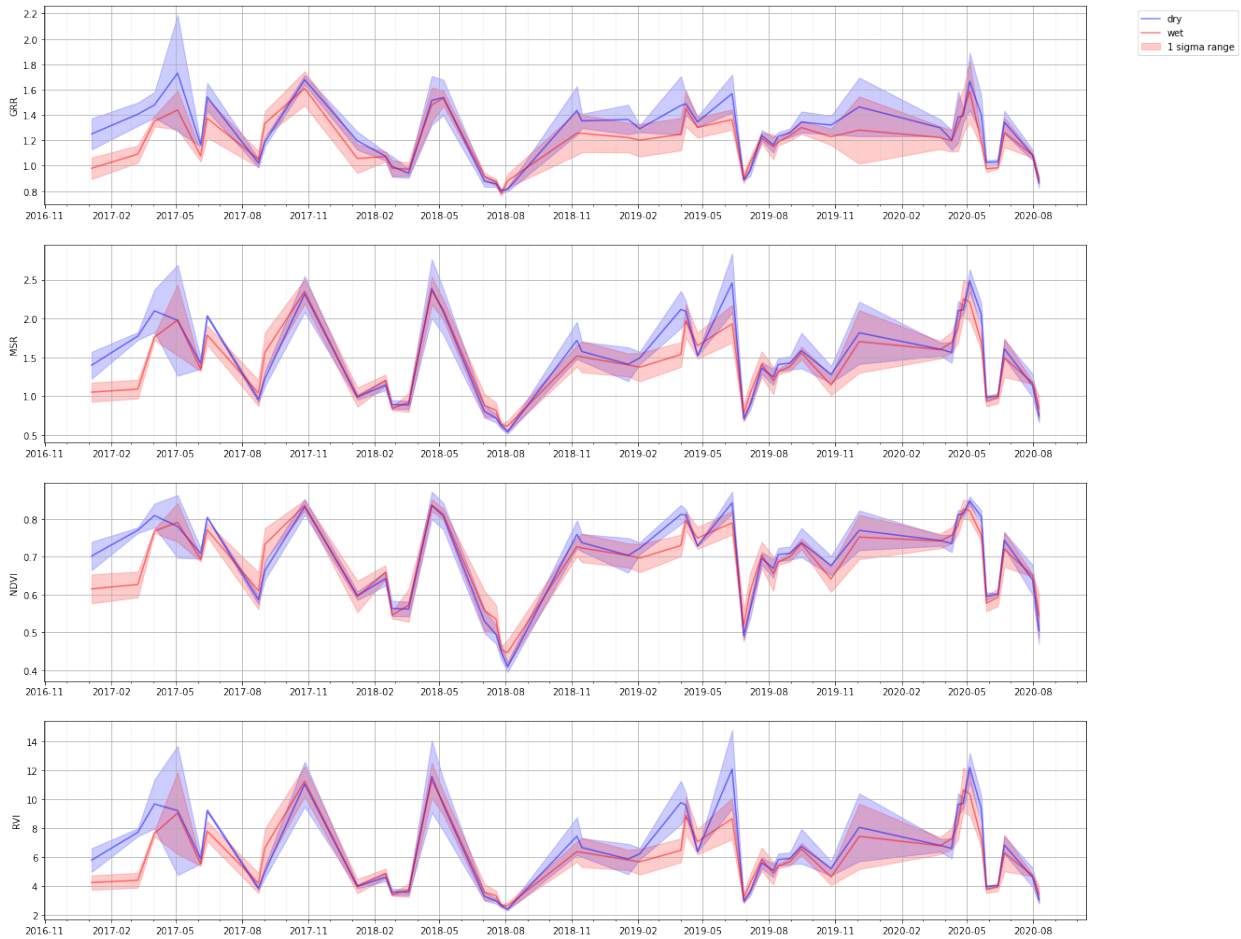

Figure E.1: Extracted vegetation indices from Landsat 8 from 2017 up until 2020. The blue line represents the mean values from the pixels within the wetted area and the red line the normal area. The shaded value represents the one standard deviation above or below the mean value.

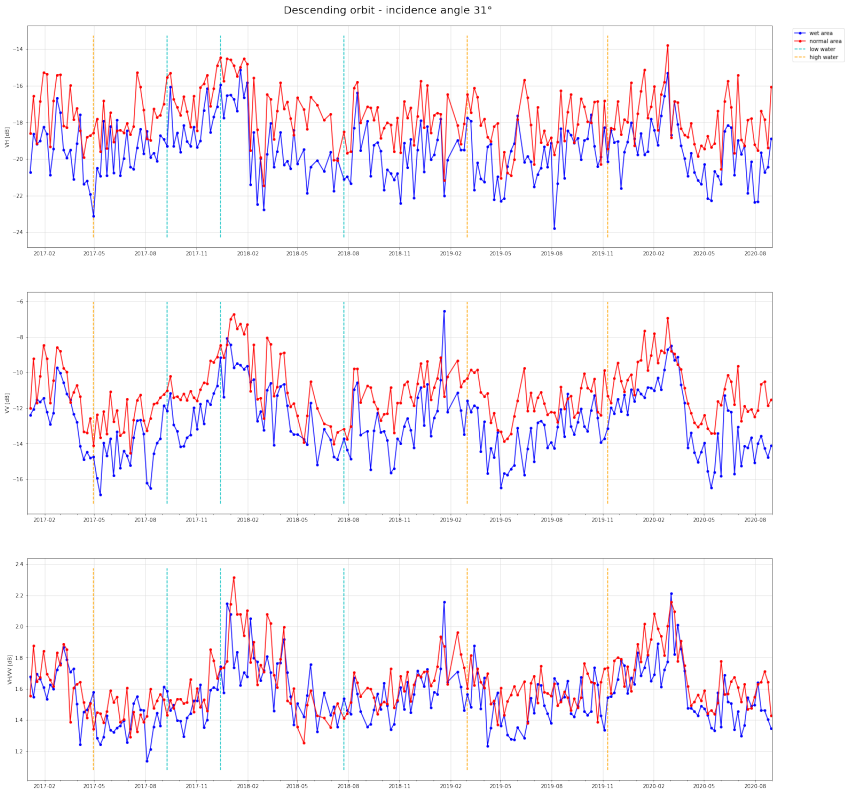

Figure E.2: Graphs showing the retrieved backscatter for polarizations VH, VV, cross-polarization ratio VH/VV at the Amsterdam-Rhine canal. Data is retrieved from satellite imagery with ascending orbit and incidence angle 37.

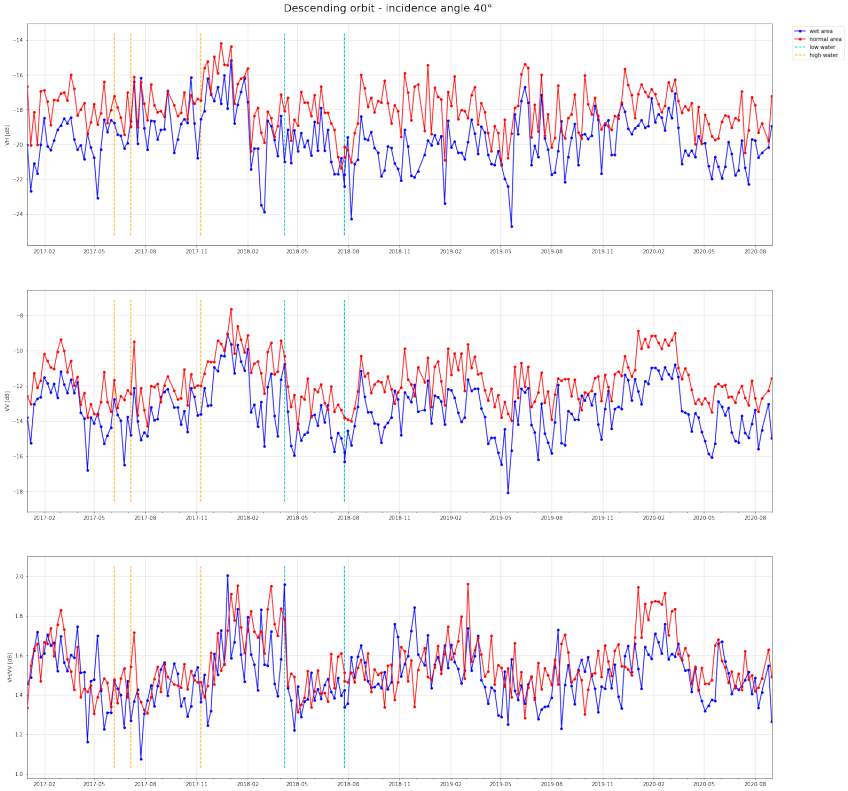

Figure E.3: Graphs showing the retrieved backscatter for polarizations VH, VV, cross-polarization ratio VH/VV at the Amsterdam-Rhine canal. Data is retrieved from satellite imagery with ascending orbit and incidence angle 45.